ADDIS ABABA UNIVERSITY,

Addis Ababa Institute of Technology

School of Mechanical and Industrial Engineering

Computational Modeling and Performance Analysis of Solar Thermal Storage Integrated with Parabolic Solar Concentrator for Cooking Application

By: Dejene Kebede Kedida

Thesis Submitted to the school of Graduate Studies of Addis Ababa University in Partial Fulfillment of the Requirements for the Degree of the Doctor of Philosophy in Mechanical Engineering (with Specialization in Thermal and Energy Systems Engineering)

Main Supervisor: Dr.-Ing. Demiss Alemu

Co – supervisor: - Dr. Yilma Tadesse

June 2020

Addis Ababa, Ethiopia

ACKNOWLEDGMENT

First of all, I would like to thank my supervisor, Dr.-ing Demiss Alemu for his support and advice during these years. His enthusiasm and expertise in this area have provided me with a wealth of knowledge and experiences that are invaluable. I would also like to send my gratitude to my co-advisor Dr. Yilma Tadesse for his patient support in the dissertation for all these years. To my colleagues at AAiT, I would like to say thank you for your friendship, assistance, and encouragement. To my wife, Asnakech Temesgen, thank you for your love, patience, and understanding. Your encouraging words and ongoing support were always there at times when I needed them most.

Last but not least, I thank my parents, sister, and brothers for their unconditional love, kindness, support, and encouragement. From the start until the accomplishment of this dissertation, they have been my source of strength and courage. To them, I dedicate this dissertation.

ABSTRACT

Cooking using biomass, which is commonly practiced in developing countries, causes rampant deforestation and exposure to hazardous emission. Hence, the utilization of solar energy for cooking can be used as solution to mitigate both problems . As solar radiation is not available at every hour of the day, thermal storage is essential for availing thermal energy at the required time of use. Therefore, this work investigates the long term efficiency of the solar cooker with a parabolic concentrating collector integrated with thermal storage using a 1D finite-difference computational model was developed under the actual cooking condition. For two type thermal storages, that is sensible pebble bed thermal storage and PCM thermal storage with air as heat transfer fluid, computational modeles are developed using MATLAB programming environment. In both case, the results of the computational models were verified using xperimental test results available in articles published in reputable journals.

In first case, a cook stove of packed pebble bed thermal storage having 0.3m diameter and 0.9m height was simulated for actual charging and cooking condition using solar radiations of Addis Ababa and Semera. The simulation resulted in thermal storage capacity of 40.1 MJ during a clear day and 12.85 MJ energy during cloudy day for Addis Ababa, and 60.3 MJ and 29.47 MJ of thermal storage for clear and cloudy day of Semera, respectively. The overall cooking efficiencies of the cookstove are 30% and 22.08% under Addis Ababa climate condition and 36.6% and 31.1% under Semera climate condition for the day of the highest and the lowest solar radiation respectively using forced convection. Hence, it can be concluded that solar concentrating cookers with pebble bed thermal storage can have an overall cooking efficiency between 22% and 30% on a clear sky day when the Sun is overhead in tropical areas.

Where as for PCM thermal storage, the thermal storage capacities of 47.42 MJ and 14.59 MJ and the overall cooking efficiencies of 53.62% and 44.10% were obtained for the day of the highest and the lowest solar radiation of Addis Ababa, respectively. For highest and lowest radaition day of Semera , the thermal stoarge capacity was 65.36MJ and 38.98MJ and the overall cooking efficiencies were 51.45% and 53.16%, respectively.

TABLE OF CONTENTS

LIST OF FIGURES

LIST OF TABLES

CHAPTER ONE

1. INTRODUCTION

1.1. Background

Energy sources such as oil, natural gas, and fossil fuel have been used extensively and have provided great benefits to humanity. Solar energy is by far the most abundant source of energy on the earth that can generate electricity, provide hot water, heat and cool a house. Solar energy applications require energy storage system due to the absence or low solar radiation during the night, morning, and evening. Energy storage is used to mitigate the mismatch between energy supply and demand in using intermittent or fluctuating energy resources such as solar, wind and hydro energy.

Cooking is an integrated part of every human being activity as food is one of the basic necessities for existence. Commonly used sources of energy for cooking are firewood, crop residue, cow dung, kerosene, electricity, liquefied petroleum gas (LPG), biogas, etc. Half of the world's population is exposed to indoor air pollution, mainly as the result of burning solid fuels for cooking and heating. Woodcut for cooking purposes contributes to 16 million hectares of forest destroyed annually. The World Health Organization (WHO) reports that in 23 countries, 10% of deaths are due to just two environmental risk factors: unsafe water, including poor sanitation and hygiene, and indoor air pollution due to solid fuels used for cooking [1]. In under-developed countries, women have to walk 2kms or more on average and spend a significant amount of time collecting firewood for cooking. The cooking energy demand in rural areas of developing countries is largely met with biomass such as fuelwood, charcoal, agricultural residues, and dung cakes, whereas LPG and electricity are predominantly used in urban areas [1],[2]. The data from the Ministry of Water and Energy Bureau indicates, 90% of the population in Ethiopia uses traditional biomass for cooking and the rest uses LPG and electricity. In Ethiopia, 83.4% of the population lives in rural areas and energy demand for cooking is mostly met by firewood, agricultural residue, and cow dung cake. Using these sources of energy for cooking creates

indoor air pollution. As a result respiratory disease are common due to the inhalation of pollutants. Although LPG, kerosene and electricity are the most chosen source of energy for cooking in urban areas, an increase in crude oil prices in the international market and an increase in demand for LPG in Ethiopia have caused the price of LPG to rise exponentially. This has forced the government to look for alternative sources of energy [2][3].

Solar energy is harnessed with solar thermal technologies such as parabolic trough, tower, and dish systems for high temperature, and flat plate collector, evacuated tube collector and box solar collectors for low-temperature applications. Although solar energy is the preferred type of renewable energy for cooking next to biomass, some shortcomings are also reported in its application. The major ones are the non-availability of solar radiation at all hours of the day, vision hazard that can be caused by reflected sun rays and its inconvenience for indoor cooking. The utilization of a thermal storage system helps avoid the limitation of solar energy to cook at all required hours of the day and makes possible indoor cooking.

Ethiopia has an abundant amount of solar insolation with almost 365 day's sunshine each year. One can confidently rely on this source of energy. Since cooking is an integral part of the activity in each household, cooking with solar energy can be used to meet the gap between supply and demand of energy in the future. With increasing population and economic growth, the utilization of solar energy is a must for sustainable development. In Ethiopia, different types of solar collectors have been disseminated by government and non-governmental organization for cooking. Such as parabolic solar cookers, box-type solar cookers, panel cookers, etc. Also, different institutions and universities have done many kinds of research concerning solar energy conversation for cooking, heating, sterilizing, etc.

A lot of researches on the design, application and performance of solar cookers from different parametrical aspects was reported in the past [4]. The design and performance of solar cookers such as panel cookers, parabolic cookers, funnel cookers and Scheffler cookers are some of the works. While most of these cookers are for outdoor cooking, scheffler's dish can be used for indoor cooking by reflecting the sunray and heating a thermal storage media. Apparently, most solar cookers mentioned are designed for day time use and lack the introduction of thermal storage [5][6]. The Literatures classify solar thermal storages as

sensible and latent heat storages [4][5][7]. Although extensive work has been done in solar thermal storage systems, still there are no conclusive remarks on the overall efficiency of the solar cooker with thermal storage under actual cooking conditions. Hence, the objective of this work is to give conclusive remarks on different efficiencies of the solar cooker with sensible and PCM thermal storage under the climatic condition of Addis Ababa and Semera in Ethiopia using the computational model.

1.2. Existing Solar Cookers and their Draw Backs

Existing solar cookers and their drawbacks are summarized in the following table.

Table 1-1: Existing solar cookers and their draw backs

No	Type of Solar Cookers	Working Principles	Draw Backs	Ref.
1	***Box Type Solar Cooker***	This type is the basic solar cooking model which is constructed from a simple rectangular box covered with either glass or plastic. Solar irradiance entering the cooker through this cover converts to energy when it is absorbed by the black colored absorber plate and cooking vessel. When the input energy is entering the cooker, the temperature inside the box cooker raises until the heat loss from the box equals the solar heat input. The box is covered by thermal insulation to reduce the heat loss to ambient, to	- Cooking has to be done outdoor and the cook has to stand in sunlight for a long time. - Very slow cooking compared to conventional cooking. This takes 2-3 hours to cook and even more time during cloudy days with respect to less than half an hour taken by conventional methods. - It is not possible to cook during rainy days.	[1][4] [8]

		attain higher temperatures and better efficiency. Hence, this trapped energy raises the temperature of the space inside the box. To improve the box temperature, reflectors are used. Single or multiple reflectors are used, which are oriented such that the incident sunlight falling on the reflector, get directed to the box	- There is no control over the rate of cooking.	
2	***Panel Solar Cooker***	This type of solar cooker is very cheap and can be easily built using reflecting material like aluminum foil and cardboard. This uses shiny material to reflect sunlight to a cooking vessel which is enclosed in a clear plastic bag. Food to be cooked is kept in a dark container covered with a tightly fitted lid.	- Cooking has to be done outdoor and not possible to cook during the rainy season. - Very slow cooking compared to conventional cooking. At least one hour is required to cook during a clear sunny day. - Control over the rate of cooking is not there.	[1][4] [8]
3	***Parabolic Cooker***	This type of solar cooker is used at a better cooking rate when it is comparable with the conventional one. The cooking pot is placed at the focus of a concentrating mirror. Using a reflector of parabolic shape, the sunbeam is reflected onto a pot or vessel kept at the focus of the parabola. The axis of the parabola	- Cooking has to be carried outdoor. Hence, not possible to cook during rainy days. - At the focal point, highly concentrated sunbeam falls which is potentially hazardous.	[1][4] [8]

		should be parallel to the sunbeam so that maximum heat energy is obtained at the pot. Since highly focused light is obtained, the temperature can go well above 1500^0C. The linear parabolic collector is also used for concentrating the sunlight on to a pot kept at the focal line.	- A parabolic collector requires either a one-axis or two-axis tracking system to track the sun. - Though cooking is as fast as compared to conventional cooking, there is no control over the cooking rate.	
4	***Funnel Cooker***	This is a type of concentric solar cooker in which the sunlight is concentrated into a cooking vessel or pot using a funnel-shaped cooker. Sunbeam is concentrated using a reflector like Aluminum foil pasted on a folded cardboard. Black colored pot is kept inside a plastic cover that traps the heat by the greenhouse effect. A simple system allows pressure-cooking to increase the cooking rate while releasing steam. This cooker can be used for cooking and pasteurizing water.	- Cooking has to be done outdoor. - There is no control over the cooking rate and very slow cooking compared to conventional cooking.	[1][4] [8]
5	***Scheffler Cooker***	This is a concentrator type solar cooker in which a paraboloid dish with a fixed focus on the ground. Cooking can be carried out in the kitchen without moving out using this type of cooker. The concentrating reflectors track the	- The seasonal variation in the height of the sun requires changing not only the angle between the concentrating reflector and its axis of	[1][4] [8]

		movement of the sun, reflecting the light of the sun and concentrating it at a fixed position. The reflected and concentrated sunlight enters a nearby kitchen directly to strike a cooking vessel or frying surface. High temperatures can be attained as it focuses the sunlight. Hence the time taken for cooking is comparable to conventional cooking. This type of cooking is suitable for preparing food for large mass. The cooking temperature is limited to around 100^0C.	rotation but also the shape of the reflector. - Since the focus point is fixed, continuous tracking is necessary. - Focused sunlight falls only on the outer part of the cooking vessel resulting in uneven cooking. - The highly focused light is very hazardous as cooking is done at the focal point. - There is no option for either decreasing or increasing the rate of cooking.	

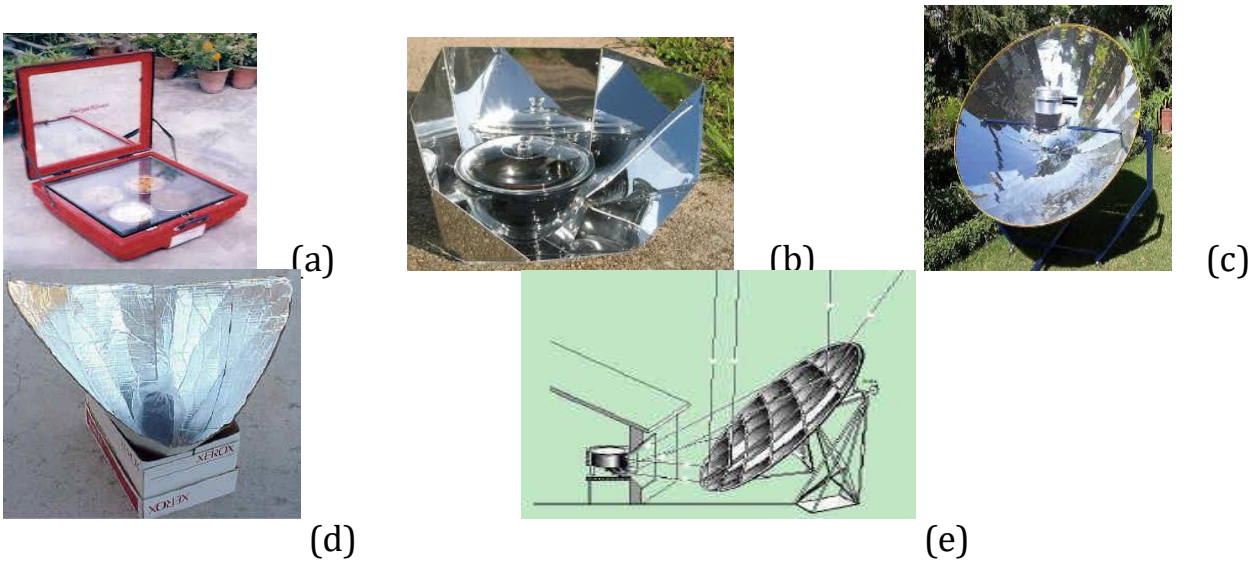

Figure 1-1: a) box type solar cooker, b) panel solar cooker, c) parabolic solar cooker, d) funnel solar cooker, e) Scheffler Cooker [9]

1.3. Statement of Problem

Due to the exhaustion of fuelwood resources in developing countries and its heavy environmental impacts such as climate change, global warming and ozone layer depletion, etc., thermal energy storage has received more attention recently to mitigate problems of solar cookers. In addition, the rapid increase in the price of fossil fuels used for cooking, forced government and non-governmental organizations to pay attention to alternative energy resources used for cooking such as solar energy, biomass, etc. As a result, different types of solar collectors used for cooking have been developed. However, they have many problems that are not still solved; cooking has to be carried out-doors which means cooking has to be carried out standing in sunlight for a long time that hazards human health and very slow cooking (box cooker, panel cooker) compared to conventional cooking. In addition to this, solar cookers have problems with storing heat and supply it during nights and cloudy days. To address these problems, solar cooker with thermal storage powered by parabolic dish are good candidates. However, the long-term performance and limitation of solar cookers with thermal storage are fully not investigated under actual cyclic cooking condition with actual climate.

1.4. Objectives

The general objective of this research activity is to model solar thermal energy storage used for cooking and analyze the long-term performance of the cooker under actual cooking conditions. The specific objectives include the following.

- Review the methods and technologies available for solar thermal energy storage
- Solar data assessment and analysis
- Size solar thermal energy storage integrated into a parabolic solar collector
- Computational simulation of the transient temperature distributions along with the storage height during charging and discharging conditions.
- Performance analysis of solar cooker with thermal storage
- Overall, the efficiency of the solar cookers with thermal will be determined.

1.5. Relevance/Significance of the Research

Solar thermal energy storage is a novel solution to bridge the time gap between energy demand and supply. This research is focused on the modeling and analysis of solar thermal storages using actual solar radiation data. The energy is stored in packed pebbles or packed PCM capsules using heat extracted from a parabolic solar concentrator. Since the cooking is carried out indoors, the users are free from the health risks due to reflection of solar radiation that happens during outdoor cooking and it is environmentally friendly since the air no pollutants or GHG emissions. In addition, it helps to relieve women and children from the burdens of collecting firewood and transporting over long distances. It also helps to reduce the rampant deforestation

The long-term goal of this research is that institutions, host communities, refugees, farmers and enterprises will be benefited from solar cooking. Small scale enterprises can get more opportunities to process food and supply to the market. Also, Health professionals can use solar heat storage solutions for the application of sterilization in clinics and health centers that are located in remote areas/ off-grid areas. Also, institutions and universities can establish support on research and education for a continuing development and improvement of solar thermal technology.

CHAPTER TWO

2. METHODOLOGY

The general methodology in this research is first to investigate the heat transfer characteristics and the ability of materials to store heat for the required time. In this chapter, methods to achieve the objective of the research work are discussed. Two types of thermal storage methods are computationally simulated and modeled separately, these are pebble bed and PCM solar thermal storages powered by a parabolic solar collector for cooking. Then, the comparison of the two cases will be discussed as per charging and discharging process for both scenarios. To address these cases, simulation of the solar cooker with thermal storage is going to be implemented. Therefore, the following methodology will be followed for both the pebble bed and PCM solar thermal storage.

2.1. Literature Review

The literature on solar collectors used for cooking with or without thermal energy storage will be reviewed. A heat transfer analysis used for modeling solar thermal storage will be carried out. Materials used as storage media and heat transfer fluids will be reviewed.

2.2. Data Collection

The following data will be collected from the literature and available sources.

- Addis Ababa and Semera solar radiation data and ambient temperatures will be collected from Ethiopia metrological agency
- The energy required for cooking and water heating
- Physical and chemical properties of storage materials from reputable references
- Experimental data on pebble beds and PCM capsules

Two main material selections, storage materials (pebbles and PCM) and insulation materials have been carried out. Materials used for storing heat can be selected based on the length of time storing energy, thermal conductivity, heat capacity, local availability, etc. Insulation materials will be selected based on low thermal conductivity and local availability. Additionally, materials used for parabolic solar collectors integrated to absorber will be

selected based on availability, reflectivity and absorbance of solar irradiance. A fan which is used to blow air from the storage during charging and discharging conditions are going to be selected based on the pressure drop and mass flow rate.

2.3. Physical Concept

In physical concept, a schematic drawing of the system integration after sizing all the components based on the amount of energy demand to be stored for the requirements will be depicted. The system flow process and working principle are going to be discussed for charging and discharging process.

2.4. Mathematical Model

The energy conversion equations of the system that integrates parabolic solar collector and thermal storage are formulated for the heat transfer fluid and the storage medium. That is, for fluid and solid for the pebble bed case (air and pebble) and fluid and for PCM capsules for the PCM case. Additionally, energy equation for the cooker which is integrated with the thermal storage is included.

2.5. Computational Model

System modeling of solar thermal storage integrated with a parabolic solar concentrator which is used for cooking will be implemented using MATLAB software. The spatial and temporal discretization of the energy balance will be done using the finite difference method. The computational model will simulate the transient temperature distributions of pebbles and air along with the spatial and temporal steps for charging and discharging conditions. The amount of energy stored along the length of the storage will be simulated for both types of solar thermal storage. Additionally, the pressure drop within the storage with respect to different flow conditions will be investigated.

2.6. Verifications of Computational Model

The validity of simulation results will be verified by comparison with experimental results in the literature. For the pebble bed case this is temperature recordings in air/rock bed

experiments. In the case of PCM solar thermal storage, this is with oil-based heat transfer fluid and PCM capsules.

2.7. Results and Discussions

The results of the computational model will be presented and discussed under this topic. Temperature distributions in the storage in case of charging and during cooking will be discussed. The thermal storage efficiencies, cooking efficiencies, thermal efficiencies, and overall efficiencies will be presented. The melt fraction of PCM thermal storage will be analyzed.

CHAPTER THREE

3. LITERATURE REVIEW

3.1. Solar Energy Technology and Theory

Since the world's population increases rapidly and resulting in the growth of industrial activities, energy requirements like fossil fuels cannot be the only source on a sustainable basis. As cooking is a vigorous part of every human being, it consumes a major element of the household energy requirement. The existing cooking fuels are mostly derived from fossil fuels like LPG, kerosene, etc. or air-polluting energy sources like crop residue, firewood, cow dung, etc. In this respect, solar cooking is a very simple, clean and environmentally friendly alternative source of energy. The advantages of solar cooking are taken as follows.

- Prevents cause for global warming and global dimming, since it is a clean source of energy. Therefore, it reduces indoor air pollution and prevents health problems.
- Solar cookers can also be used to heat water, sterilization, and food processor.
- Solar cooking reduces deforestation.
- Cooking fires are dangerous, especially for children, and can cause damage to the building also. In this regard, the solar cooker is fire-free and safer compared to conventional cooking.
- Using solar cooking helps in reducing the load on fossil fuels and hence it is a sustainable one. Many poverty-stricken families around the world's income spent on cooking fuel. Since Sunlight is free and abundant, Money saved can be used for quality food, health care, etc.

3.2. Solar Energy Conversion

Several researches have been done on the conversion of solar energy into different forms of energy. This means, it converts to thermal energy, electrical energy, etc. This energy conversion requires different types of solar collectors. Flat plate solar collectors, evacuated

tube solar collectors and parabolic solar collectors are among the types of solar collectors used to convert solar energy to other forms of energy.

Veslum et al. [10] described different types of air heating absorber for a parabolic solar collector for different mass flow rates and found stainless steel fiber mesh absorber and silicon carbide honeycomb monolith absorber to have similar performance at a concentration factor of 300. However, the cost of stainless fiber mesh absorber is quite lower than that of the honeycomb. In addition, Sharma et al. [11] conducted research on design and evaluation of open volumetric air receiver. Veremachi et al. [12] analyzed the parabolic dish concentrating collector for indirect solar cooking. Ibrahim et al [13] also studied the design and development of a parabolic dish solar water heater analytically with the energy conversion model.

3.3. Solar Thermal Energy Storage

Thermal energy storage describes to any technology where the heat is stored in a thermal reservoir for the use at the time of need. Traditionally, humans store heats that are needed for the short time and therefore the technical solutions for storage may be quite simple. The applications of thermal energy storage are necessary for reducing mismatch between energy supply and energy demand, and intermittent and unpredictable energy sources such as solar energy can be captured for use at a later time. Thermal energy storage can be stored as a change in the internal energy of a material as sensible heat, latent heat and thermochemical or a combination of these [6], [7], [14], [15]. Depending on its forms of storage, they can be classified as it is shown in Figure 3-1.

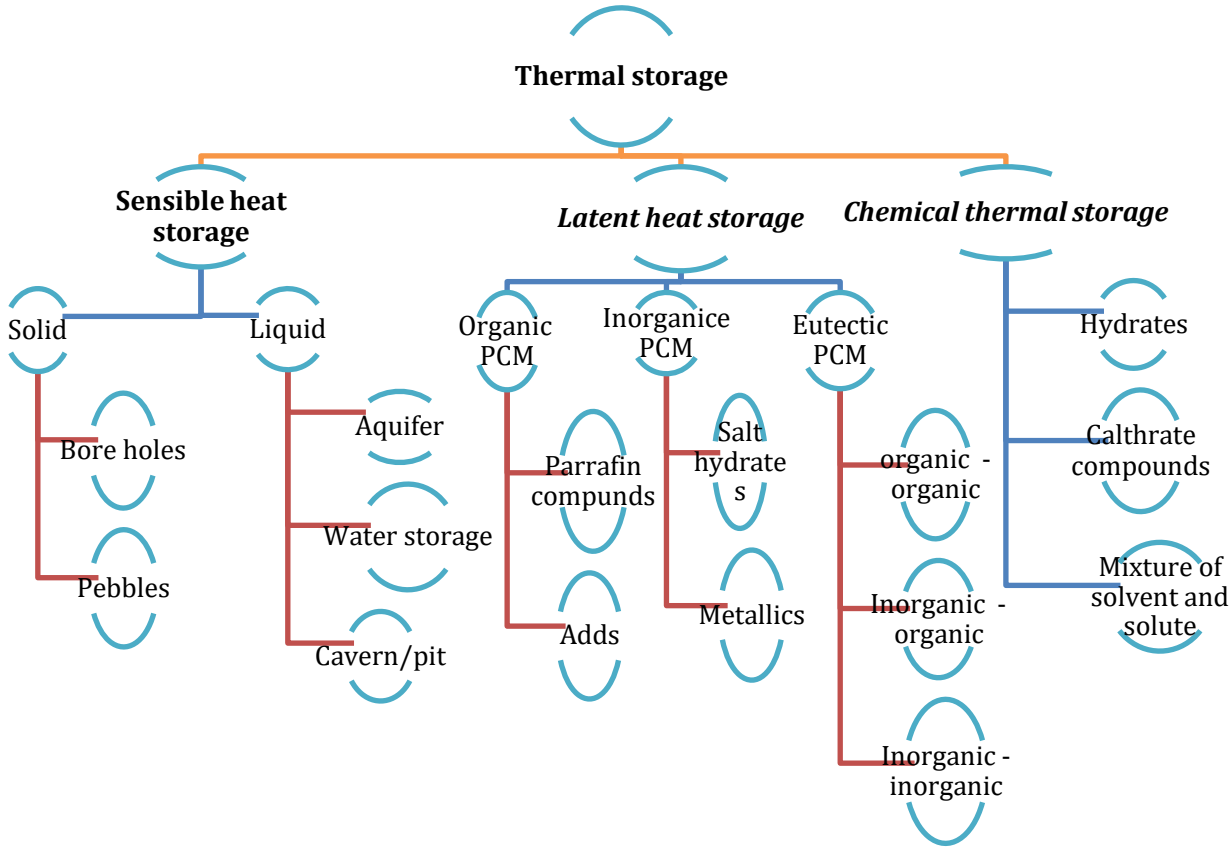

Figure 3-1: Flow chart of classification of thermal storage

3.3.1. Sensible Heat Solar Thermal Storage

The thermal storage occurs when adding heat, the temperature of material becomes elevates and it would be classified as a sensible type. Likewise, it would be sensible heat when the temperature of materials drops while heat is removed from the material.

Zanganeh et al. [16], Hänchen et al. [17], Zavattoni et al. [18] and Barton et al. [19] investigated performance analysis of sensible thermal storage system by numerical methods. Furthermore, experimental investigations of sensible thermal storage for solar cooking were done by Okello et al. [20], Hänchen et al. [17] and Allen et al. [21].

Hänchen et al. [17] carried out the heat transfer analysis of high-temperature thermal storage using a packed bed of rocks with the computational method which was validated experimentally for constant heat inflow. They used a transient one-dimensional two-phase

energy conservation equation for combined convection and conduction heat transfer, and the numerical solutions were obtained for charging and discharging cycles with a constant heat inflow. Okello et al. [20] and Barton et al. [19] developed a computational model for pebble bed thermal storage and verified them with the experimental results of Hänchen et al. [17].

Allen et al. [22] investigated convective heat transfer coefficients and pressure drops throughout the thermal storage and discussed two-phase energy equations through the packed bed of rocks.

The amount of energy stored in the material depends on the specific heat capacity of the medium, the change of the temperature of the material, and the amount of storage material [15].

$$Q_{st} = \int_{T1}^{T2} mC_p dT \tag{3.1}$$

Where Q_{st} is stored heat, m is mass of sensible material, C_p is the specific heat capacity of sensible material, and T_1 and T_2 are initial and final temperatures rise in the material. Some sensible materials properties are discussed in Table 3-1.

They have the disadvantages of being when sensible materials are larger. For this reason, the proper selection of the storage material considers specific heat capacity per unit volume (ρc_p). Another drawback of this sensible heat thermal storage systems is that they are not able to store or deliver energy at a constant temperature.

In the packed bed thermal storage media, the porosity of the bed or void fraction must be taken into consideration. Therefore, the energy-stored capacity in the packed media gives as

$$Q_{st} = \rho c_p (1 - \varepsilon) V \Delta T \tag{3.2}$$

Where, (ρc_p) is heat capacity per unit volume of the solid media, V is the volume of the storage, and ε is porosity or void fraction of the packed bed. Similarly, the heat stored in the heat transfer fluid phase is given as

$$Q_f = \rho_f c_{p,f} \varepsilon V \Delta T \tag{3.3}$$

Where ($\rho_f C_{p,f}$) is heat capacity per unit volume of fluid.

3.3.2. Latent Heat Solar Thermal Storage

Similar to sensible heat storage several researches have been done regarding latent heat thermal storage for different applications [23]–[36]. Latent heat thermal storage is based on the heat absorption or heat release when storage materials undergo phase change from solid to liquid or liquid to gas or vice versa [15].

Fortunato et. al [25] developed a simple mathematical model of thermal storage with PCM by characterizing the thermodynamics of a thermal storage system based on the latent heat of a paraffic phase change material (PCM) used for low-temperature requirements. He investigated heat transfer analysis between heat transfer fluid and PCM. The temperature distributions within the PCM and the time required to complete the melting process were found by simulation. However, the dynamic characteristics of heat transfer fluid were not considered during the simulation. Besides, the simulation was conducted for constant heat transfer inflow rather than actual solar radiation. Haopeng et. al [29] investigated PCM-based high-temperature thermal energy storage in packed bed, where molten salt was used as heat transfer fluid and 60% $NaNO_3$ & 40% KNO_3 mixture as PCM capsules. From their study, it was concluded that the heat transfer between capsules and molten salt can be significantly influenced by capsule diameter. They have shown, that the effective charging time is shortened by decreasing the capsule diameter. As aresult, the charging efficiency is increased.

Several researchers conducted modeling, simulation and experimental investigation of PCM thermal storage with oil as heat transfer fluid for different applications wth constant heat inflow case [23], [26], [29], [31], [34], [37]–[39]. In most cases , the temperature variation of the heat transfer fluid under actual solar radiation condition were not considered. Korti and Tlemsani [34] conducted an experimental investigation of latent heat storage of PCM storage unit when water as heat transfer fluid flows through a coil surrounded by PCM for low-temperature requirements less than 80 ^{0}C. As a result, it can not be applied cooking where frying requires temperature above 160 ^{0}C. Even the experimental work was not done under actual solar conditions, rather it was a laboratory experiment with resistant heating.

Raul et. al [23] conducted numerical modeling and experimental investigation of latent heat thermal energy storage with encapsulated A164 PCM with Hytherm 600 as heat transfer fluid for solar thermal applications. This PCM has a melting temperature of 168.70^{0}C and 249700 J/kg of the heat of fusion. By optimizing the diameter of PCM capsules and the inlet temperature of the heat transfer fluid, 75.69% thermal storage efficiency was obtained. In addition, they studied the variations in PCM temperature in the radial direction in the lab-scale and found the radial heat fow is negligible compared to the axial heat flow which justifies the use of one dimensional numerical model. Tarwidi [26] analyzed the modeling and numerical simulation of PCM packed in several hollow cylinders as thermal energy storage placed in cylindrical tank. In this work, different types of PCM materials were simulated and magnesium chloride hexahydrate was found to yield highest capacity for thermal storage. However, the results of the simulation showed that the maximum temperature of PCM is not more than 90 ^{0}C. Thus, it can not be used for cooking only for heating water.

Latent heat energy storage can store more heat due to large thermal energy storage density and phase changing of storage material that is called Phase Change Material (PCM). The storage capacity of the latent heat thermal storage system with a PCM medium [15] is given as:

$$Q_{st} = \int_{Ti}^{Tm} mC_P dT + ma_n \Delta h_m + \int_{Tm}^{Tf} mC_P dT \tag{3.4}$$

$$Q_{st} = m\left(C_{sp}(T_m - T_i) + a_m \Delta h_m + C_{lp}(T_f - T_m)\right) \tag{3.5}$$

Where Q_{st} is quality of heat stored m is the mass PCM

C_{sp} is the average specific heat b/n T_i and T_m for solid PCM

T_m is the melting temperature of PCM Δh_m is the heat of fusion per unit mass

a_m is the fraction melted T_f is the final temperature

C_{lp} is average heat capacity b/n T_m and T_f T_i is the initial temperature PCM

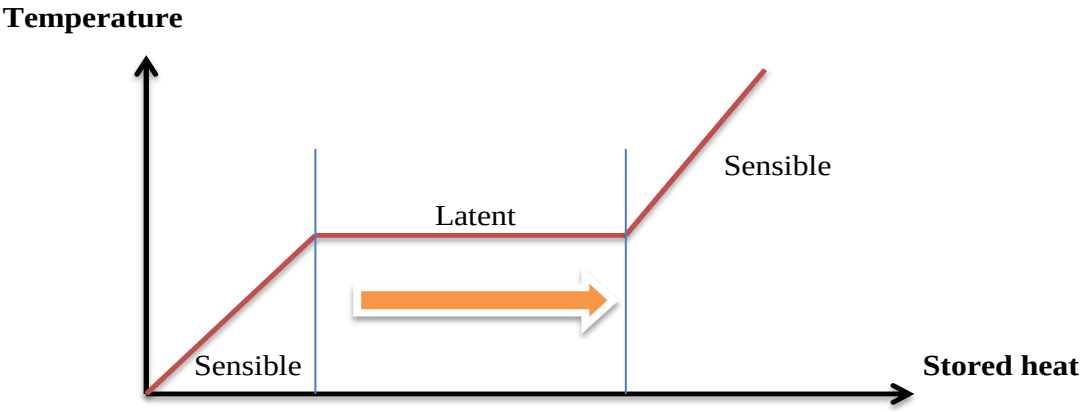

Figure 3-2: Comparison of sensible and latent heat temperature with heat storage

Latent heat thermal storage is more attractive than sensible heat storage because of its energy storage density with smaller temperature fluctuation. Because the phase transition occurs at a constant temperature taking some time to complete, it is possible to smooth temperature variations in LHTES systems [15].

However, many practical problems are stumbled upon with latent heat thermal storage due to low thermal conductivity, a variation in thermo-physical properties under extended cycles, phase separation, sub-cooling, incongruent melting, volume change, and high cost. For practical applications, PCMs usually undergo from solid to liquid phase transformations. However, liquid to vapor Phase changes is not practically applicable due to the large volumes and high-pressures requirements to store the material in the vapor phase. Classifications of PCMs are illustrated in Figure 3-1 and their thermo-physical properties are in Table 3-4.

3.3.3. Thermo – Chemical Heat Storage

Thermochemical systems rely on the energy absorbed and released in breaking and reforming molecular bonds in a completely reversible chemical reaction. In this case, the heat stored depends on the amount of storage material, the endothermic heat of reaction, and the extent of conversion [15]. The amount of heat storage can be given as:

$$Q_{st} = a_r m \Delta h_r \tag{3.6}$$

Where, a_r is the extent of the conversion reaction, m is mass of storage material and Δh_r is change of endothermic heat of reaction

3.4. Sensible thermal Storage Materials and Heat Transfer Fluids

Solid materials like concrete, rock, brick, sand, soil, silicon carbide, graphite, cast iron, and even waste metal chips, have been considered or applied for thermal energy storage purposes [40]. The main properties of some of these materials are discussed in Table 3-1.

Table 3-1: Main properties of sensible materials [40]

Medium	Melting (^{0}c)	ρ (kg/m^3)	C(kJ/kg.^{0}C)	ρ.C(kJ/m^3.^{0}C)	k(W/m.^{0}C)
Aluminum	660	2700	0.92	2484.0	250
Fireclay	1800	2100-2600	1.0	2100-2600	1-1.5
Soil (dry)	1650	1200-1600	1.26	1512-2016	1.5
Sandstone	1300	2000-2600	0.92	1840-2392	2.4
Brick (common)	1800	1920	1.0	1920.0	1.04
Granite	1215	2400	0.79	1896	1.7-4.0
Rocks	1800	2480	0.84	2086.6	2-7
Concrete	1000	2240-2400	0.75	1680-1800	1.7
Graphite	3500	2300-2700	0.71	1633-1917	85
Silicon carbide	2730	3210	0.75	2407.5	3.6
Taconite	1538	3200	0.8	2560	1.0-2.0
Cast iron	1150	7200	0.54	3888	42-55

Rock properties vary substantially from one rock to another rock type, and the thermal conductivities are generally between 0.5 W/mK and 5 W/mK depending on the moisture content in the rock and rock types [40].

Table 3-2: Sample pebbles density and thermal conductivity at 27 ºC (Özkahraman et al. 2004) [40][22]

Pebbles	Density,ρ_s (kg/m^3)	Thermal conductivity, k_s(W/m^{0}C)
Concrete (stone mix)	2300	1.4
Cement mortar	1860	0.72
Granite (Barre)	2630	2.79
Limestone (Salem)	2320	2.15
Marble (Halston)	2680	2.80
Quartzite (Sioux)	2640	5.38
Sandstone (Berea)	2150	2.90

Note that if large diameter rocks with low thermal conductivity are used for storage, the inner volume of the rock may not heat up or cool down completely during the charging and discharging process. This means the rock mass and bed volume is not efficiently used to store heat.

Hänchen et.al [17] states that there are three advantages when air used as heat transfer fluid in a packed bed of rocks heat storage. These are:

- Operating temperature constraints due to chemical instability of the heat transfer fluid in the rocks are eliminated.
- Operating pressure can be near to ambient with avoiding the need for complex sealing.
- The thermal storage can be integrated directly after the receiver, eliminating the need for a heat exchanger.

It is an advantage to use air since it is free and non-degradable. However, at high temperatures, air density is low, so the volumetric flow of air is very high and may require pumping power that is significant compared to the power generated utilizing the heat extracted from the bed. Hughes (1975) designates that, since the airflow requires large cross-sectional area ducts, thermal losses from the duct can be significant even with insulation [40].

Table 3-3: Thermo-physical properties of air at 1atm and T_{av}= 30^0C [41].

Heat transfer fluid	ρ [kg/m^3]	C_p [J/kg.K]	k [W/m.K]	μ [kg/m.s]
Air	1.08	1008	0.028	2.20×10^{-5}

However, the thermo-physical properties of air depend on the temperature is explained in appendix table A.

3.5. Latent Thermal Storage Materials

Sharma, et.al [15] reviewed various types of PCM materials. The PCM to be used in the design of thermal-storage systems should consider desirable thermo-physical, kinetics, and chemical properties which are as follows.

The thermal properties of PCM materials should be:

(i) Suitable phase-transition temperature. (ii) High latent heat of transition. (iii) Good heat transfer.

The physical properties of PCM materials should

(i) Favorable phase equilibrium. (ii) High density. (iii) Small volume change. (iv) Low vapor pressure.

Kinetic properties of PCM materials should

(i) No supercooling. (ii) Sufficient crystallization rate.

Chemical properties of PCM materials should

(i) Long-term chemical stability. (ii) Compatibility with materials of construction. (iii) No toxicity. (iv) No fire hazard.

Also, M. D. Muhammad [42] carried out a review of PCMs and heat transfer enhancement methods applied in parabolic trough solar plants thermal storage systems. The study conducted the potential PCMs to come up with commercially available ones that have suitable properties. These suitable properties are like: physical requirements such as high latent heat of fusion, high thermal conductivity, reversible phase change, negligible subcooling, and supercooling, and high density. Technical requirements like small density change, low vapor pressure chemical stability, and compatibility with other materials of the system. Economic requirements like low specific cost and availability and non-toxic and recyclable.

Table 3-4: The properties of phase change materials used in the TES of solar cookers [7].

Material	Class	T_m [^{0}C]	Δh_{fus} [J/g]	C_P [J/g.K]	ρ [kg/m^3]	k [W/mK]
Magnesium nitrate hex hydrate	In – organic	89.0	134	0.55	1643	0.55
Stearic acid	Organic	55.1	160	2.83	965	0.18
Commercial grade acetamide	Organic	82	263	1.94	1159	0.43
Commercial grade erythritol	Organic	118	339	1.38	1480	0.73
Commercial grade acetanilide	Organic	119	222	2.00	1210	0.14
Nitrate salts (KNO_3 – $NaNO_3$)	Inorganic	220	146	4.10	2200	0.8
PCM – A164	Organic	164	290	2.42	1500	-

3.6. Solar Cooking Systems

A solar cooker is a device that uses energy extracted from the Sun to cook. Solar cookers have been present for more than a century with one of the first ones being reported in India by Adams in 1878 [7]. Different researchers reviewed these solar cookers and concluded based on stages to cooking load. For instance, Lameck Nkhonjera, et.al [7] concluded the review into three categories as 2-stage, 3-stage, and 4-stage solar cookers as in Table 3-5.

Table 3-5: Block diagrams of the setups of solar cookers with the TES unit [7].

Cooker category	Block diagram of system set up
2 – stage categories	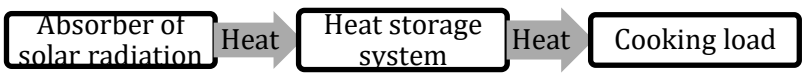

3 – stage categories

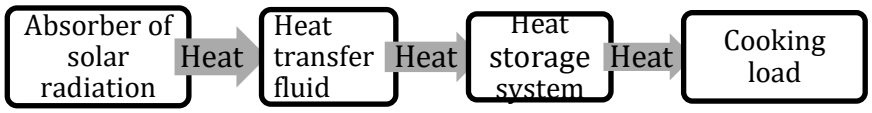

4 – stage categories

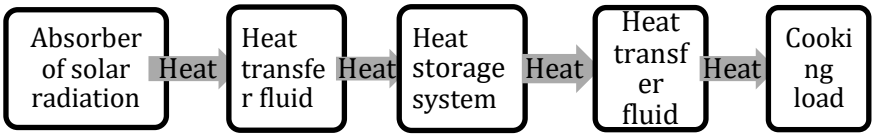

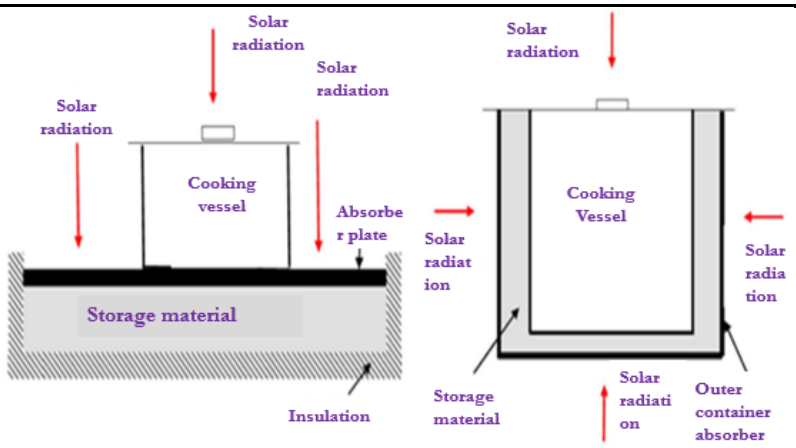

(a)

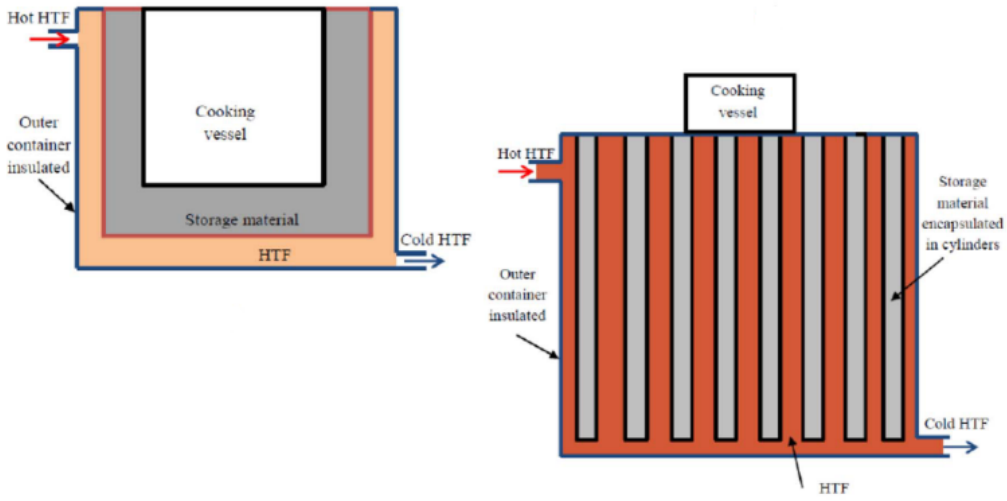

(b)

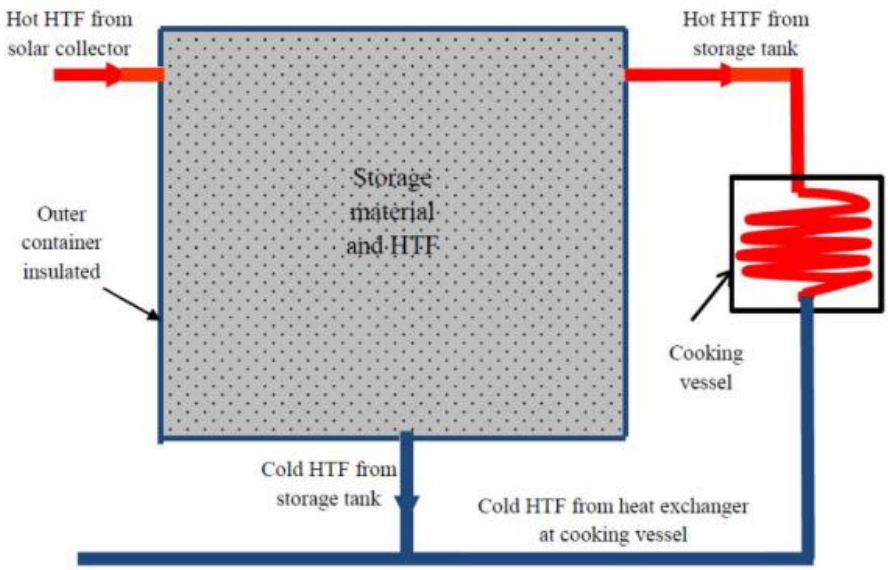

(c)

Figure 3-3: (a) Schematics of a thermal energy storage unit in 2-stage cookers, (b) Schematics of general designs of a thermal energy storage unit in 3-stage cookers, (c) General design of the thermal energy storage unit and cooking vessel in the 4-stage cookers [7].

Besides, Muthusivagami, R M, et.al [4] and Mawire, Ashmore [43] described three types of solar cookers that are classified based on their design: direct focusing solar cookers, oven cookers, and indirect solar cookers.

3.6.1. Solar Cookers Without Thermal Storage

Direct focusing solar cookers: They use reflectors to focus and concentrate the Sunlight directly onto a usually smaller and darker cooking pot. The pot is either suspended or set on at a stand of the focal area. The type of reflectors used for these cookers includes parabolic dish reflectors, spherical reflectors, plane mirror reflectors, and parabolic trough reflectors. The principle of operation of this type of solar cookers involves the concentration of reflected solar irradiance from a larger aperture onto a smaller absorbing material usually referred to as the absorber or receiver. The receiver absorbs energy and can cook food contained in it. They are relatively cheap to construct and can attain the highest cooking temperatures in the shortest space of time for faster cooking.

A lot of researches have been done on these types of solar cookers. For instance; Mussard and Nydal [44] tested their experimental work by using this device. The parabola was held by a structure that allows rotation to follow the sun. A holder was placed so that the vessel was exactly at the focal point and the experimental work was tested as it is illustrated in Figure 3-4 (g).

The ratio of the larger reflecting aperture area to the smaller absorber area is the geometric concentration ratio given as [12]

$$CR = C_{geo} = \frac{A_{ap}}{A_{abs}} \tag{3.7}$$

where Aap is the aperture area and A_{abs} is the absorber area.

The absorbed power from the solar radiation onto the absorber from the reflector aperture is given as:

$$P_{abs} = \eta_{op} I_b A_{ap} \tag{3.8}$$

where P_{abs} is the incident power, η_{op} is the optical efficiency, I_b is the beam solar radiation power flux measured in W/m^2, and A_{ap} is the aperture area.

If the amount of water m_w is placed in a pot at the focal region of the solar cooker, the energy transferred to the water for a time interval Δt or (the output energy) is given as:

$$Q_w = m_w c_w (T_{wf} - T_{wi}) \tag{3.9}$$

where c_w is the specific heat capacity of water, and T_{wf} and T_{wi} are the final and initial water temperatures in the time interval.

The over all useful efficiency u is calculated as the ratio of the output energy to the incident absorbed beam solar radiation, and is expressed as:

$$\eta_{use} = \frac{m_w c_w (T_{wf} - T_{wi})}{\eta_{op} I_b A_{ap} \Delta t} \tag{3.10}$$

Direct-focusing cookers are reasonably priced and cheap to construct and reach high temperatures in a short interval of time. These cookers have several disadvantages, some of which may be improved by the use of a TES system. Some of the other disadvantages are:

- The reflective surface material degrades;
- The cooking pot is exposed to many hazards because of unprotected;
- They are less adaptable;
- Some designs with long focal points may injure the eyes of the users and
- They perform poorly during cloudy or hazy periods since they utilize direct solar radiation.

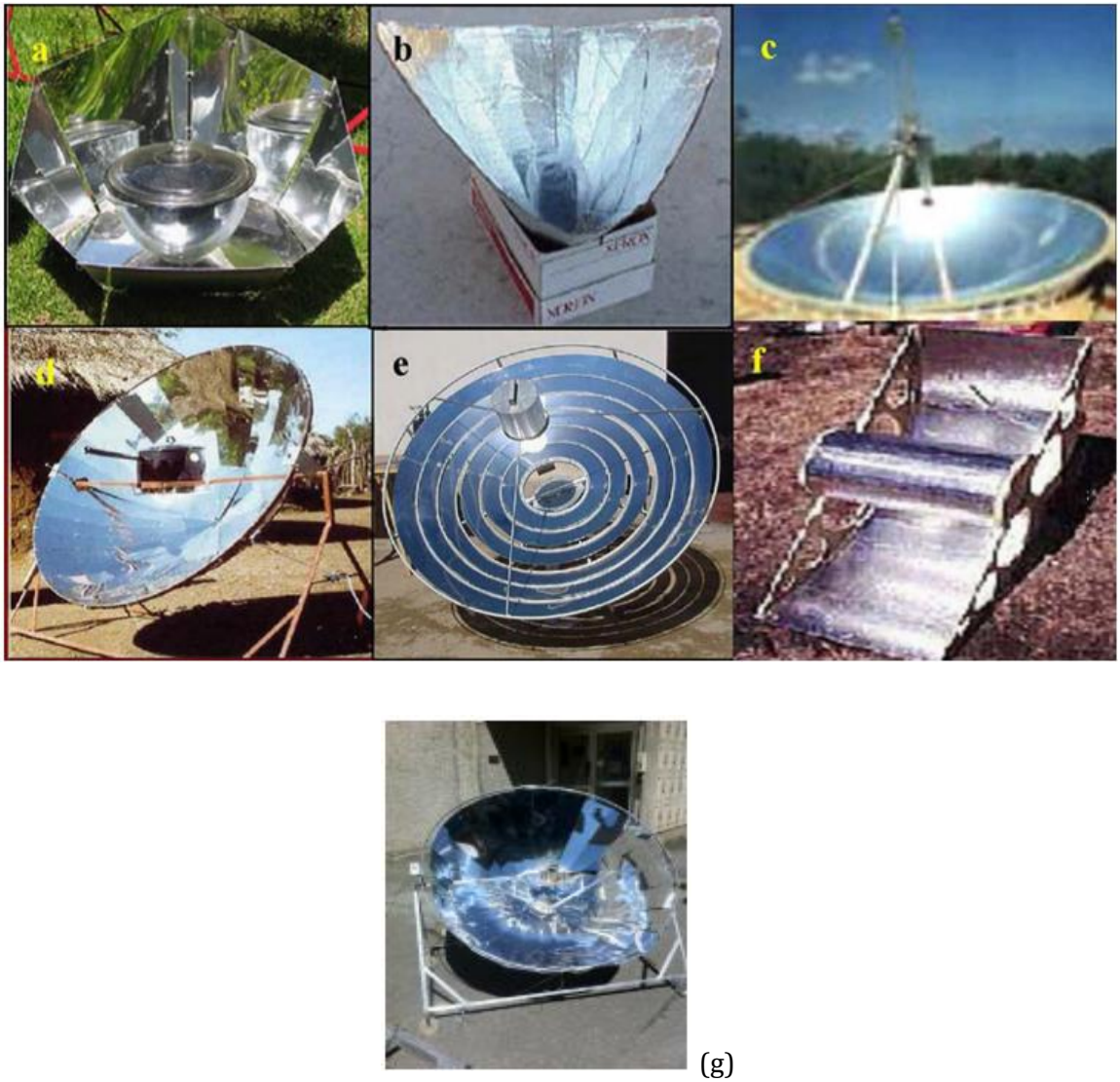

(g)

Figure 3-4*:* Direct-focusing types of solar cookers: (a) panel cooker, (b) funnel cooker, (c) spherical reflector, (d) parabolic reflector, (e) Fresnel concentrator, and (f) cylindro – parabolic concentrator [43]. (g) SK14 solar cooker [9]

Oven Solar Cookers: They are insulated boxes with the bodies that are glazed covers that cook food using the solar radiation effect. The solar radiation that enters the oven cooker through a glazed window (plastic or glass) heats the darker inside walls and the cooking is processed. Because heat does not out through the glazed window, the oven becomes hot. A principal advantage of oven solar cookers over direct- focusing cookers is that they can use both the direct and the diffuse components of solar radiation. An advantage of these cookers is that no solar tracking is required to focus the solar radiation. The operating temperatures of about 200 °C can be realized with these solar cookers when booster mirrors are exploited. These temperatures are adequate for cooking most types of food, except for prolonged frying.

For very simple solar box cookers with no reflectors, the energy entering the glazed collecting window Q_c which is given as [43]

$$Q_c = A_{ag}\tau_g I_p \tag{3.11}$$

Where A_{ag} is the area of the glazed collecting window, τ_g is the transmissivity of the glazing material, and I_p is the global solar radiation that is incident normal to the collecting window. In the actual case, the apparent area of the window will change concerning the angle of the sun's rays. This variation is given as

$$A_{agp} = A_{per} cos\,(\theta) cos\,(\varphi) \tag{3.12}$$

where A_{agp} is the apparent area, A_{per} is the perpendicular area, θ is the solar azimuth, and φ represents the difference between the solar elevation angle and the collecting window tilt angle. The useful energy efficiency η_{use} is defined as the ratio of the energy output to the energy input can be expressed as

$$\eta_{use} = \frac{M_w C_{pw} \Delta T_w}{I_{av} A_{ap} \Delta t} \tag{3.13}$$

where M_w and C_{pw} are the mass and the specific heat capacity of the cooking fluid inside a pot, respectively. ΔT_w is the change in the cooking fluid temperature, Δt is Δt is the time required to achieve the maximum temperature of the cooking fluid, and I_{av} is the average solar incident at the time difference with a reference value is 900 W/m^2. Different solar cookers are presented in [4] as shown in Figure 3-5, according to the number of reflectors.

Even though oven solar cookers have more advantageous than direct – focusing cookers, the main drawbacks are:

- They have low efficiencies compared to others,
- They require more time to complete cooking,
- They have restricted capacity depending on the size of the cooker,
- They have limited varieties, and they cannot be used for indoor applications.

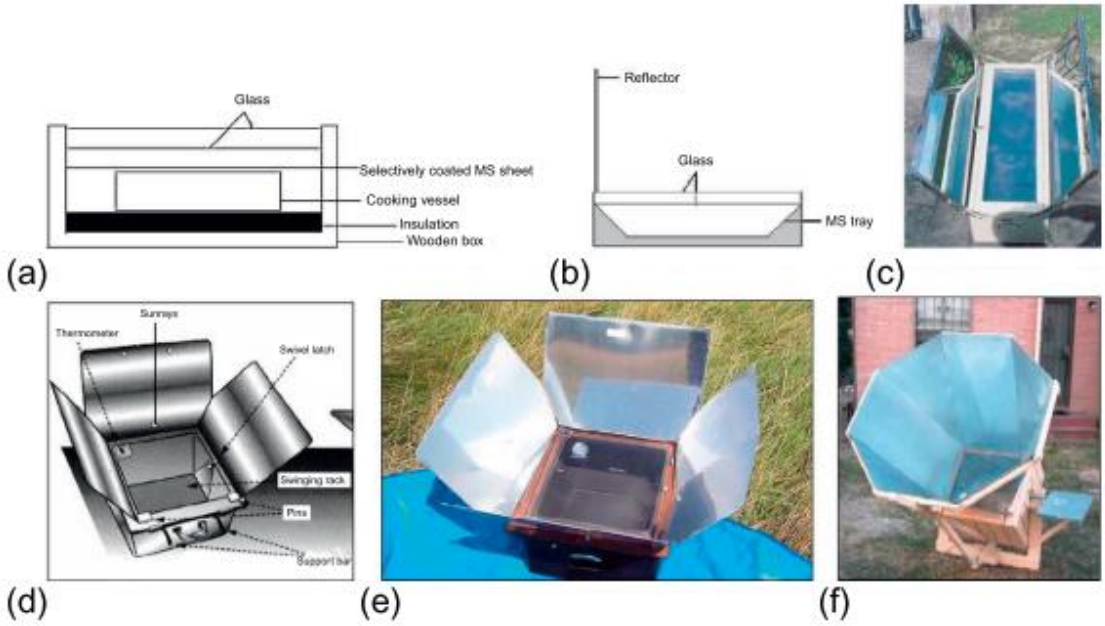

Figure 3-5: Oven types of solar cookers: (a) without reflector, (b) with a single reflector, (c) with double reflectors, (d) with three reflectors, (e) with four reflectors, and (f) with eight reflectors [4].

Indirect Solar Cookers: These types of solar cookers are constructed such that the solar energy collectors are separated from the cooking vessels. A heat transfer medium is required to transfer the collected energy into the cooking vessel. The cooking vessel can be placed at the distance from the solar energy collector allowing for an indirect cooking mode [45]. Asfafawu et al.[46] designed and developed solar thermal Injera baking with steam-based direct baking. They introduced a technology that enables Injera baking using the indirect solar stove. Heat transfer was made by the principle of natural circulation (boiling-condensation) between receiver and stove as pictured in Figure 3-6.

Solar energy collectors with forced convection can be placed on the roof, while the cooking vessel can be placed indoors. Indirect solar cookers have the advantage like indoor cooking,

ease of use, stability, controlled cooking, and easy integration into a thermal energy storage unit.

In indirect solar cookers, a heat transfer fluid circulates heat extracted from the solar energy collector. The rate of energy absorption by the circulating fluid is given by

$$\dot{Q}_f = \dot{m}_f C_{pf}\left(T_{fout} - T_{fin}\right) \tag{3.14}$$

Where $\dot{m}_f$ is the mass flow rate, c_{pf} is the specific heat capacity, T_{fout} is the outlet fluid temperature, and T_{fin} is the inlet fluid temperature. The instantaneous efficiency of the solar collector is defined as the ratio of heat transfer to the incoming solar power, and is expressed as:

$$\eta_{ins} = \frac{\dot{m}_f C_{pf}\left(T_{fout} - T_{fin}\right)}{IA_C} \tag{3.15}$$

Where A_C is the solar collector area and I is the solar radiation

The thermal sensible efficiency η_{th} is the ratio of the energy used to heat a certain mass of water in the cooking vessel from the ambient temperature to boiling temperature of water to the absorbed solar energy in a time interval dt. This is expressed as:

$$\eta_{th} = \frac{m_f C_{pf}\left(T_{wb} - T_{fin}\right)}{\int_0^t IA_C dt} \tag{3.16}$$

where m_w is the mass of the water in the cooking vessel, c_w is the specific heat capacity of the water, and T_{amb} is the ambient temperature. The thermal sensible power is the rate of energy used to heat the water in the cooking vessel, and it is given as:

$$\dot{Q}_w = \frac{m_f C_{pf}\left(T_{wb} - T_{fin}\right)}{\Delta t} \tag{3.17}$$

Where, $\dot{Q}_w$ is the thermal sensible power

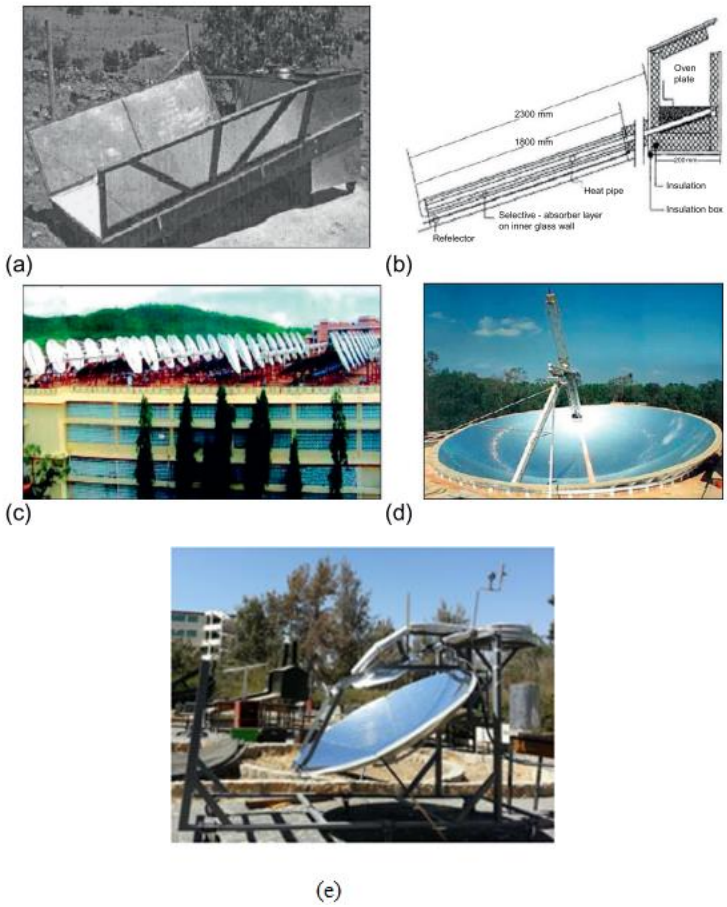

Figure 3-6*:* Indirect types of solar cookers: (a) with flat plate collector, (b) with evacuated tube collector, (c) with parabolic concentrators, and (d) with spherical reflectors [43], (e) actual ring during the test [46].

A major disadvantage of indirect solar cookers is that

- They are expensive to build and maintain since they consist of many parts.
- Some of the solar cookers, especially those using solar concentrators, require constant tracking mechanisms.

3.6.2. Solar Cookers with Thermal Storage

3.6.2.1. Solar cookers with sensible heat storage

This section has revised different types of solar cookers which have been designed and experimentally evaluated at different temperature regions. Of these, the following types of

solar cookers have been presented for the sensible heat storage solar cooking. Mawire et.al [43] reviewed different types of solar cookers with sensible and latent heat storage.

Direct focusing solar cookers with sensible heat storage:

They are few reports on this type of solar cooker. The heat storage has direct contact with the thermal cooking part at a focal point of solar irradiance. In Mawire et al. [43] reviewed article, Chandra et al. (2013) designed an umbrella type parabolic dish that uses oil thermal energy storage material to heat the oil that was in thermal contact with the cooking surface. The water in the pipes gets heated by exchanging heat with the hot oil inside the storage container. Then, the water becomes vaporized and comes out through pores that are used to cook rice.

Oven solar cookers using sensible heat storage:

In this type of solar cooker; sensible heat storage materials are incorporated with an oven solar cooker to store heat for the night or cloudy times when the cooking is required. Oven solar cookers with sensible heat thermal storage have the disadvantages of achieving low temperatures due to low efficiencies, slow cooking speeds, and limited capacity depending on the size of the cooker.

Indirect solar cookers with sensible heat storage:

Many researchers are studying the design and development of indirect type solar cookers with sensible heat storage. Substantial research has been done on these solar cookers. Using an evacuated tube, flat plate, and concentric solar cookers have been designed and experimentally tested by many researchers.

Abdulkadir Aman Hassen and Demiss Alemu Amibe [47] investigated a finite model and experimental tests of Solar powered Injera baking by using Addis Ababa solar irradiances. A system diagram of solar power Injera baking oven was developed as it is shown in Figure 3-7 and the system consists of a parabolic trough, pumps, heat storage tank, and the injera baking pan ('Mitad'). The parabolic trough is used to collect solar energy and increase the temperature of the fluid. A simulation model, showed that the heat up time could be reduced by reducing the thickness of the baking pan for the given oil temperature. They concluded that an oil based solar system worked well together with a novel ceramic mitad in the kitchen.

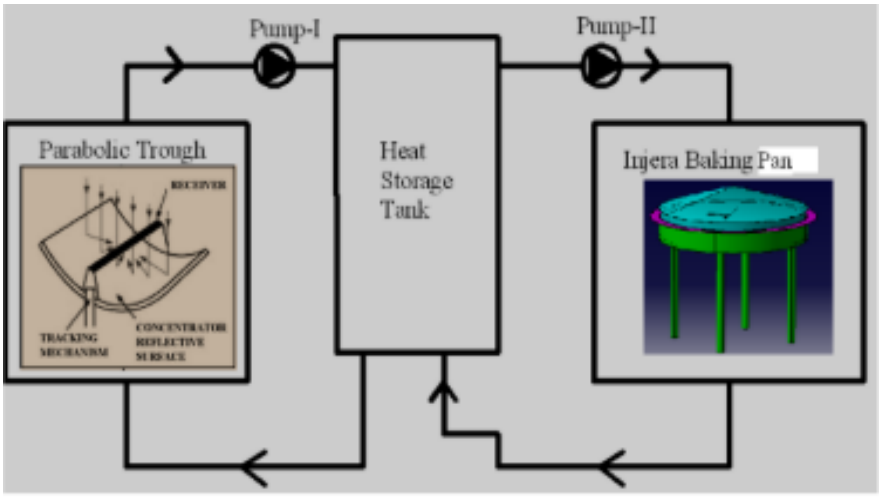

Figure 3-7: Block diagram of solar-powered Injera baking oven [47]

Okello et al.[48] experimentally investigated charging and discharging of rock bed heat storage system for cooking applications. The cooking pot is set on the top of the packed bed pebbles as shown in Figure 3-8. Charging tests were made with a hot air blower. By reversing the air flow the discharging rate to the cooker could be controlled.

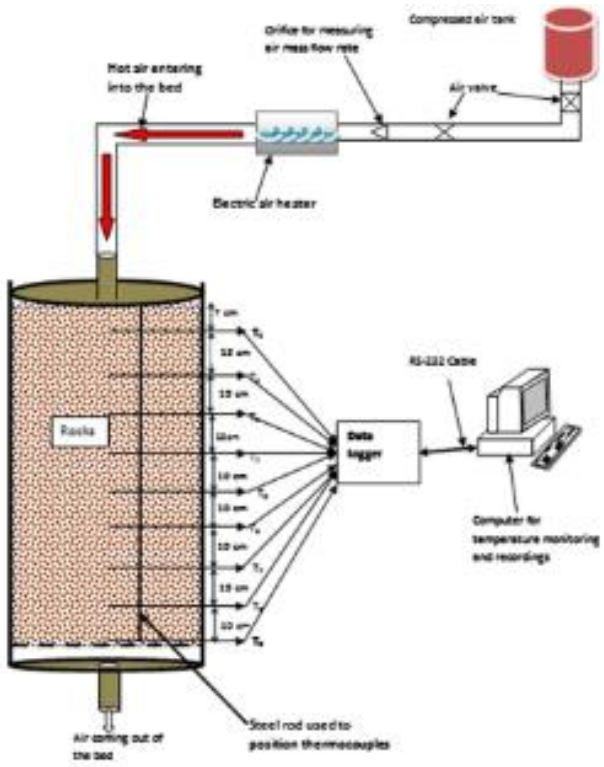

Figure 3-8: Block diagram showing the experimental setup, the layout of thermocouples and data acquisition systems of rock bed with air as heat transfer fluid [49].

3.6.2.2. Solar Cookers using Phase Change Materials

These types of solar cookers use phase change materials (PCM) for different temperature ranges. A heat transfer fluid is used for carrying heat from the collector to the storage and the cooking pot gets heat from the storage.

Sharma et al. [50] analyzed the thermal performance of solar cookers based on an evacuated tube solar collector using PCMs. They developed a model that consists of a componentssuch as evacuated tube solar collector, a closed-loop pumping line containing water as the heat transfer fluid (HTF), a PCM storage unit, cooking unit, pump, relief valve, flow meter, and a stainless steel tube heat exchanger. Some tests [51] [2], [46], [52] ,[53] have been carried out on these types of solar cookers by using oil and staem as heat transfer fluid and PCM storage units.

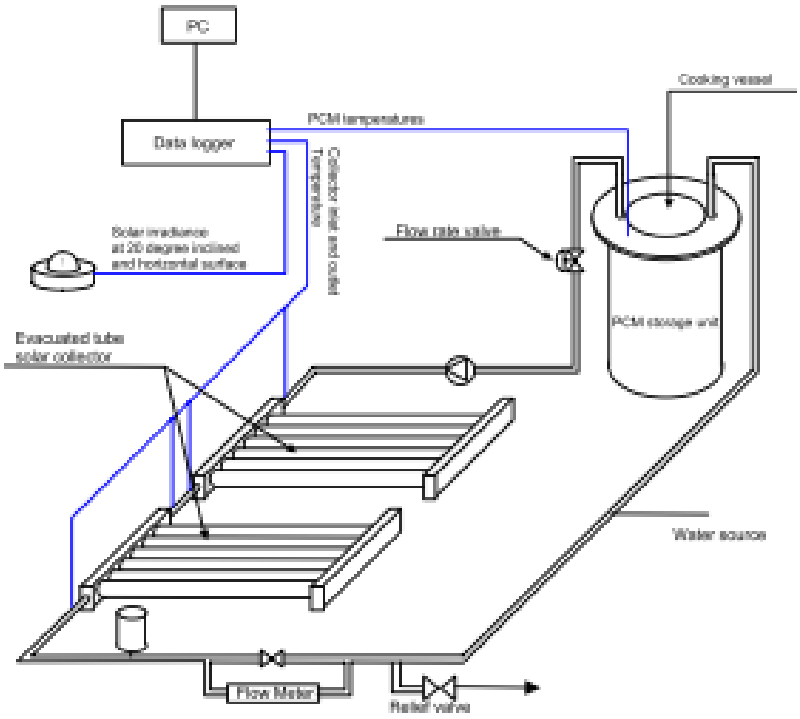

(b)

Figure 3-9: Outline of the prototype solar cooker based on evacuated tube solar collector with PCM storage unit [50].

3.7. Thermal Storage Design Considerations

The following basic requirements for thermal storage, which should be considered when storage media are chosen and thermal storage is designed:

- Good utilization of the storage at affordable cost, from available materials;
- High thermal conductivity and heat transfer capabilities;
- High energy storage density;
- High resistance to thermal cycling damage;
- Clearly and carefully thought out design;
- Simple and quick to build;
- Environmentally friendly/compatible;
- Safety

This topic provides details on material properties and various design considerations and requirements found in the literature. Two important considerations are involved in the design and operation of packed bed storage. Firstly, the rate of heat transfer that will take place between the airflow and solid particle is characterized by the volumetric heat transfer coefficient. Secondly, the sizing of the bed involving determining the four critical parameters like; the airflow rate per unit of collector surface area, the equivalent particle diameter, the bed length, and the bed frontal area. The design and sizing of the storage unit require: collector, storage unit, heating load, and the auxiliary unit should be taken in to consideration [54]. Al Azawiet.al [55] had concluded the following on the effects of the design parameter on stored energy.

- Materials that have high thermal capacity cause an increase of the charging period and increase of storage capacity of the unit.
- Increasing of mass velocity of fluid accelerates the charging process for the storage unit and give maximum pressure drop and also cause fast arrival to steady-state.
- The increase of particle size caused a reduction of the quantity of stored heat and reduction of pressure drop.
- The choice of the ratio between the diameter and height of the packed bed is important because the increase of this ratio diameter to length causes an increase

of the cross-sectional area and increases the mass flow rate. This causes the increase of the stored energy, also that increase of the ratio diameter to length cause a reduction of the pressure drop.

3.8. Solar Radiation Analysis

Solar radiation incident outside the earth's atmosphere is called extraterrestrial radiation or total solar irradiance (TSI), and is in fact, the amount of global radiation that a location on earth would receive in the absence of the atmosphere. As extraterrestrial radiation passes through the atmosphere, some of it is scattered back into space, another part is absorbed by air, aerosols and water vapor. The part of solar radiation that reaches the surface of the earth with essentially no change in direction is called direct or beam radiation. Solar radiation scattered in the atmosphere is referred to as diffuse radiation. The sum of the beam and diffuse radiation on a surface is called total or global solar radiation. On a clear day, direct solar irradiance constitutes about 80 to 90 % of the total amount of solar energy reaching the earth's surface. Localized blockage of the direct component of solar irradiance produces shadows. In overcast weather or on a foggy day, 'when we can't see the sun', the direct component of solar irradiance is essentially zero and there are no shadows. Beam radiation is of great interest to designers of high-temperature solar energy systems because it can be concentrated, whereas the diffuse component cannot [56][57].

CHAPTER FOUR

4. Solar Data Analysis and System Sizing

4.1. Over All Concept Description

The schematic diagram used for the research work is given in Figure 4-1. A parabolic dish collects energy from the solar irradiation. A receiver absorbs the heat reflected from the collector and heats the air that flows through the porous media. The charging pipe takes the hot air from the receiver to the storage. Storage media like pebbles and capsules of eutectic salts are selected to store heat. The pattern of storage media is arranged randomly along with the storage. The parabolic dish consists of carrying the dish couple with a tracking structure, and the tracking structure rotates the parabolic dish in a two-way axis.

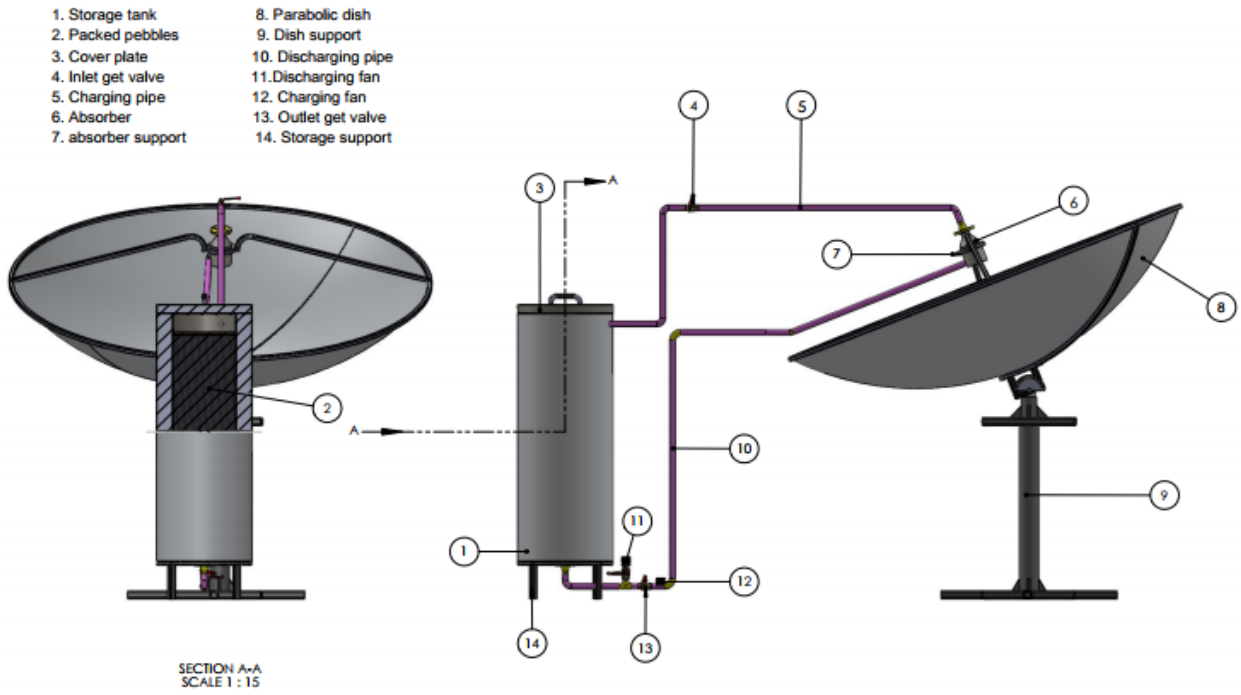

Figure 4-1: Schematic diagram of packed bed pebbles thermal storage integrated with parabolic solar collector and fan.

4.2. Solar Data Analysis

Solar data is collected from the Ethiopian metrological agency for Addis Ababa the capital city of Ethiopia which is located at 9.023 ^{0} latitudes and 38.747^{0}longitude, and Semera is a new town established on the Awash–Asseb highway in north-east Ethiopia, planned to replace Asaita as the capital of the Afar Region. Semera is located at latitudinal 11^{0}47'32'' N ^{0} and longitudinal 41^{0}0'31'' E. Duffie et al. [56] proposed a solar radiation representative days for each month as shown in Table 4-1.

Table 4-1: Recommended average days for months and values of n by months

Month	n for ith day of the month	For Average Day of Month		
		Date	n	δ
January	i	17	17	-20.9
February	31+i	16	47	-13.0
March	59+i	16	75	-2.4
April	90+i	15	105	9.4
May	120+i	15	135	18.8
June	151+i	11	162	23.1
July	181+i	17	198	21.2
August	212+i	16	228	13.5
September	243+i	15	258	2.2
October	273+i	15	288	-9.6
November	304+i	14	318	-18.9
December	334+i	10	344	-23.0

Note: From Klein (1977). Do not use for $|\phi|>66.5^0$

In Figure 4-2 and Figure 4-3, the average hourly total solar radiation of Addis Ababa and Semera for 5 years data's can be analyzed, and the values are presented in Appendix table B.

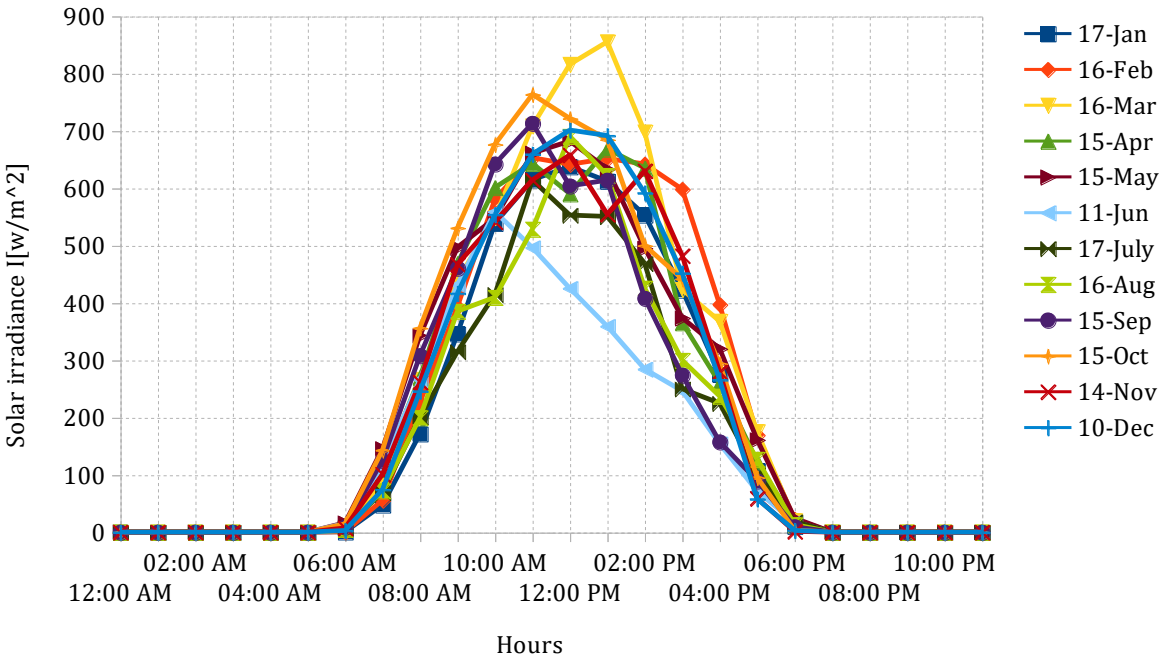

Figure 4-2: Hourly total solar radiation of Addis Ababa for recommended days in months

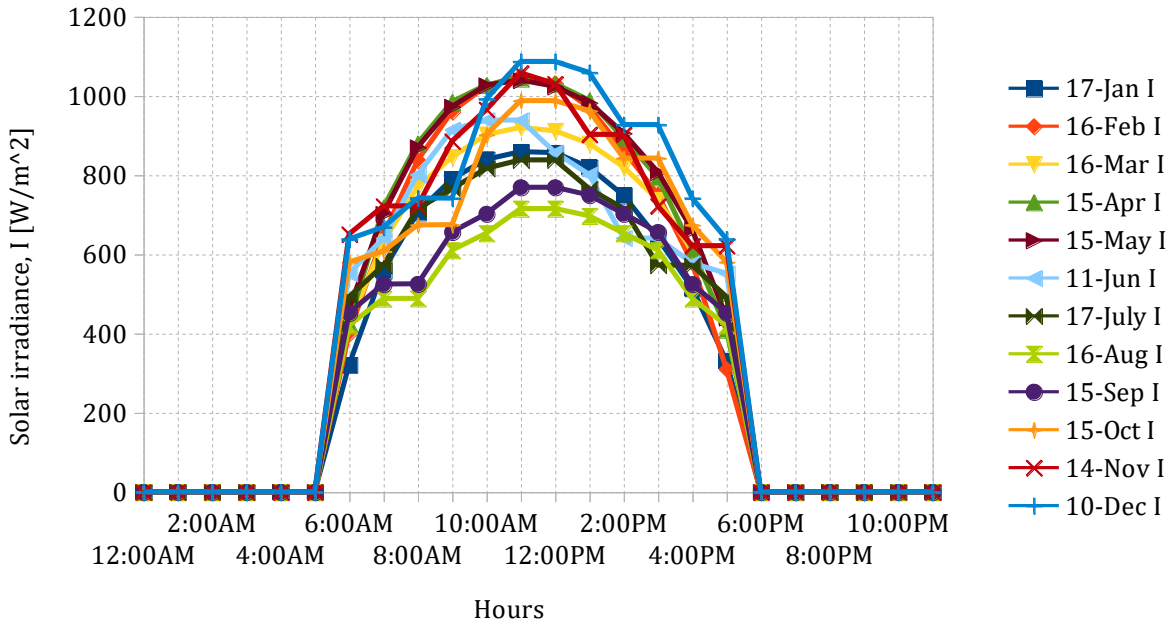

Figure 4-3: Hourly total solar radiation of Semera for represented days in months

4.3. Estimation of Beam and Diffuse Hourly Solar Radiation

To convert the total solar radiation into the beam and diffuse, first daily solar clearness index, K_T is calculated as it is given below

$$K_T = \frac{H}{H_0} \tag{4.1}$$

An hourly clearness index k_T can also be defined

$$k_T = \frac{I}{I_0} \tag{4.2}$$

$$H_0 = \frac{24 \times 3600 \times G_{sc}}{\pi}\left[1 + 0.033\cos\left(\frac{360n}{365}\right)\right] \times \left(\cos(\phi)\cos(\delta)\sin(\omega_s) + \frac{\pi\omega_s}{180}\sin(\phi)\sin(\delta)\right) \tag{4.3}$$

Then, the values of the parameters in the equation can be given as:

G_{sc} is solar constant $= 1367\text{W/m}^2$

$\phi_{Addis\ Ababa} = 9.023^0$

ω_s is sunset hour angle, $\cos(\omega_s) = -\tan(\phi)\tan(\delta)$

δ is declination angle $= 23.45\sin\left(360\dfrac{284+n}{365}\right)$

n is number of days

H is the average daily solar radiation in $\dfrac{\text{J}}{\text{m}^2\text{day}}$

Average Hourly Solar Radiation before the atmosphere is given as:

$$I_0 = \frac{12 \times 3600 \times G_{sc}}{\pi}\left[1 + 0.033\cos\left(\frac{360n}{365}\right)\right] \times \left(\cos(\phi)\cos(\delta)sin(\omega_2 - \omega_1) + \frac{\pi(\omega_2 - \omega_1)}{180}sin\phi sin\delta\right) \tag{4.4}$$

The Erbs et al. [56]correlates for the fraction of diffuse hourly solar irradiance to total solar irradiance which can be given as:

$$\frac{I_d}{I} = \begin{cases} 1.0 - 0.09k_T & for\ k_T \le 0.22 \\ 0.9511 - 0.1604k_T + 4.388k_t^2 - 16.638k_t^3 + 12.336k_t^4 & for\ 0.22 < k_T < 0.8 \\ 0.165 & for\ k_T > 0.8 \end{cases} \tag{4.5}$$

Therefore, average beam solar radiation is calculated as

$$I_b = I - I_d \tag{4.6}$$

The total, beam and diffuse solar irradiance of Addis Ababa and Semera for the represented days in the months are given in appendix table B and C.

Figure 4-4 explains the total, beam, and diffuse solar irradiance of Addis Ababa for the days of 16 March and 11 June.

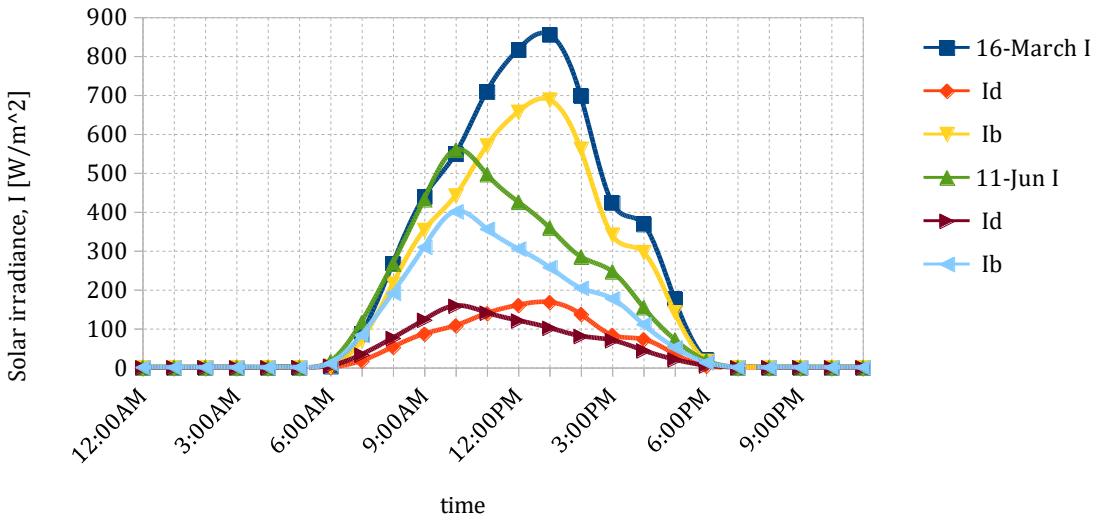

Figure 4-4: Total, beam and diffuse solar irradiance of Addis Ababa for the represented days of 16 March and 11 June

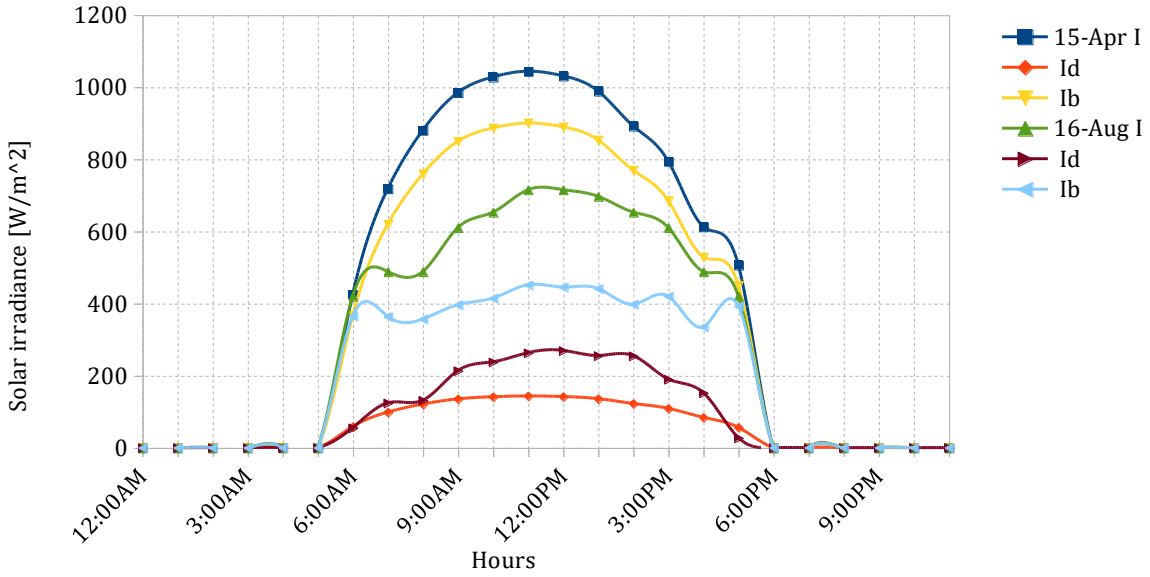

Figure 4-5: Total, beam and diffuse solar radiation of Semera for represented days of 15 Apr and 16 Aug.

4.4. Energy Demand Analysis for a Household

Commonly, most of the Ethiopian household use the following diets. These foodstuffs need energy from different sources. Here in the following Table 4-2 shows the specific heat capacity of foodstuffs above and below freezing points.

Table 4-2: The specific heat capacities of common food items [61]

No	Common foodstuffs for a household in Ethiopia	Specific heat capacity above freezing	Specific heat capacity below freezing
1	Beets	3.77	1.8
2	Butter	2.72	1.42
3	Clams, meat only	3.52	1.51
4	Mushrooms dried	1.26	0.96
5	Olives, green	3.35	1.67

In Ethiopia, there are at an average 6 persons per household according to the Ethiopian statistical agency. In day to day activities, the following cooking preparations have been

practiced in each household. These are water heating, preparation of 'Shiro wet', preparation of coffee and tea. Other data required to determine energy demand for one household during food preparation are specific heat capacity of water is 4185.5J/ (kg k), the density of water is 1000kg/m3, and initial temperature which is assumed as a constant of 23^0c (ambient temperature of Addis Ababa). Water is boiled at 93^0C in Addis Ababa. Therefore, the energy required for one household is calculated as;

$$Q_{demand} = mC_p\Delta T \quad (4.7)$$

Table 4-3: Energy demand for different cooking items for a house hold

Items	Quantity	The energy needed per unit quantity (MJ)	Total Energy Demand (MJ)
Water heating	5liter	0.113	0.565
Coffee preparation	2 liter	0.3696	0.7392
Tea preparation	1liter	0.3696	0.3696
Wet	2liter water +0.5kg bee powder	5	5
Others	-	-	2.5
Sum			= 9.1738

Note: There are convection, radiation, and conduction heat transfer between the cooking pot and the environment. Considering the efficiency of an improved cooking stove the total amount of energy required for the model is 24MJ.

4.5. Design of Parabolic Solar Collector

The parabolic dish collects energy from the solar irradiation. A receiver absorbs the heat reflected from the collector and heats the air that flows through the porous absorber. The charging pipe takes the hot air from the receiver to the storage. To design the size of the parabolic solar concentrator, the amount of energy demand and availability of solar radiation should be taken in to consideration.

a) Concentrating solar collector

The word collector will be applied for both the receiver and concentrator. The receiver is an element of the system where the radiation is absorbed and converted to heat. The concentrator, or optical system, is the part of the collector that directs radiation onto the receiver.

b) Collector configurations

Many concentrator types are used to direct a heat flux on the receiver. They can be 2 dimensional (trough) to focus on a ''line'' or 3 dimensional to focus on a ''point.'' Receivers can be concave, flat, or convex. In general, concentrators are effective only for beam radiation. It is evident also that the angle of incidence of the beam radiation on the concentrator is important and that sun-tracking will be required for these collectors. A variety of orienting mechanisms have been designed to move focusing collectors so that the incident beam radiation will be reflected on the receiver.

c) Concentration ratio

The concentration ratio is a ratio of aperture area of a collector to the area of a receiver. Also, a flux concentration ratio is the ratio of the average energy flux on the receiver to that on the aperture. There can be substantial variations in energy fluxes over the surface of a receiver. A local flux concentration ratio can be defined as the ratio of the flux at any element on the receiver to that on the aperture, which will vary across the receiver.

The area concentration ratio can be given as

$$CR = \frac{A_{ap}}{A_{abs}} \tag{4.8}$$

Where, A_{ap} is aperture area A_{abs} is absorber area

d) Optical performance of concentrating collectors

Consider Q_{opt} is the absorbed radiation per unit area of the unshaded aperture which can be written as

$$Q_{opt} = I_b \rho (\gamma\tau\alpha)_n K_{\gamma\tau\alpha} \tag{4.9}$$

The incident solar radiation on the collector is the beam solar irradiance, I_b. ρ is the specular reflectance of the concentrator, . If the concentrator is a refractor, it will be the

transmittance of the refractor, τ is the transmmitance and α is the absorbance. The next three factors, γ, τ, and α, are functions of the angle of incidence of radiation on the aperture. The intercept factor (γ) is defined as the fraction of the reflected radiation that is incident on the absorbing surface of the receiver. Values of γ greater than 0.9 are common.

4.5.1. Sizing Analysis

To calculate the parabola, mathematical analysis can be performed to find the values that satisfy the design criteria, like diameter, aperture angle and concentration ratio. Figure 4-6 shows geometry of the solar collector parabolic dish.

4.5.2. Geometric Sizing

Under this topic, the geometric analysis of the parabolic solar collector can be determined. All the required parameters are calculated as in the following equations. From the parabola geometry as shown in Figure 4-6, the rim angle is calculated as

$$\tan(\phi_r) = \frac{\frac{D_a}{2}}{f - H_d} \tag{4.10}$$

Where, from the parabolic equation the height of dish can be given as

$$H_d = \frac{\left({}^{D_a}/_{2}\right)^2}{4f} = \frac{D_a^2}{16f} \tag{4.11}$$

Substituting equation (4.10) in to equation (4.11) the rim angle is given as

$$\phi_r = \arctan\left(\frac{D_a/2}{f - H_d}\right) = \arctan\left(\frac{D_a/2}{f - \frac{D_a^2}{16f}}\right) \tag{4.12}$$

Where, D_a the diameter of the aperture

At the maximum angle that defines it is related by equation (4.13) derived from parabola geometry at half of the rim angle which is given as

$$\phi_{\mathrm{r}} = 2\arctan\left(\frac{D_a}{4f}\right) \tag{4.13}$$

The half acceptance angle θ can be determined as a function of concentration ratio is obtained as

$$CR = \frac{1}{\sin^2(\theta)} \tag{4.14}$$

Therefore, the acceptance angle θ can be given as

$$\theta = \sin^{-1}\sqrt{\frac{1}{CR}} \tag{4.15}$$

The optimum rim angle $\emptyset_r$ is given as

$$\phi_r = 90^0 - \theta \tag{4.16}$$

The focal length, f of parabolic dish is derivedfrom

$$sin\ (\phi_r) = \frac{D_a/2}{r_r} \tag{4.17}$$

Where, maximum distance between the focal point and the paraboloid extreme which is defined as

$$r_r = \frac{2f}{1+\cos(\phi_r)} \tag{4.18}$$

Substituting equation (4.18) in to equation (4.17), the ratio of focal length to the diameter of aperture is derived as

$$\frac{f}{D_a} = \frac{1+\cos(\phi_r)}{4\sin\phi_r} \tag{4.19}$$

The height of the dish H_d is given as

$$H_d = \frac{D_a^{\ 2}}{16f} \tag{4.20}$$

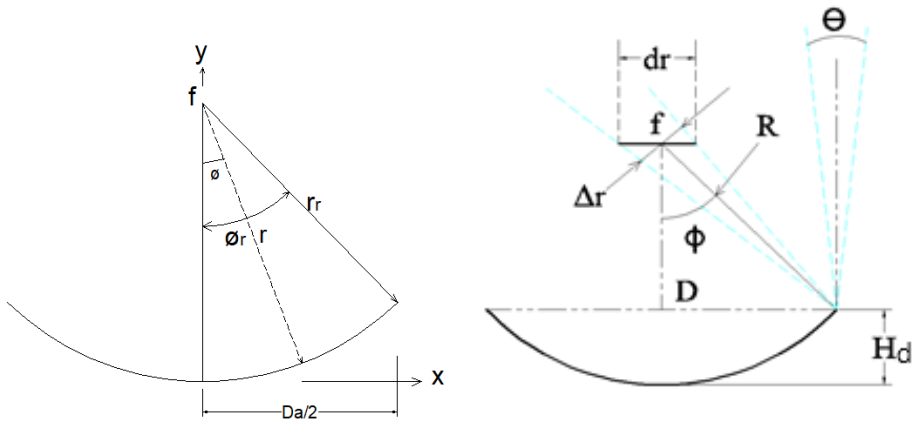

Figure 4-6: Geometry and dimension of the solar collector parabolic dish

4.5.3. Thermal and Optical Calculation

After performing the theoretical analysis for the design of the solar collector parabolic dish, the following presents its thermal and optical analysis. The optical efficiency of the collector is given by equation 4.21

$$\eta_{op} = \rho_c \tau_v \rho Q_{opt} \tag{4.21}$$

Table 4-4: Necessary values to calculate the optical efficiency

Parameter	Nomenclature	Value
Receptor absorptance	α_c	0.87
The transmittance of the glass coating the (if it exists). In this case, it does not exist, then it is equal to 1	τ	1
The reflectivity of the glass mirror	ρ	0. 95
Shape factor	S	0.916

The shape factor (S) is given by equation (4.22):

$$S = \frac{A_a - A_t}{A_a} \tag{4.22}$$

Where, A_t represents the fraction of the concentrator's aperture area, which is not shadowed by the receptor. Equation (4.23) gives the fraction of the aperture area not shadowed by the receptor.

$$A_t = A_a - A_{abs} \tag{4.23}$$

Assume that the shape factor is very small due to small size of the receiver, the total concentration area used in the thermal analysis equation is A_a

The direct radiation measured in the area is I_b. With this radiation, it is possible to estimate the rate of energy (power) absorbed by the receptor through the following equation.

$$\dot{Q}_{abs} = \eta_o A_a I_b \tag{4.24}$$

Where A_a is the aperture area, ρ_c is the receptor absorptance, τ_v is the transmittance, S is the shape factor, and I_b is the mean direct radiation. The useful energy in the receiver, depends on the receiver's power loses to the environment, which is given by:

$$\dot{Q}_{loss} = A_r U_{lr} (T_{rm} - T_{amb}) \tag{4.25}$$

Where U_L is the mean coefficient of heat losses, which is represented by:

$$U_{lr} = \left[\frac{1}{h_c + h_r} \right]^{-1} \tag{4.26}$$

The terms h_c and h_r correspond to the convection coefficient and radiation coefficient, respectively. The radiation coefficient is given by:

$$h_r = \sigma \varepsilon_r \frac{\left(T_r^4 - T_{amb}^4\right)}{T_r - T_{amb}} \tag{4.27}$$

Where, σ stefan boltzman constant and ε_r emmisivity of the receiver

To calculate the convection coefficient (h_c), we consider the thermal conductivity of air (k_a) the receiver outer diameter (D_{out}) and the Nusselt number (Nu), which must be calculated from the Reynolds number (R_e).

$$h_c = \frac{k_a}{D_{out}} \times Nu \tag{4.28}$$

The Reynolds number is represented by the following equation:

$$R_e = \frac{V_a D}{\nu_a} \tag{4.29}$$

Where, V_a is the approximate average wind velocity in Addis Ababa (3m/s) and v_a is the kinematic viscosity of air.

$$\nu_a = \frac{\mu_a}{\rho_a} \tag{4.30}$$

Where μ_a is the dynamic viscosity of air, ρ_a is the density of air

4.5.4. Sizing of Focal Point Receiver

The focal point receiver is used to absorb radiation reflected from the solar concentrator. The size of the receiver – absorber is calculated based on the concentration ratio. The maximum concentration ratio determined for this research is 400. The area of an absorber can be determined as:

$$A_{abs} = \frac{A_a}{CR} \tag{4.31}$$

The silicon carbide (SiC) absorber chips are contained in the shell of the receiver as shown in Figure 4-7. The air inflow to the absorber come from the storage outlet and passes throughout the porous of Si – C chips along the length of the receiver. The hot airflow from the receiver is used to charge the thermal storage. The side wall of the receiver is covered by an insulation fiber glass which is used to reduce the heat loss to the surrounding along the side channel. The bottom part of the reciver is porous and black painted.

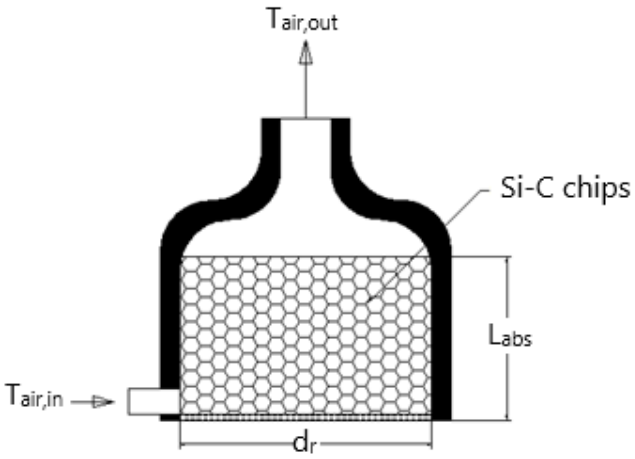

Figure 4-7: Schematic drawing of focal point receiver

Heat transfer SiC – air is calculated assuming the uniform flow and temperature in all channels.

By assuming the length of absorber L_{abs}= 0.15m, the diameter absorber can be given as

$$d_r = \sqrt{\frac{4A_{abs}}{\pi}} \tag{4.32}$$

Where, d_r is diameter of receiver/absorber

The time taken to heat air in the receiver is calculated as

$$\dot{m} = \frac{\rho_a V_{air}}{t} \tag{4.33}$$

Where V_{air} is the volume of the absorber is given as

$$V_{air} = \pi\varepsilon\left(\frac{L_{abs}}{4}(d_r)^2\right) \tag{4.34}$$

ε is the porosity in the receiver and is selected 0.4

The diameter of the pipe (d_{pipe}) through which a heat transfer fluid is flowing can be given as

$$d_{pipe} = \sqrt{\frac{4\dot{m}_a}{\pi\rho_a V_a}} \tag{4.35}$$

Where, V_a is velocity of air

Thermal Analysis on the Receiver

The rate of useful energy from the absorber is the power reflected on the receiver minus the power loss from the receiver and power absorbed in the receiver which is given as

$$\dot{Q}_{use} = \eta_{op} A_{ap} I_b - A_{abs} U_{lr}(T_{abs,av} - T_{amb}) - \rho_{abs} V_{abs} c_{p,abs} \frac{dT_{abs}}{dt} \tag{4.36}$$

The ratio between the rate of useful energy carried by the heat transfer fluid and the rate of energy incident concentrator aperture can be obtained as

$$\eta_{th} = \frac{\dot{Q}_{use}}{A_{ap} I_b} = \frac{(\dot{m} C_p)_a (T_{a,out} - T_{a,in})}{A_{ap} I_b} = \eta_{op} - \frac{A_{abs} U_{lr} (T_{abs,av} - T_{amb)}}{A_{ap} I_b} - \frac{\rho_{abs} V_{abs} c_{p,abs}}{A_{ap} I_b} \frac{dT_{abs}}{dt} \quad (4.37)$$

Therefore, the rate of temperature of the absorber can be determined from equation and given as

$$\frac{dT_{abs}}{dt} = \frac{\eta_{op} A_{ap} I_b - A_{abs} U_{lr} (T_{abs} - T_{amb}) - (\dot{m} C_p)_a (T_{a,out} - T_{a,in})}{\rho_{abs} V_{abs} C_{p,abs}} \quad (4.38)$$

Where, the loss from the absorber is due to convection and radiaton on the absorber which is revealed to the ambient air temperature.

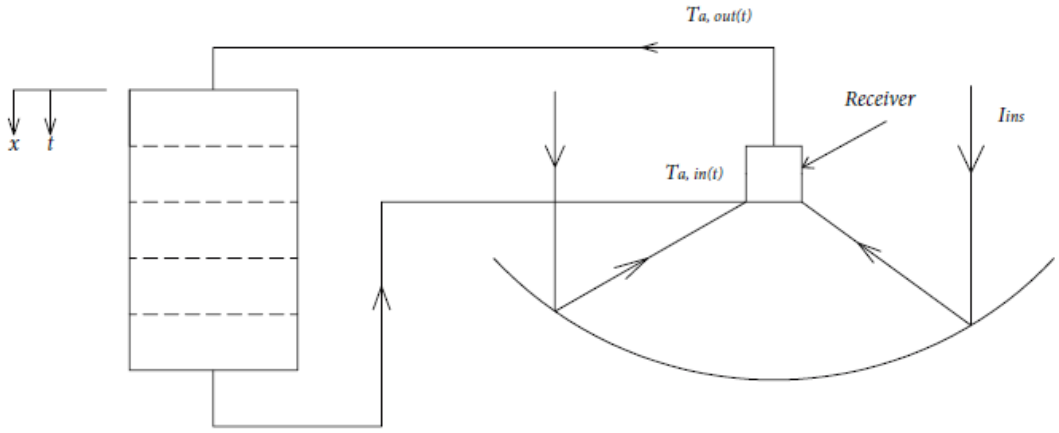

Figure 4-8: Schematic diagram showing the heat transfer process in integrated packed bed with parabolic solar collector

Note that: most of the receiver thermal analysis and the discretization of equation (4.38) are discussed in chapter 5.

4.5.5. Sun Tracking System

The main purpose of this tracking mechanism is used to trace the path of Sun movement through the entire day. In this study, manual tracking system which consists of a hollow cylinderic stainless steel for the support of the dish as shown in Figure 4-9. The manual tracking system is operated by hand in two – axis. The tracking is up and down the dish for adjusting or setting the reflector as per the solar altitude angle using hand rod pin to the holes adjusted at an angle of 15^0 at each hour and also rotates along the axis of rotation to

adjust azimuth angle. The operator carefully adjusts the orientation of the reflector normal to the beam solar radiation

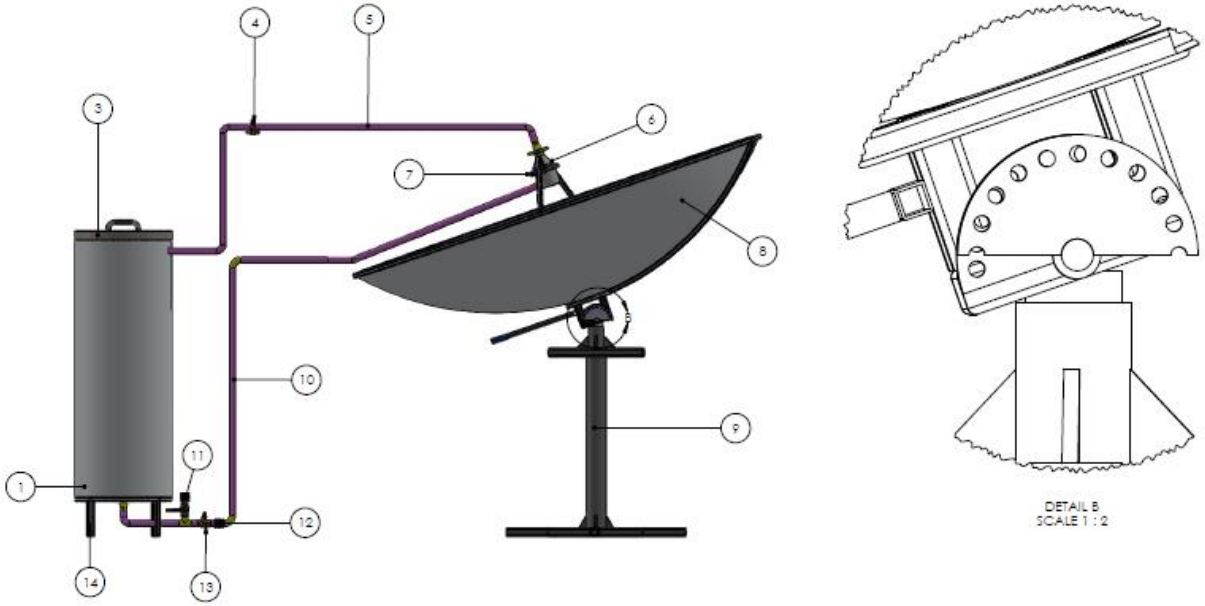

Figure 4-9: Two-axis Sun tracking mechanism

Table 4-5: The results of geometric parabolic dish

Parameters	Nomenclature	Values	Units
Aperture diameter	D_a	2.00	[m]
Concentration ratio	C	400	[-]
Rim angle	ϕ_r	85.14	[^{0}]
Acceptance angle	θ	4.86	[^{0}]
Edge radius	r_r	1.0033	[m]
Focal point	f	0.54	[m]
Height of dish	H_d	0.45	[m]
Aperture area	A_{ap}	3.14	[m^2]
Absorber area	A_{abs}	0.00785	[m^2]
Absorber diameter	d_r	0.05	[m]

4.6. Sizing Packed Pebble Bed Thermal Storage

To model the size of a pebble bed thermal storage, the amount of energy to be stored, and the mass flow rate of a heat transfer fluid used for charging the storage should be known. An average temperature of the storage which is applicable to cook should be considered. The initial temperature of storage, average temperature inflow to the storage, porosity, pebbles size and physical and chemical properties of pebbles are of concern during the sizing of the storage.

In this system, the porous medium is a bed of closely packed pebbles. The pebbles are essentially spherical and of uniform diameter. Hot air is forced through the bed in the axial direction.

Based on the above energy demand; the diameter and length of the storage can be determined from the sensible heat of the storage.

$$E_{st} = \rho_p c_{pp} V_{st} (1-\varepsilon)(T_{P,ave} - T_{init}) \tag{4.39}$$

Where, E_{st} is the stored energy, ρ_p is pebble density, c_{pp} is the specific heat capacity of pebbles, V_{st} is the volume of the storage, ε is the void fraction or porosity, $T_{p,ave}$ is an average find the temperature of pebble particle, T_{init} is the initial temperature of the pebble. By using energy stored formula, we can determine the total volume of the storage

$$V_{st} = \frac{E_{st}}{\rho_p c_{pp} (1-\varepsilon)(T_{s,ave} - T_{init})} \tag{4.40}$$

From the volume of storage, the diameter of the storage tank can be given as

$$D_{st} = \sqrt{\frac{4V_{st}}{\pi L_{st}}} \tag{4.41}$$

Where, L_{st} is length of the storage

To describe the thermal and geometric properties of a packed bed, a number of characteristics are used; typically, these are particle size (and particle size to container size ratio), void fraction, bed cross-sectional area and bed length, superficial air velocity and Reynolds number. Generally, particle sizes are not spherical but of irregular shape. In such cases, the equivalent diameter of pebbles d_p is given as [55]

$$n_p = \frac{6(1-\varepsilon)V_{st}}{\pi d_p^3} \tag{4.42}$$

Where, V_{st} is the total volume of storage, n_p is the number of pebbles. The porosity or void fraction ε is given as

$$\varepsilon = \frac{V_{void}}{V_{st}} \tag{4.43}$$

The porosity of closely-packed pebble beds would lie between 0.38 and 0.42 [41]. Assuming that ε =0.4. We can determine the void volume from the above equation.

4.7. Sizing of Packed PCM Capsules Thermal Storage

To model the size of a Packed PCM capsules thermal storage, the amount of energy demand used for one house and mass flow rate of hot air circulates in the system should be known. The average temperature desirable for the cooking should be justified.

Eutectic 40% kNO_3 - 60% $NaNO_3$ is selected for the model which have the following characteristics as shown in Table 4-6

Table 4-6: Properties of eutectic 40% KNO_3-60% $NaNO_3$ [20]

Parameters	Nomenclature	Values	Units
Density at temp≤220 °C	$\rho_{pcm,s}$	1800	[kg/m^3]
Density at temp≤220 °C	$\rho_{pcm,l}$	1700	[kg/m^3]
Thermal conductivity	k_{pcm}	0.8	[W/mK]
Latent heat of fusion	h_{fus}	108.67±1.43	[kJ/kg]
Melting temperature of PCM	T_m	220	[^{0}C]

The amount of energy stored in the packed PCM capsules is given as

$$Q_{pcm} = Q_{pcm,solid} + Q_{pcm,latent} + Q_{pcm,liquid} \tag{4.44}$$

Where, Q_{pcm} is the amount of energy stored in PCM, $Q_{pcm,solid}$ is the amount of energy stored in solid PCM, $Q_{pcm,latent}$ is the amount of energy stored in PCM latent phase and $Q_{pcm,liquid}$ is the amount of energy stored in liquid phase

The specific heat capacity of PCM (C_{ppcm}) is given as a function of temperature [52].

$$C_{ppcm} = \begin{Bmatrix} 0.75\ if\ T < 110\ oC \\ 4.2\ if\ 110\ oC \leq T \leq 120\ oC \\ 1.4\ if\ 120\ oC < T < 210\ oC \\ 12\ if\ 210\ oC \leq T \leq 220\ oC \\ 1.6\ if\ T > 220\ oC \end{Bmatrix} \tag{4.45}$$

Therefore, energy stored in the packed PCM capsules can be given as

$$Q_{PCM} = \int_{T_{init}}^{T_m} m_{pcm} c_{ppcm,s} dT + m_{pcm} \Delta h_{fus} + \int_{T_{init}}^{T_m} m_{pcm} c_{ppcm,l} dT \tag{4.46}$$

Where, m_{pcm} is mass of PCM, $c_{ppcm,s}$ specific heat capacity of PCM for solid state, $c_{ppcm,l}$ is specific heat capacity of PCM for liquid state, ρ_{pcm} is density of PCM and Δh_m is change enthalpy in latent phase

$$m_{pcm} = \rho_{pcm} V_{st} (1 - \varepsilon) \tag{4.47}$$

From this equation, the volume storage can be determined as

$$V_{st} = \frac{E_{store,in\ PCM}}{\int_{T_{init}}^{T_m} \rho_{pcm,s}(1-\varepsilon) c_{ppcm,s} dT + \rho_{pcm}(1-\varepsilon)\Delta h_m + \int_{T_{init}}^{T_m} \rho_{pcm,l}(1-\varepsilon) c_{ppcml} dT} \tag{4.48}$$

The length of storage as a function of its diameter can be given as

$$D_{st} = \sqrt{\frac{4V_{st}}{\pi L_{st}}} \tag{4.49}$$

Assuming 25mm diameter of PCM capsules, the number of PCM capsules required for the storage can be given as,

$$n_{PCM,capsules} = \frac{6(1-\varepsilon)V_{st}}{\pi d_{pcm}^3} \tag{4.50}$$

Where, d_{pcm} is diameter of PCM and $n_{PCM,capsules}$ is number of PCM capsules

4.8. Material Selection for System Design

a) Material for the body of the dish

Aluminum is chosen over steel because of its lightness, lower cost, ease of fabrication, and energy effectiveness in the use of material. It also reduces the amount of work to be done during the tracking mechanism.

b) Material for the reflecting surface

To reduce the overall weight of the collector, a light glass mirror having 2mm thickness, high surface quality, and good specular reflectance was selected. A glass mirror was selected over the polished aluminum surface because its reflectivity of (95%) is better than aluminum sheet with its reflectivity 85%. Also, the glass surface is easier to clean than the aluminum surface.

c) Material for tracking structure

Two – axis tracking mechanism with pipe, hollow, stainless steel was selected for the support of the dish. This is because of its strength, rigidity, resistance to deflection by commonly encountered winds, and its ability to withstand transverse and cross-sectional loads of the entire heating portion of the parabolic dish.

d) Material of receiver

The materials used for absorbing heat energy are selected based on the absorbance of the material properties. Depending on this, SiC chips materials have good absorbance which is experimentally proved. The shell and insulation materials selected for the receiver are stainless steel and fiberglass which resists high temperature and low the thermal conductivity respectively.

e) Material for storage tank

The materials selected for the storage tank is stainless steel. Because it resists the high temperatures and corrosions. Fiberglass material is selected for the insulation since it has low thermal conductivity and commercially available.

f) Heat transfer fluid

Air is selected as the heat transfer fluid for the solar heater because of its stability at high temperatures, low material maintenance, and transport costs, safe to use, and is the most commonly used fluid for pebble bed thermal storage.

CHAPTER FIVE

5. PERFORMANCE ANALYSIS OF PEBBLE BED THERMAL STORAGE

5.1. Pebble Bed Thermal Storage Modeling

5.1.1. Physical Concept

In this work, the heat transfer fluid that transports heat from the solar receiver to the thermal storage unit is hot air and direct normal irradiance is concentrated on the receiver by parabolic dish as shown in Figure 5-1. The thermal storage media is a packed pebble bed with assumed uniform spherical shape which is suitable for the storage due to its abundance and stability in chemical and mechanical properties.

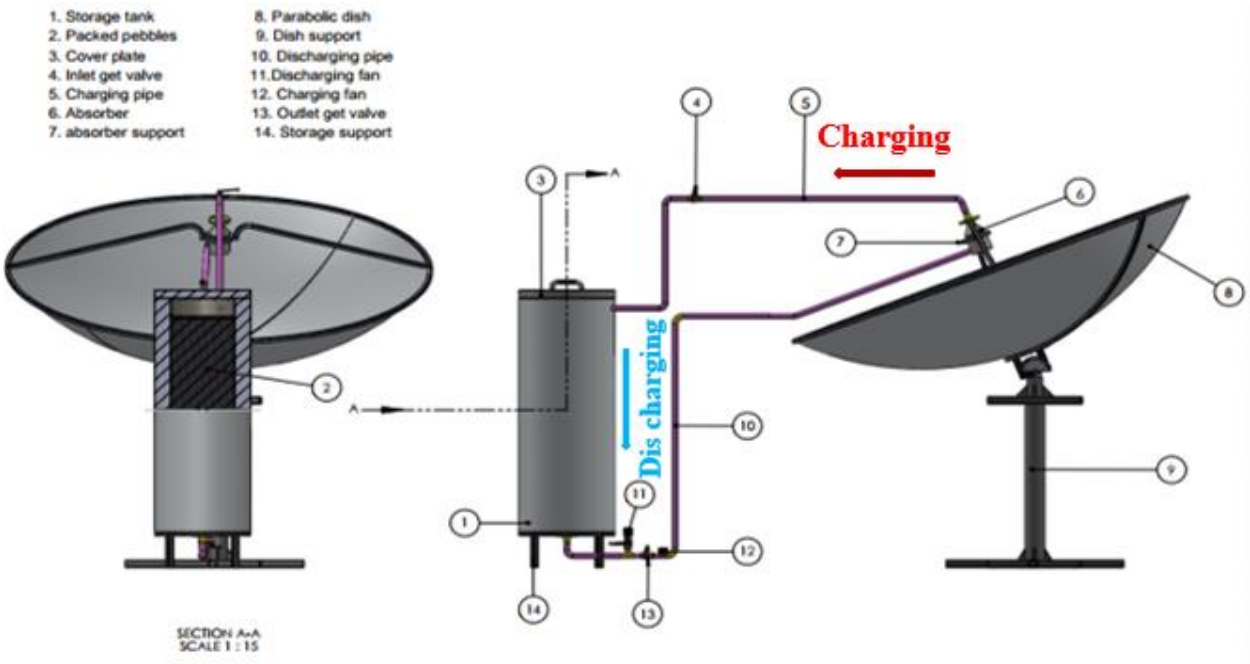

Figure 5-1: Schematic diagram of pebble bed thermal storage integrated with parabolic solar collector and fan.

The method of discharging heat when the cooking pot is placed on the pebble bed thermal storage and the heat is transferred to the pot with convection and conduction. There is direct

contact with the pot and the storage thermocline and most part of the circumferential is contact with air passing through pebbles as shown in Figure 5-2.

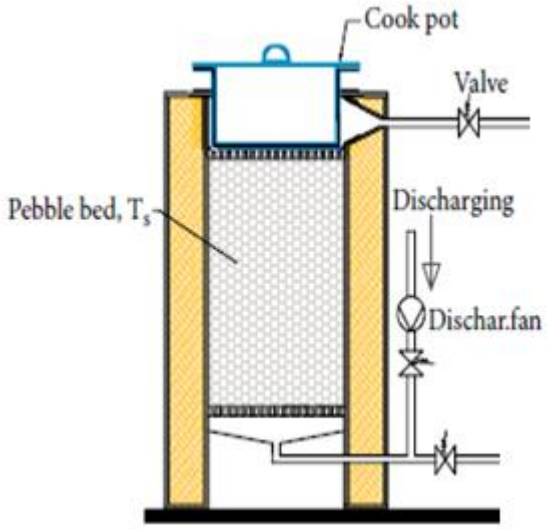

Figure 5-2: Schematic diagram of pebble bed thermal storage integrated with parabolic solar collector and cooking pot during the discharging period

5.1.2. Solar Thermal Storage Model

The solar thermal energy storage is modeled when hot air heated in the receiver enters the packed pebble beds and the returns to the receiver. The thermal storage media is a packed pebble bed with the assumed uniform spherical shape which is suitable for the storage due to its stability in chemical and mechanical properties. The size of the storage is modeled based on the amount of energy demand for the required application as follows.

$$E_{stored} = \rho_p c_{pb} V_{st} (1-\varepsilon)(T_{st,av} - T_{st,initial}) \quad (5.1)$$

Where ρ_p is density of pebble, c_{pb} is Specific heat capacity of pebble and V_{st} storage volume

Parameters and dimensions of the packed bed storage stack model of Figure 5-3 is presented in Table 5-1

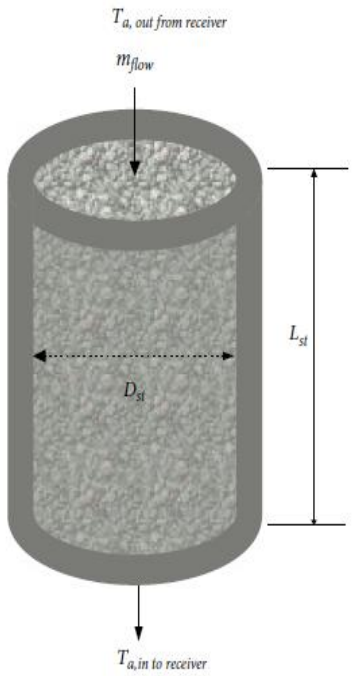

Figure 5-3: Schematic diagram of packed pebble bed storage

5.2. Mathematical Model

5.2.1. Heat transfer analysis of parabolic solar collector receiver

A mathematical model for solar thermal storage integrated to the parabolic solar collector as shown in Figure 4-8. The beam radiation is concentrated on the receiver (absorber) which heats the air that returns from the thermal storage.

The rate of energy incident on the absorber is equated to the rate of useful heat gained by the air plus the rate of heat loss from the absorber. The energy balance equation at the receiver can be written as [14, 16]:

$$\dot{Q}_{abs} = \dot{Q}_{use} + \dot{Q}_{l} \tag{5.2}$$

Where $\dot{Q}_{abs}$ is the rate of energy incident on the receiver, $\dot{Q}_{use}$ is the rate of useful heat gained and $\dot{Q}_{l}$ is the rate of heat loss from the absorber.

The power on the absorber is given as a function of aperture area beam radiation and concentration efficiency as follows

$$\dot{Q}_{abs} = \eta_{op} A_{ap} I_b \tag{5.3}$$

η_{op} is optical efficiency of the concentrator, A_{ap} is aperture area and I_b is beam solar radiation

Where the useful power gain of the air through the receiver is formulated as:

$$\dot{Q}_{use} = \dot{m}C_{pa}(T_{a,out} - T_{a,in}) \tag{5.4}$$

And heat loss from an absorber becomes:

$$\dot{Q}_l = A_{abs}U_{lr}.(T_{abs,av} - T_{amb}) \tag{5.5}$$

Where, A_{abs} is absorber area and U_{lr} is over all heat transfer coefficient through the absorber

The useful power gain is elaborated by substituting equations (5.4) and (5.5) into equation (5.2).

$$\dot{Q}_{use} = \eta_{op}A_{ap}I_b - A_{abs}U_{lr}(T_{abs,av} - T_{amb}) - \rho_{abs}V_{abs}c_{p,abs}\frac{dT_{abs}}{dt} \tag{5.6}$$

To characterize the thermal performance of a solar concentrating collector, the concept of thermal efficiency is used. This concept refers to the ratio between the rate of useful energy carried by the heat transfer fluid and the rate of energy incident concentrator aperture:

$$\eta_{th} = \frac{\dot{Q}_{use}}{A_{ap}I_b} = \frac{(\dot{m}C_p)_a(T_{a,out} - T_{a,in})}{A_{ap}I_b} = \eta_{op} - \frac{A_{abs}U_{lr}(T_{abs,av} - T_{amb)}}{A_{ap}I_b} - \frac{\rho_{abs}V_{abs}c_{p,abs}}{A_{ap}I_b}\frac{dT_{abs}}{dt} \tag{5.7}$$

The outlet temperature of air from the receiver storage is given as a function of inlet temperature of air and solar radiation as follows.

$$T_{a,out}(t) = T_{a,in}(t) + \frac{\eta_{op}A_{ap}I_b(t)}{(\dot{m}C_p)_a} - \frac{A_{abs}U_{lr}(T_{abs,av} - T_{amb})}{(\dot{m}C_p)_a} - \frac{\rho_{abs}V_{abs}C_{p,abs}}{\dot{m}c_{pa}}\frac{dT_{abs}}{dt} \tag{5.8}$$

Where U_{lr} is the mean coefficient of heat losses for the absorber, which is represented by [58], [59]:

$$\frac{1}{U_{lr}} = \left[\frac{1}{h_c + h_r}\right] \tag{5.9}$$

Where the radiation heat transfer coefficient (h_r) is given by:

$$h_r = \sigma\varepsilon_{abs}(T_{abs}^4 - T_{amb}^4)\Big/(T_{abs} - T_{amb}) \tag{5.10}$$

Where, T_{abs} is temperature of absorber, σ is absorbance and ϵ is emmisivityof absorber

The convective heat transfer coefficient (h_c) is calculated by considering thermal conductivity of air k_{air} the absorber diameter (d_r) and Nusselt number (Nu)

$$h_c = \frac{k_{air} Nu}{d_r} \tag{5.11}$$

The Reynolds number (Re) is given as follows for fluid flow in the pipe.

$$\mathrm{Re} = \frac{\rho_{air} d_r}{v_{air}} \tag{5.12}$$

Where v_{air} *is* kinematic viscosity of air

5.2.2. Packe d Bed Thermal Energy Storage Mathematical Model

One dimensional two-phase energy equations describe the heat exchange between air (fluid phase) and pebbles (solid phase) as shown in Figure 5-4 during charging and discharging, from which the transient temperature profiles in packed pebbles during charging and discharging times are determined. The pebble bed consists of a cylindrical tank which can be divided into subdomains of packed pebbles with fixed thickness with the air flowing through the porous space around the pebbles.

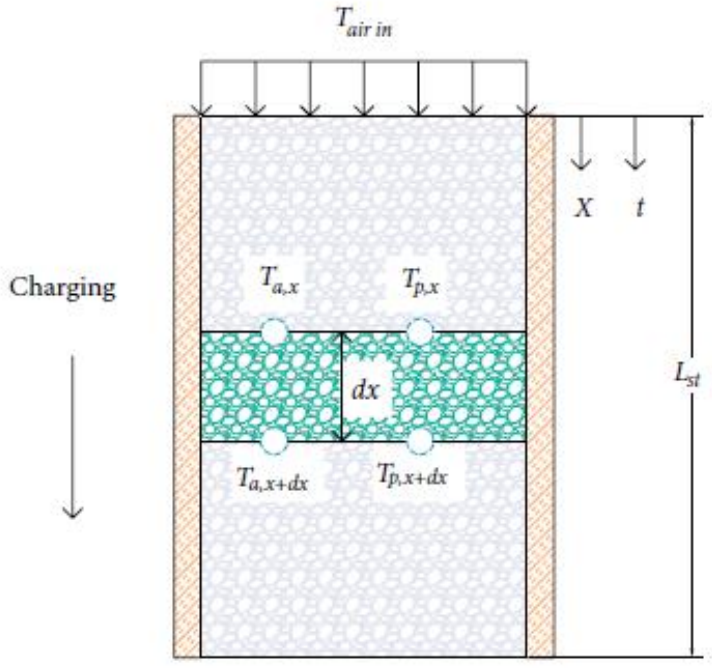

Figure 5-4: Schematic diagram showing the heat transfer process occurring within packed bed pebbles of storage.

In formulating the mathematical model of the system, it was assumed that the porosity, mass flow rate and pebble geometry are uniforms, air temperature is constant in the radial direction, and radiation heat transfer in the pebble bed (radiation heat transfer is neglected due to low temperature) and the conduction heat transfer in the air were neglected. From an energy balance, the change of enthalpy of air during time dt of the differential element is determined as negative of the sum of heat transferred from the air to the pebbles by convection, energy transported by air from the control volume and heat loss to the surrounding as shown in equation (5.13). Hence, the energy equation for air (fluid phase) is obtained as follows.

$$\varepsilon A_{cs}\rho_a c_{pa}\frac{\partial T_a}{\partial t}+h_v A_{cs}(T_a-T_p)+\dot{m}c_{pa}\frac{\partial T_a}{\partial x}+U_w PL(T_a-T_{amb})=0 \tag{5.13}$$

It shall be noted that ε (porosity) is the volume fraction of air while 1-ε is the volume fraction of pebbles. Where, P is perimeter of the storage tank and L is the length of storage.

Considering the energy balance of pebbles on the differential element of the pebble bed, the rate of change of internal energy of the pebbles is determined as the sum of the heat transferred from the air to the pebbles, the heat conducted to the neighboring pebbles in the longitudinal direction. Hence, the energy equation for pebbles (solid phase) is obtained as follows.

$$\rho_p(1-\varepsilon)A_{cs}c_{pb}\frac{\partial T_p}{\partial t}-h_v A_{cs}(T_a-T_p)-\frac{\partial}{\partial x}(k_{eff}A_{cs}\frac{\partial T_p}{\partial x})=0 \tag{5.14}$$

ρ_p is density of pebble, h_v convective heat transfer coefficient and k_{eff} is effective thermal conductivity of pebble

5.3. Computational Model

Discretization of the partial differential equation for air equation (5.13) by using forward finite difference method, approximating the time and spatial first-order derivates, the following explicit algebraic equation for air temperature variation is obtained:

$$\frac{T_{a,i}^{n+1}-T_{a,i}^{n}}{\Delta t}=\frac{h_v}{\varepsilon\rho_a c_{pa}}(T_{p,i}^{n}-T_{a,i}^{n})-\frac{\dot{m}}{\varepsilon A_{cs}\rho_a}\frac{T_{a,i+1}^{n}-T_{a,i}^{n}}{\Delta x}-\frac{U_w P}{\varepsilon A_{cs}\rho_a c_{pa}}(T_{amb,i}^{n}-T_{a,i}^{n}) \tag{5.15}$$

While *i* and *i+1* designates the current and front spatial nodes in the longitudinal directions, *n* and *n+1* indicates the current and next time step.

Discretizing the partial differential equation of the pebble, equation (5.14), approximating first-order spatial and temporal derivatives by forwarding difference and the second-order spatial derivative by central difference scheme, the following explicit algebraic equation is obtained for the temperature variation of the pebbles.

$$\frac{T_{p,i}^{n+1}-T_{p,i}^{n}}{\Delta t}=\frac{h_v}{\rho_p(1-\varepsilon)c_{pb}}\left(T_{a,i}^{n}-T_{p,i}^{n}\right)+\frac{k_{eff}}{(1-\varepsilon)\rho_p c_{pb}}\left(\frac{T_{p,i+1}^{n}-2T_{p,i}^{n}+T_{p,i-1}^{n}}{\Delta x^2}\right. \tag{5.16}$$

Kay et al. [22] analyzed different convection heat transfer correlations among which the following was found to give better convective heat transfer between the air and the pebbles.

$$h_p=\frac{k_a}{d}\left(\frac{0.26}{\varepsilon}\right)\mathrm{Re}^{0.7}\ \mathrm{Pr}^{1/3} \tag{5.17}$$

The volumetric convective heat transfer coefficient, h_v is related to the surface area of heat transfer coefficient of the particle h_p becomes.

$$h_v=h_p a=h_p\sum(\ )A_p/V_t=h_p\sum A_p/\left[\sum V_p/(1-\varepsilon)\right]=h_p(1-\varepsilon)\sum A_p/\sum V_p \tag{5.18}$$

Where a is the particle surface area per unit volume of thr bed. In the case of spherical shape of pebbles,

$$\sum V_p\Big/\sum A_p=d_p/6 \tag{5.19}$$

Therefore, the volumetric heat transfer coefficient becomes

$$h_v=\frac{6h_p(1-\varepsilon)}{d} \tag{5.20}$$

The effective thermal conductivity for the packed pebbles is determined considering the volume fraction of the pebble and the air as follows [17]:

$$k_{eff}=\frac{1}{\left[\varepsilon\frac{1}{k_a}+\frac{(1-\varepsilon)}{k_{pb}}\right]} \tag{5.21}$$

Prandtl number is given as

$$p_r=\frac{c_{pa}\mu}{k_a} \tag{5.22}$$

The overall heat transfer coefficient through the wall is calculated from the equation below.

$$\frac{1}{U_w A} = \frac{1}{h_i A_i} + \frac{x_{ins}}{k_{ins} A} + \frac{1}{h_o A_o} \tag{5.23}$$

Where, U_w is overall heat transfer coeffiecient throughout the wall, A is surface area of storage, A_i is inner surface area of the storage wall, A_o is outer surface of the storage wall, h_i internal convective heat transfer coefficient , h_o is outer convective heat transfer coefficient , x_{ins} is thickness of insulation and k_{ins} is thermal conductivity of the insulation.

The natural convection heat transfer coefficient for the wall of the packed bed is determined from the correlation of the Nusselt number as a function of the Rayleigh and Prandtl numbers as follows.

$$h_o = \frac{k_a}{D}\left[0.825 + \frac{0.387 Ra_D^{1/6}}{(1+(\frac{0.492}{pr})^{\frac{9}{16}})^{\frac{8}{27}}}\right]^2 \tag{5.24}$$

The natural convection heat transfer coefficient for the horizontal pipe is determined from the correlation of Nusselt number as a function of the Rayleigh and Prandtl numbers as follows.

$$h_o = \frac{k_a}{D}\left[0.6 + \frac{0.387 Ra_d^{1/4}}{(1+(\frac{0.559}{pr})^{\frac{9}{16}})^{\frac{8}{27}}}\right]^2 \tag{5.25}$$

For hot air circulation pipe from receiver to the thermal storage, the following inside forced convective heat transfer coefficient is valid for laminar flow [60]

$$Nu = 1.86(\mathrm{Re}\,\mathrm{Pr})^{\frac{1}{3}}(\frac{D}{L})^{\frac{1}{3}}(\frac{\mu_b}{\mu_w})^{0.14} = \frac{h_i D}{k_a} \tag{5.26}$$

For the charging of the pebble bed, the air is heated with the concentrating parabolic solar collector absorber. Hence, the air temperature coming from the pebble bed and heated in the receiver is updated as follows considering the loss from the receiver to the inlet of the pebble bed.

$$T_{a,out}^{n+1} = T_{a,in}^{n} + \frac{\eta_{0p} A_{ap} I_b(t)}{\dot{m} c_{pa}} - \frac{A_{abs} U_{rl} (T_{abs}^{n} - T_{amb})}{\dot{m} c_{pa}} - \frac{\rho_{abs} V_{abs} C_{p,abs} (T_{abs}^{n} - T_{abs}^{n-1})}{\Delta t \dot{m} c_{pa}} \quad (5.27)$$

Where, the temperature of absorber T_{abs} obtained from back ward finite difference methos which is given as

$$T_{abs}^{n} = T_{abs}^{n-1} + \frac{\left(\eta_{0p} A_{ap} I_b(t) - A_{abs} U_{rl} (T_{abs}^{n-1} - T_{amb}) - \dot{m} c_{pa} (T_a^{n} - T_a^{n-1})\right) dt}{\rho_{abs} V_{abs} C_{p,abs}} \quad (5.28)$$

During discharging heat is transferred from storage to the material to be cooked. Simplifying the cooking process as water boiling, the temperature variation is given as follows from the heat transferred to the pan minus the radiative and convection losses of the pan:

$$T_w^{n+1} = T_w^{n} + \frac{\dot{Q}_{pan}(t) - (\dot{Q}_r(t) + \dot{Q}_{cv}(t))}{m_w c_{pw}} \Delta t \quad (5.29)$$

Where,

$\dot{Q}_{pan}$ is the rate of heat of pan $= \dfrac{T_{st} - T_w}{R_{th}}$

$\dot{Q}_r$ is the rate of radiation heat loss $= \sigma S_{pan} (T_w^4 - T_{amb}^4)$

$\dot{Q}_{cv}$ is the rate of convective heat loss $= hA_{csp}(T_w - T_{amb})$

Where, m_w is mass of water, C_{pw} is specific heat of water, R_{th} is thermal resistance of pan, T_w is temperature of water, T_{st} is temperature of storage, T_{amb} is ambient air, σ is Stefan boltzman constant S_{pan} is surface area of pan, h is convective heat transfer coefficient and A_{cspan} is cross-sectional area of pan

The stored thermal energy is obtained from the change in the average temperature of the pebble and evaluating the change in enthalpy of the pebble bed during charging. The thermal storage efficiency is determined as the ratio of the stored thermal energy to the solar energy incident on the receiver as follows.

$$\eta_{TS} = \frac{\int_0^L \rho_p c_p A_{cs} (1-\varepsilon)(T_{p(x)} - T_o) dx}{\int_0^{t_c} I_b A_{ap} dt} \quad (5.30)$$

The cooker thermal efficiency is evaluated as the ratio of the useful heat transferred to the cooking media during discharging to the charges in the stored thermal energy for cooking.

$$\eta_{th} = \frac{m_w c_w (T_{w,f} - T_{w,i})}{\int_0^L \rho_p c_p A_{cs} (1-\varepsilon)(T_{p(x)} - T_o) dx} \quad (5.31)$$

The overall efficiency of the cooker is evaluated as the ratio of the useful heat in the cooking media to the solar energy incident on the receiver surface used for charging. This means the heat is accumulated in the storage and the cooking is made by reversed flow rate.

$$\eta_o = \frac{m_w c_w (T_{w,f} - T_{w,i})}{\int_0^{t_c} I_b A_{ap} dt} \quad (5.32)$$

5.4. Verification of Computational Model

An experimental investigation of thermal storage under constant heat input was conducted by Okello [20] with 0.048 kg/s air mass flow rate for the pebble bed thermal storage of 0.3 m diameter and 0.9m length as indicated in Table 5-1. During the charging process, constant temperature hot air with a fixed mass flow rate (heated by electric resistance) flows from top to bottom of the thermal storage in the experimental set-up selected for verification. In the computation model of this system, 10 spatial nodes and 18000 time steps were used for the simulation. Stratification of temperature throughout the packed bed pebbles is observed. The initial and boundary conditions to be used during the charging of heat to packed bed pebbles for the simulation required to verify experimental data are given in Table 5-2.

Table 5-1: Bench mark experimental data [20] and calculated results

Parameters	Nomenclature	Values	Unit
Porosity	ε	0.38	[-]
Length of the storage	L	0.9	[m]
The diameter of the storage	D	0.3	[m]
Optimum diameter of pebbles	d	0.02	[m]
Mass flow rate	$\dot{m}$	0.0495	[Kg/s]
Inlet/outlet pipe diameter	d_p	0.05	[m]

The thickness of the stainless steel of the storage stack.	S	0.002	[m]
Pebble specific heat capacity	c_{pb}	880±50	[J/kg.k]
Pebble thermal conductivity	k_p	2.5	[W/mk]
Density of absorber	P_{abs}	2940	[kg/m^3]
Specific heat capacity of absorber	$C_{p,abs}$	1194	[J/kgK]
Inflow Temperature	T_{in}	355	[^{0}C]
Overall heat transfer coefficient	U_{wall}	0.4	[W/m^{2}k]

Table 5-2: Initial and boundary conditions

$T_{a(t,x=0)} = 355\ ^0C$	$T_{P(t,x=0)} = T_{p(t,x=1)}$	Space step = 0.1m
$T_{a(t=0,x=L)} = 23^0C$	$T_{P(t,x=L)} = T_{p(t,x=L+1)}$	Number of space step = 10
$T_{P(t=0,x=L)} = 23^0c$	Time step $(\Delta t) = 1s$	Maximum time charging = 5h
	Number of time step=18000	

The experimental results were compared with the results of simulation using the computational model developed in this work and good agreement with an average error 1.87% after charging for 5 hours as shown in Figure 5-5. Hence, it can be concluded that the accuracy of the model is sufficient to simulate an integrated system of concentrating parabolic dish and thermal storage during charging and cooking conditions. Since an average error is small after charging for 5 hours and 0.1m space grid is considered for simulation. The grid sensitivity is tested for dx=0.1m (10 spatial nodes), 0.05m (19 spatial nodes) and 0.025m (37 spatial nodes) and the temeperature gradient along the length of the storage relatively similar with insiginificant errors after charging for 5 hours as shown in Figure 5-6.

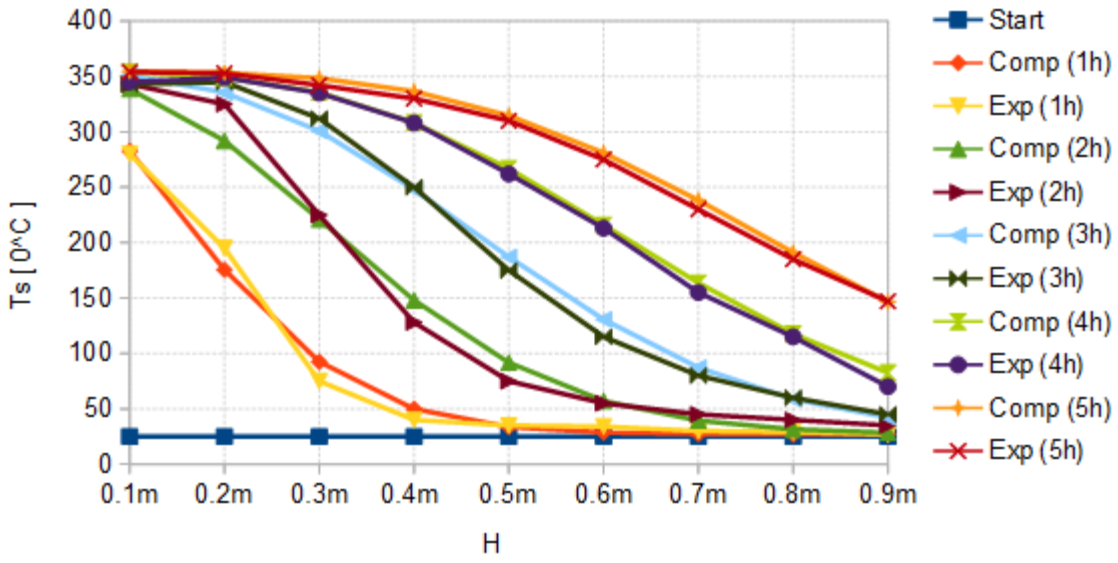

Figure 5-5: Validating the numerical model with the experimental results at different space steps for dx=0.1m. (Comp is computational and Exp is experimental)

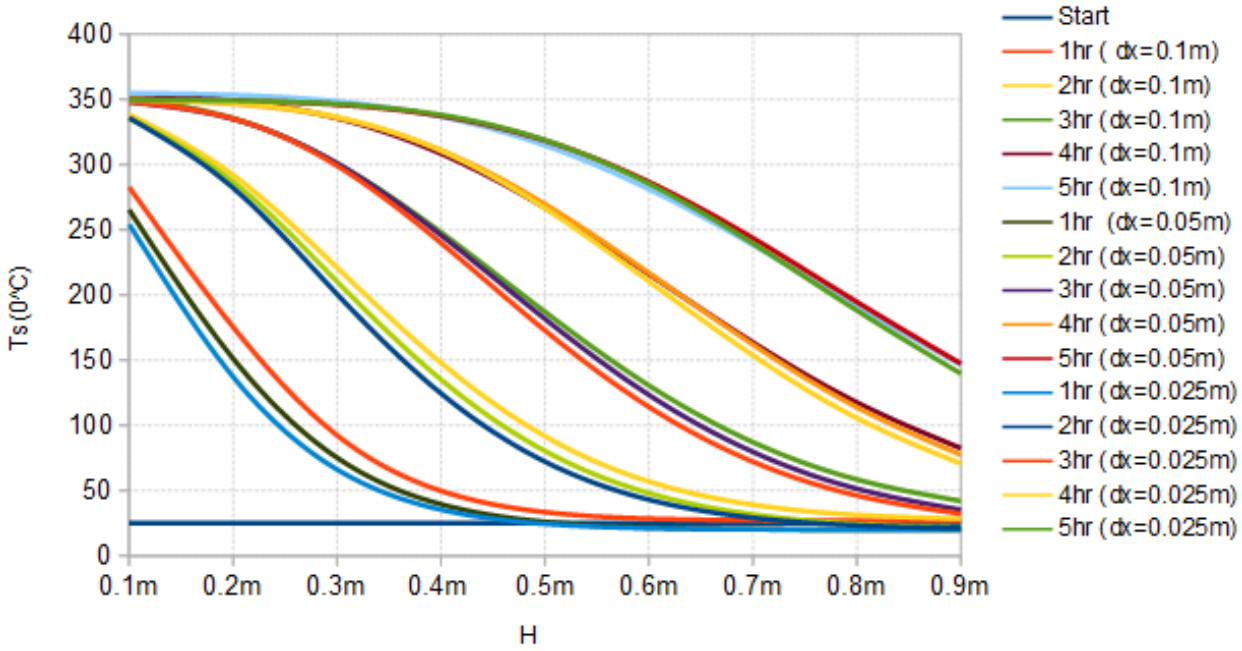

Figure 5-6: Grid sensitivity test

Figure 5-7 show the validation of temperature degradation after discharging for 2 hours with an experimental result using forced convection [48]. Therefore, the good agreement is obtained from this validation and the discharging equation is valid for the case of using the actual solar data.

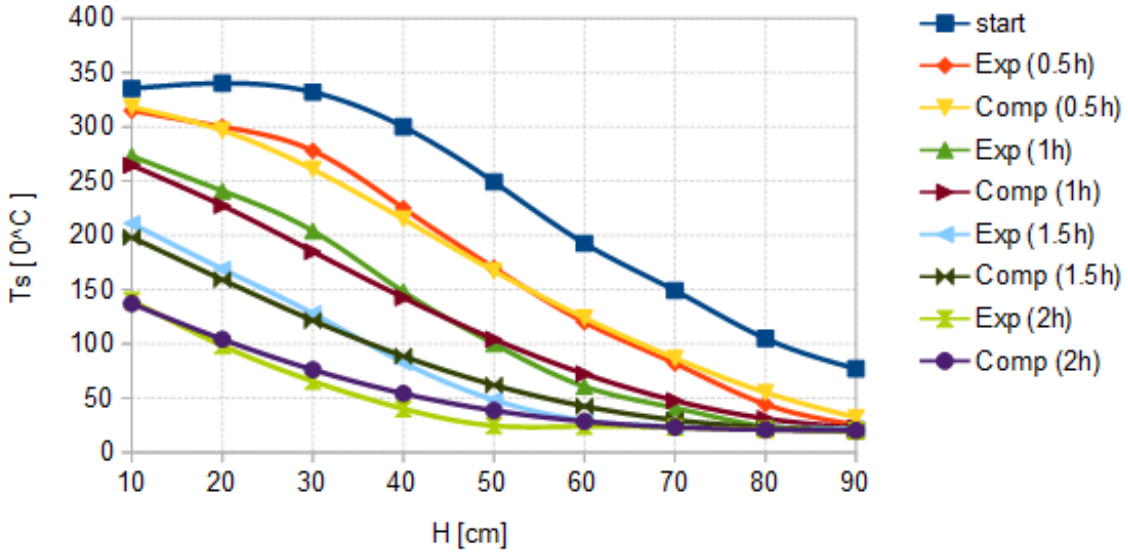

Figure 5-7: Validating an experimentalresuls with simulation model during discharging [48]. (Comp is computational and Exp is experimental)

5.5. Results and Discussions

5.5.1. Charging with Solar Energy and Discharging with Water Boiling

Figure 5-8 shows the maximum and minimum direct normal irradiance (DNI) for Addis Ababa selected for modeling of the parabolic solar collector from Sunrise to Sunset.

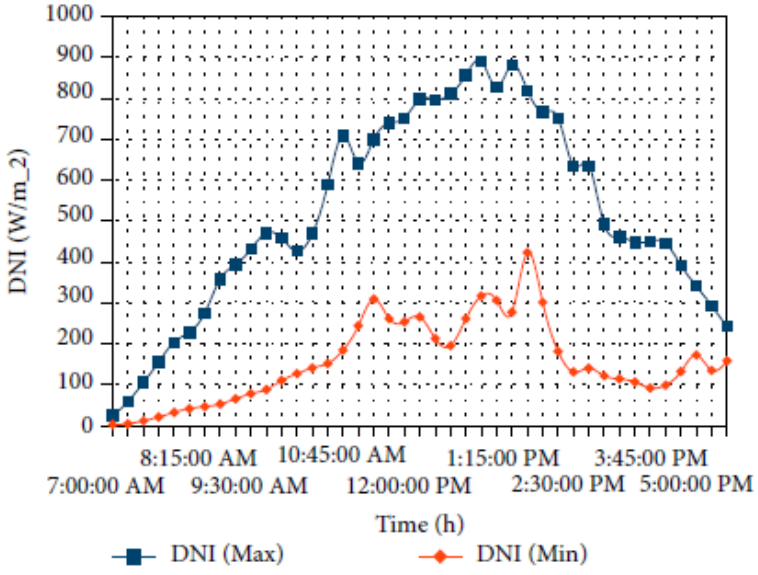

Figure 5-8: The day's of the maximum and minimum direct normal irradiance in the year from 7 AM To 5 PM

Parameters of the solar collector are calculated and the results are explained as it is shown in Table 4-5 which is used to investigate the variable charging of heat to storage.

The charging of the pebble bed thermal storage was investigated in typical days of March and June in which the highest and lowest direct normal irradiance occurs in Addis Ababa from 7 AM to 5 PM by recirculating the hot air through the receiver of the parabolic solar collector for the thermal storage in consideration and initial conditions of the pebbles given in Table 5-1 and Table 5-2. Figure 5-9 shows the variation of air temperature at the outlet of the receiver of the parabolic solar collector when the air is circulating throughout the storage and returned to the receiver for the days with the highest and lowest beam solar irradiance.

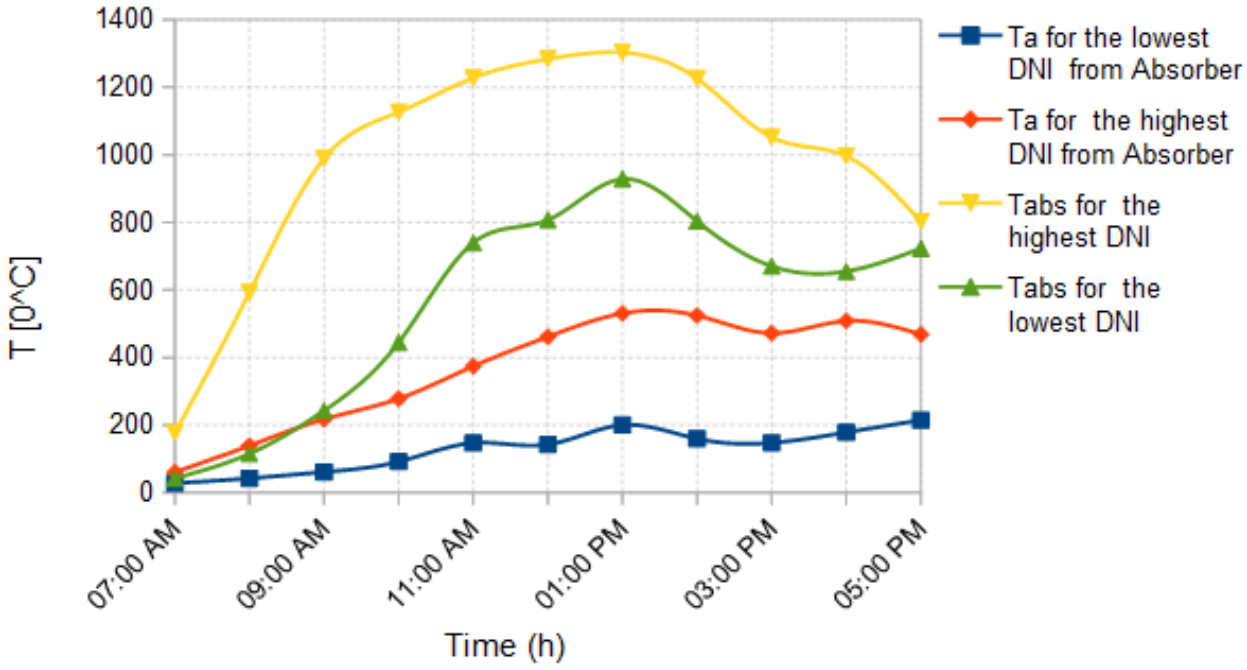

Figure 5-9: Temperature of air and absorber when the air returns from the storage to the receiver heating from 7 AM to 5 PM for for the day of the highest and lowest solar radiation.

Figure 5-10 and Figure 5-11 show the temperature distributions in the thermocline storage and the recirculated air with respect to sunshine hours during charging for the day with the highest DNI for Addis Ababa. After charging for 11 hours, the maximum temperatures of packed pebbles and air reached 459.71^{0}C and 468.42^{0}C, respectively at the top surface of the storage. The minimum temperatures of the air and the thermal storage were 383.22^{0}C and 414.41^{0}C, respectively.

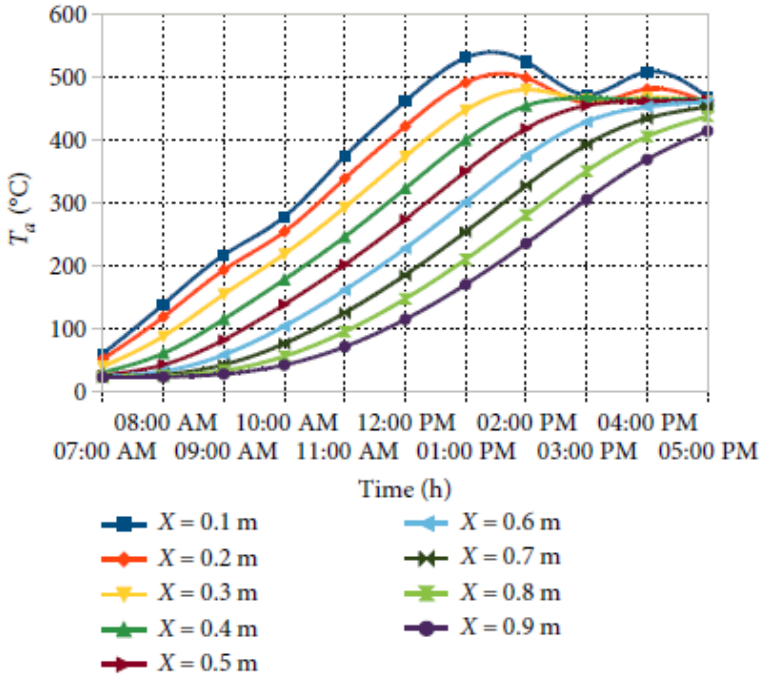

Figure 5-10: Temperature of air cycling throughout the storage and receiver with respect to charging time from 7 am to 5 pm for the higher DNI.

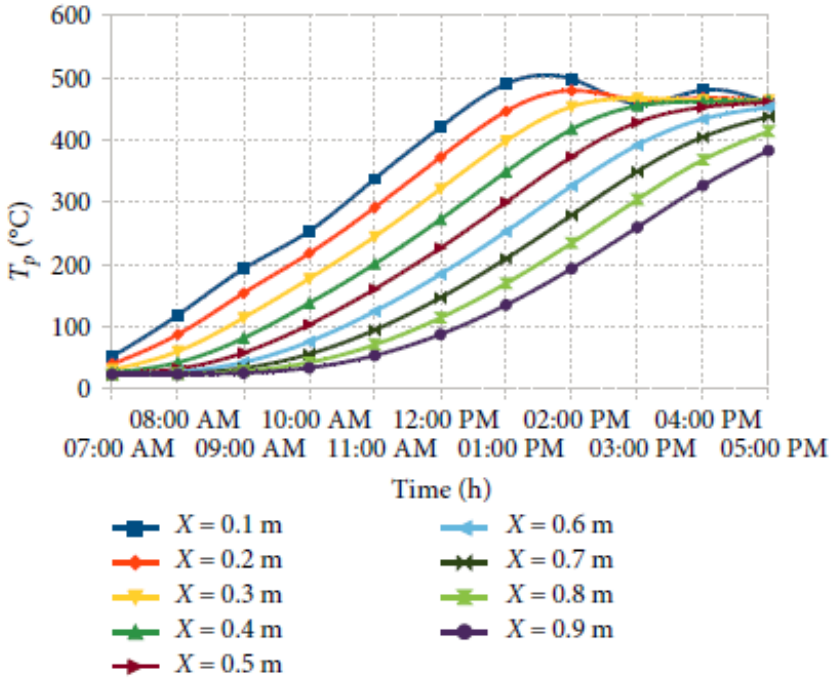

Figure 5-11: Temperature of thermocline storage charged with respect to charging hours from 7 AM to 5 PM for the higher DNI.

Figure 5-12 and Figure 5-13 show temperature distributions within thermocline storage and the air within storage with respect to charging hours simulated for the lowest direct normal irradiance (DNI) of Addis Ababa. After charging for 11h hours, the maximum temperatures of packed pebbles and air reached 199.75^{0}C and 214.49 ^{0}C, respectively at the top surface of the storage. The minimum temperatures were 129.48^{0}C and 139.16^{0}C for packed pebbles and air, respectively.

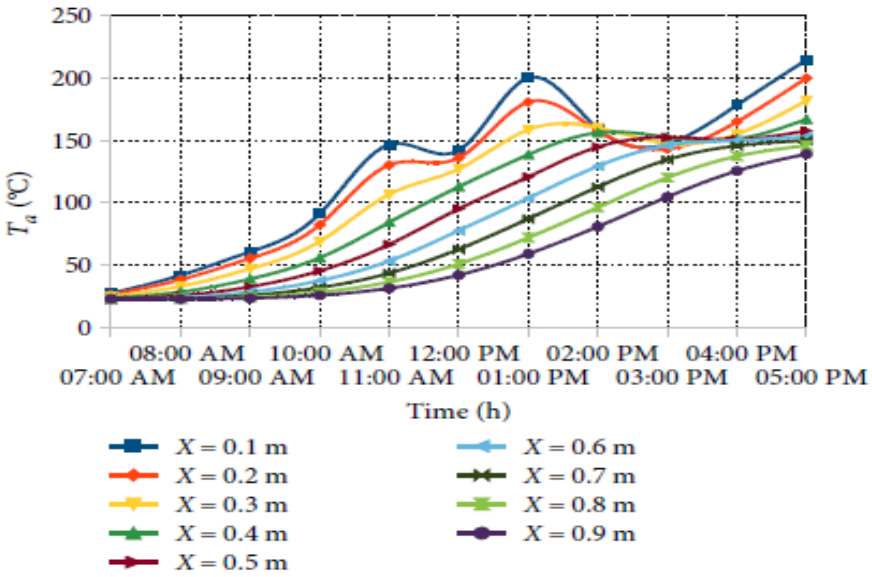

Figure 5-12: Temperature of air charging the storage versus charging time from 7 AM to 5 PM for the lower DNI

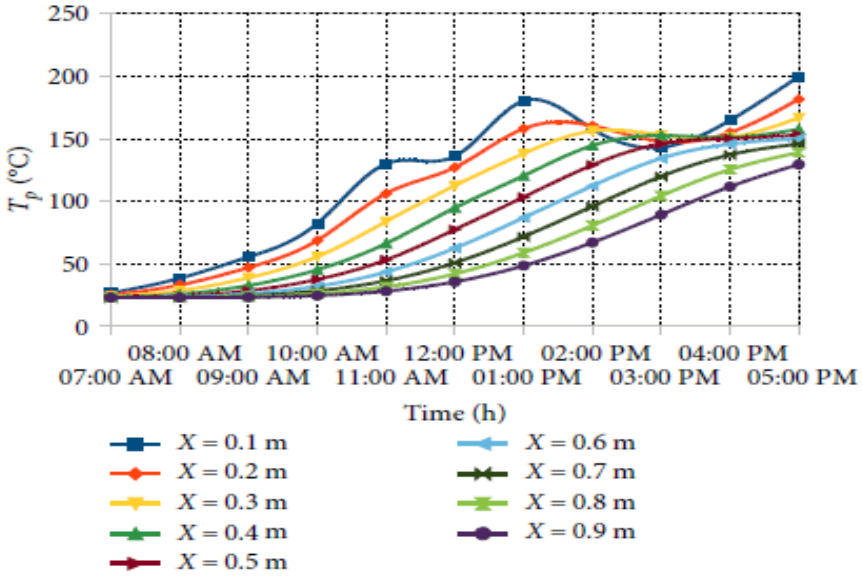

Figure 5-13: Temperature of thermocline storage versus charging time from 7 AM to 5 PM for the lowest DNI

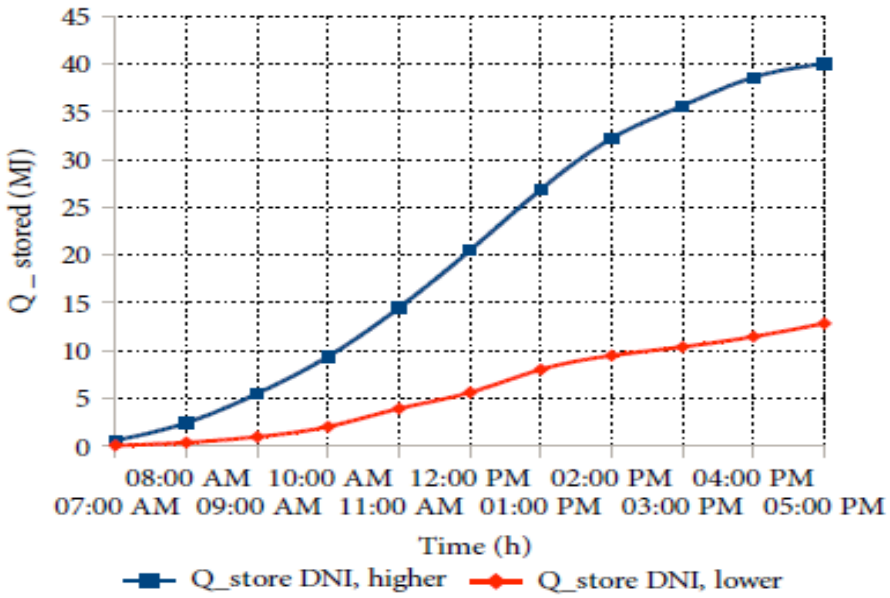

Figure 5-14: Energy stored versus charging hours for both maximum and minimum direct normal irradiance.

Figure 5-14 shows the amount of energy stored in thermocline storage for the days with maximum and minimum direct normal irradiance. The total stored energy was 40.10MJ and 12.85 MJ for both conditions respectively.

Discharging Conditions

Heat is extracted from the storage when the ambient air is recirculated with 0.0048kg/s mass flow rate of air throughout the storage from bottom to top. The discharging of heat from the storage was considered in the following two cases.

- When the cooking is carried out only by conduction heat transfer, the pot is placed on the top of storage, and the heat is transferred from the storage to the pot by conduction.
- When the cooking is carried out by forced convection circulation of air.

Figure 5-15 and Figure 5-17 Compare discharging of heat during water boiling to simulate cooking with forced convection versus conduction and natural convection heat transfer in the pebble bed. From the comparison, forced convection discharging gives higher heat transfer rate discharging by conduction without air recirculation. For 5 liters of water boiling, 53 minutes discharging time is required to reach a temperature 93^{0}C for forced

convection heat discharge. In the case of the conduction and natural convection discharging, 5liters water requires 56 minutes to reach 93^{0}C and the storage temperature decreases gradually as it is shown in Figure 5-15 and Figure 5-17. The parameters and values required during the discharging condition (during water boiling) are presented in Table 5-3.

Table 5-3: Dimensions and values required during water boiling simulation [44]

Parameters	**Symbols**	**Values**	**Unit**
Diameter of pan	d_{pan}	0.273	[m]
Length of pan	L_{pan}	0.17	[m]
Specific heat capacity of water	C_{pw}	4180	[J/kgK]
Stefan Boltzmann constant	σ	$5.67x10^{-8}$	[W/m^{2}K^4]
The emissivity of the steel pan	ϵ	0.4	[-]
The thermal resistance of the pan	R_{th}	0.865	W/K

The initial and boundary conditions during discharging of heat from packed bed pebbles for water boiling test simulation are given in Table 5-4.

Table 5-4: Initial and boundary conditions for the discharging process

$T_{a(t=t_{max},\ x=0)} = 23\ ^0C$	Space step = 0.1m	Time step $(\Delta t) = 1s$
$T_{p\ (t=0,\ x=L)} = T_{p,\ 11h\ charge}$	Number of space step = 10	t_{max} = 11h

The temperature degradation for the case of the day with the highest solar radiation during boiling 5 liters of water when the pot is placed on the top of the storage and the heat is transferred to the pot using conduction. The average temperatureof the storage is degraded to 350.15 ^{0}C and the temperature of water reach to 93 ^{0}C after 1.4 discharing hours as it is shown in Figure 5-15.

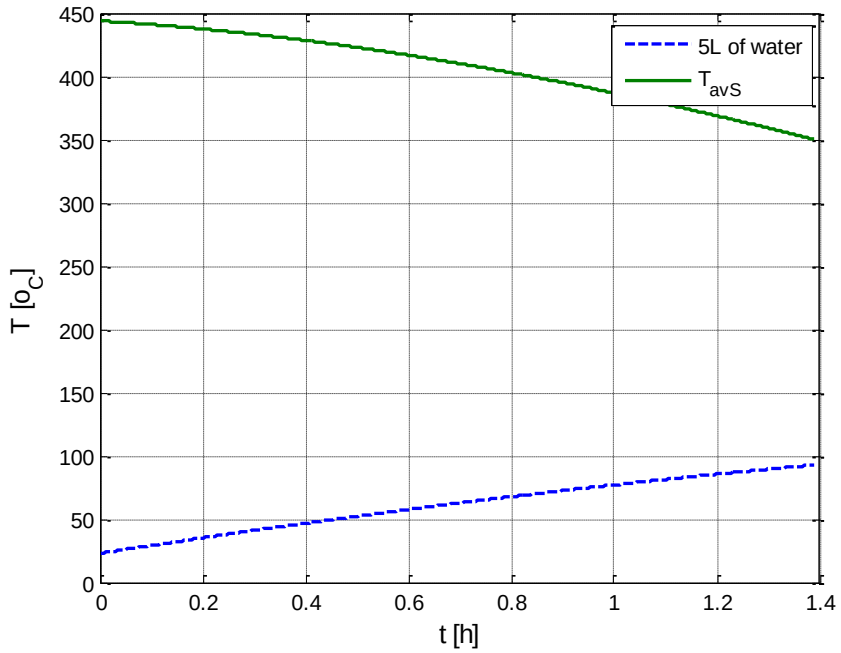

Figure 5-15: Average temperature of storage versus temperature of water during boiling of 5 liters of water where the pot is placed on the storage for higher DNI

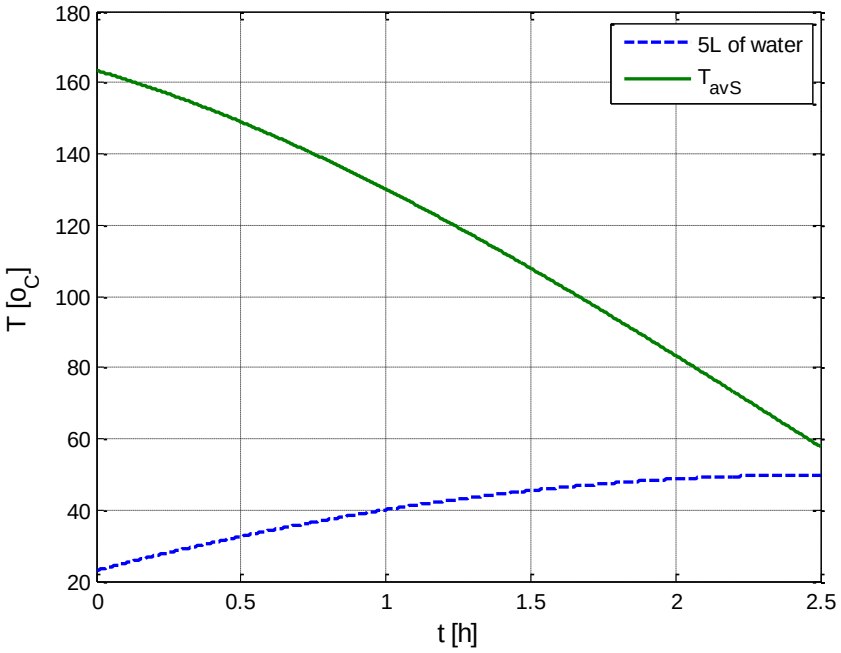

Figure 5-16: Average temperature of storage versus water heat by conduction for the day of the lowest DNI

For the case of the lowest solar radiation, 5 liters of water heat to 49.88 ^{0}C and an average temperature of the storage degraded to 57.88^{0}C after discharging for 2.5 hour as shown in Figure 5-16.

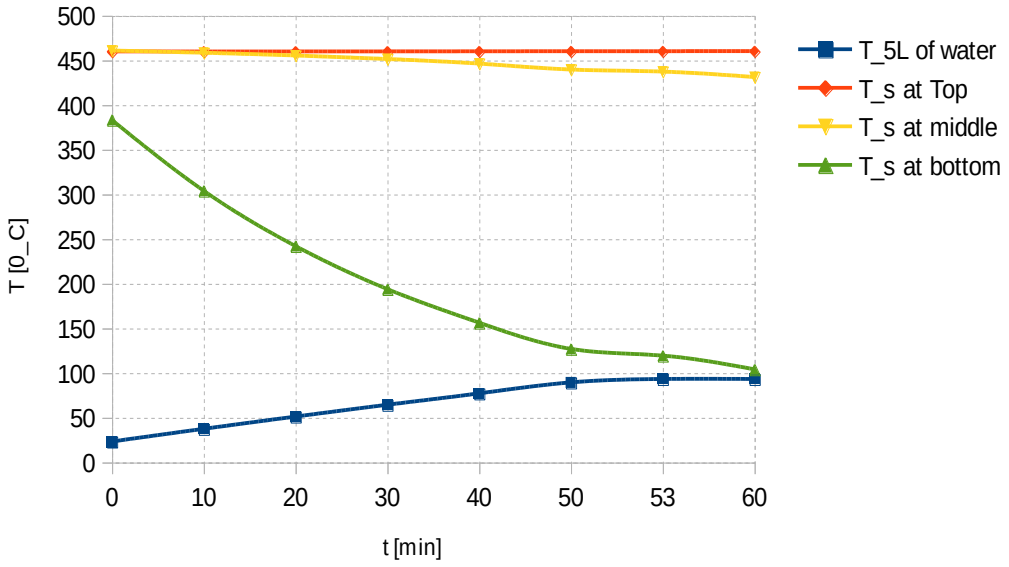

Figure 5-17: temperature of storage versus temperature of water during the boiling of 5 liters of water with 0.0048kg/s mass flow rate for the maximum direct normal irradiance.

In the previous simulation, 5 liters of water was heated in a short time with an insignificant change of pebble bed temperature profile on the top of the storage as shown in Figure 5-17. However, the thermal storage can heat at a maximum of 28 liters of water as shown in Figure 5-18 over a longer time, with considerable cooling in pebble stack. From the results of the simulation, the temperature of water reached 93 ^{0}C after 8h discharging time and the top surface of the thermal storage temperature reached 109 ^{0}C. Therefore, the storage has a capacity of boiling 28 liters of water for the day with the highest DNI.

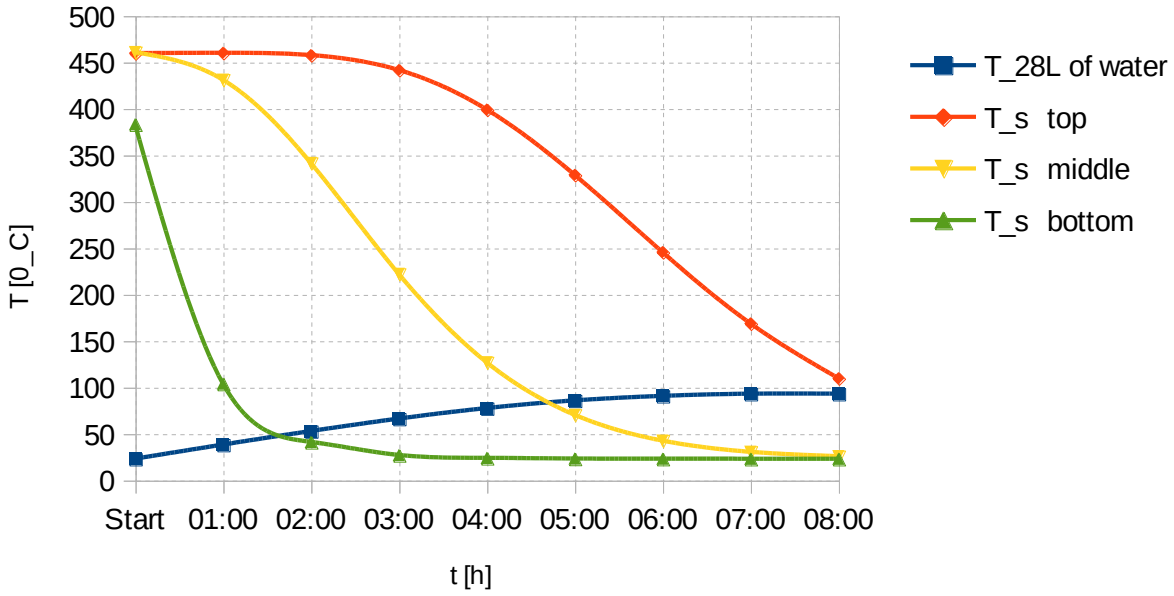

Figure 5-18: Temperature of thermal storage and 28 liters of water during discharging with 0.0048kg/s mass flow rate of air for the higher dni.

On the day of lowest DNI, the storage temperature degraded during boiling of 5 liters of water in 4 hours as it is shown in Figure 5-19. From the results of the simulation, the temperature of water reached 93 ^{0}C after 4 hours of discharging time and the top surface of the thermal storage temperature reached 138 ^{0}C. Therefore, the storage has a capacity of boiling only 5 liters of water during the day of lowest DNI. The rest of the energy in the storage will be available for the next day or for heating water.

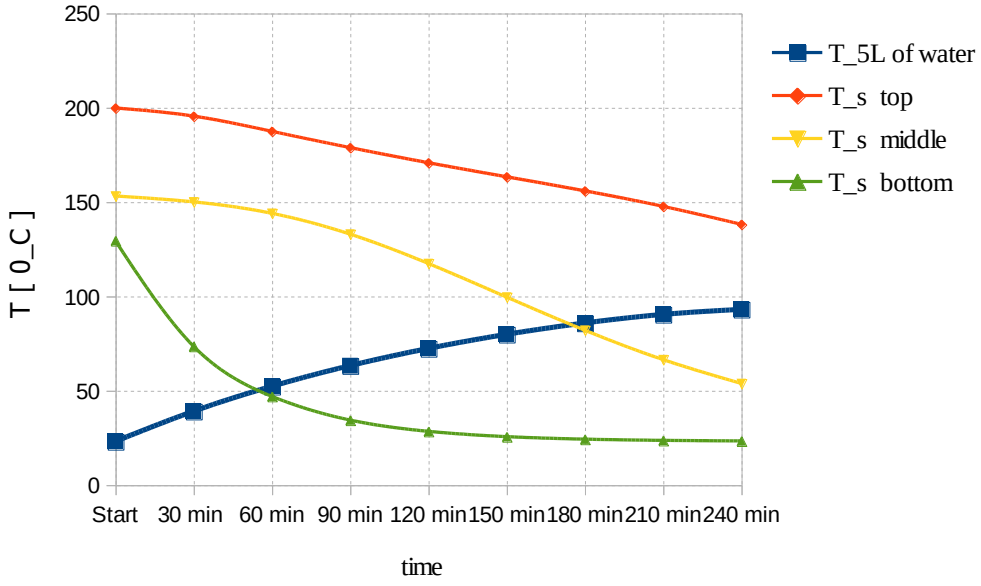

Figure 5-19: Temperature of storage versus temperature of water during the boiling of 5 liters of water with 0.0048kg/S mass flow rate for the lower direct normal irradiance.

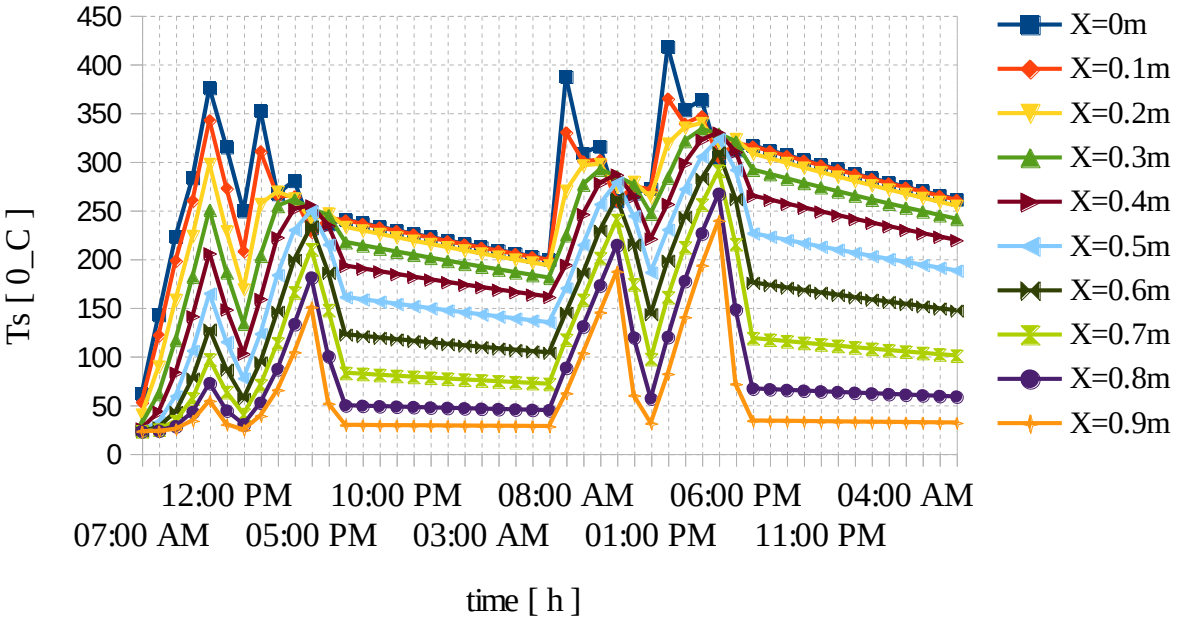

Figure 5-20: Temperature of storage versus time for two consecutive days.

Figure 5-20 shows the temperature of storage during charging and discharges for two consecutive days. The cooking was done for 2 hours from 11:00 AM to 1:00 PM and 5:00 PM to 7:00 PM for two reasonable cycles in a day. The simulation was carried out on March 16 and March 17 of beam solar irradiance. The cooking is conducted using valves.

Table 5-5 explains the different amounts of energies and efficiencies of cooking for the conditions of the highest and lowest DNI from sunrise to sunset (7 AM to 5 PM).

Table 5-5: Comparison of efficiencies for the conditions of higher and lower DNI

Energy and Efficiency	DNI, highest	DNI, Lowest
Solar energy on Aperture area [MJ]	60.11	18.11
Stored energy [MJ]	40.11	12.85
Storage efficiency (%)	66.71	70.90
The volume of water boiled	5liter in 53 min	5liter in 4h
Useful cooking energy [MJ]	1.45	1.45
The thermal efficiency of the cooker (%)	45	31.12
The overall efficiency of the cooker (%)	30	22.08

Table 5-6 explains the results of the temperatures and efficiencies when the cooking is carried out by conduction and enhanced by forced convection.

Table 5-6: Efficiency for the condition of the highest DNI

Energy and Efficiency	Conduction	Forced Convection
Water temperature at 53 min for 5 liters [^{0}C]	87	93
Useful cooking energy [MJ]	1.344	1.45
Stored energy for 11h charging [MJ]	40.10	40.10
Solar energy on aperture [MJ]	60.11	60.11
Storage efficiency (%)	66.71	66.71
The thermal efficiency of the cooker (%)	28.72	45
The overall efficiency of the cooker (%)	19.14	30

Table 5-7: Efficiency for the condition of the lowest DNI

Energy and Efficiency	Conduction	Forced Convection
Temperature of 5 liters of water [^{0}C]	49.88 at 2.5h	93 at 4h
Useful cooking energy [MJ]	0.562	1.463
Stored energy for 11h charging [MJ]	12.85	12.85
Solar energy on aperture [MJ]	18.11	18.11
Storage efficiency (%)	70.90	70.90
The thermal efficiency of the cooker (%)	19.26	31.12
The overall efficiency of the cooker (%)	13.65	22.08

Figure 5-21 shows the degradation of the thermal storage without cooking operation in 8 days with a final average temperature of 38 ^{0}C. In this context, the storage interacts with the environment through fiberglass insulation having a thickness of 75 mm.

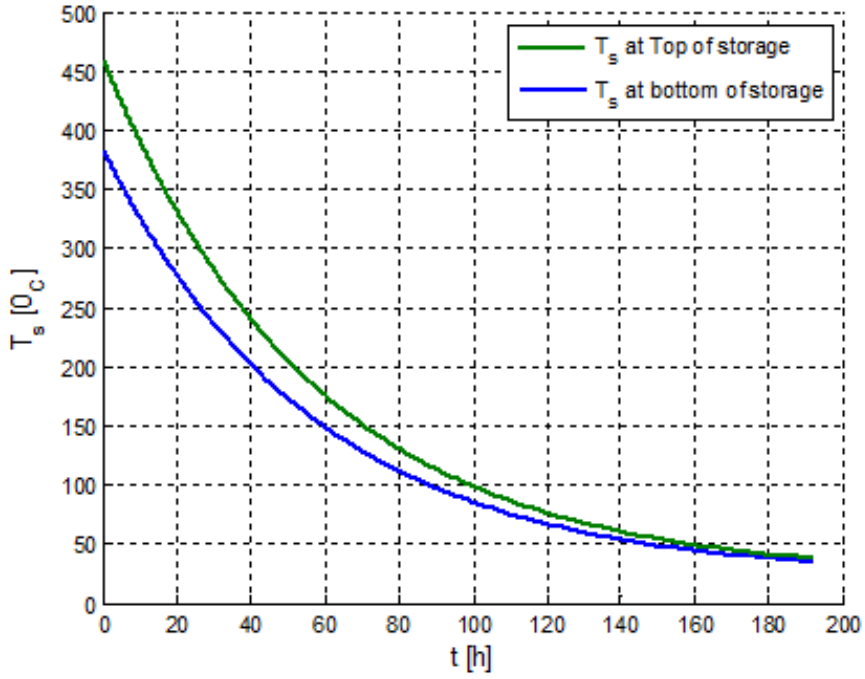

Figure 5-21: Temperature of storage when without operation with heat losses to the environment through insulation thickness of 75mm

5.5.2. Charging and Discharging of a Pebble Bed Thermal Storage using Semera Solar Radiations

Charging Conditions

In this charging condition, the beam solar radiations of Semera have been taken as the source of energy for heating the air in the receiver of the parabolic solar concentrator, and the heated air is used for charging the packed bed storage. This is used in analyzing the performance of a pebble bed thermal storage for the Semera site location. The solar radiations of Semera were analyzed in chapter 4 and categorized as diffuse and beam solar irradiance. In Figure 5-22 and Figure 5-24 temperatures of a pebble bed, thermal storage for the daily minimum beam solar irradiance in August and maximum in April in the recommended days were analyzed with respect to charging hours from 7:00 AM to 5:00 PM. The maximum temperatures of a packed pebble reach 410^{0}C and 742.8^{0}C at the top, and 250.1 ^{0}C and 529.46^{0}C at bottom surfaces of the storage for August and April respectively.

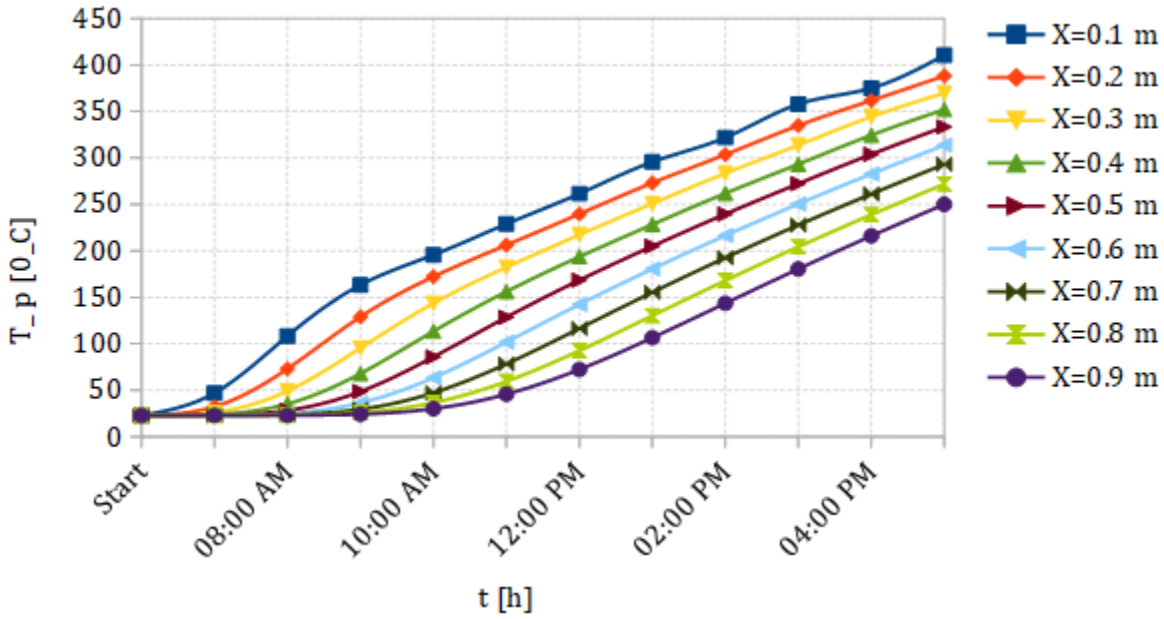

Figure 5-22: T_p versus charging hours from 07:00 AM to 6:00 PM for Semera solar radiation in August for the recommended day.

On the other hand, the temperatures of air in the storage are simulated for the days of maximum and minimum beam solar irradiance as it is shown in Figure 5-23 and Figure 5-25.

Therefore, the maximum temperatures of the air are 435^{0}C and 765.6^{0}C at the top of the storage for minimum and maximum beam solar irradiance respectively.

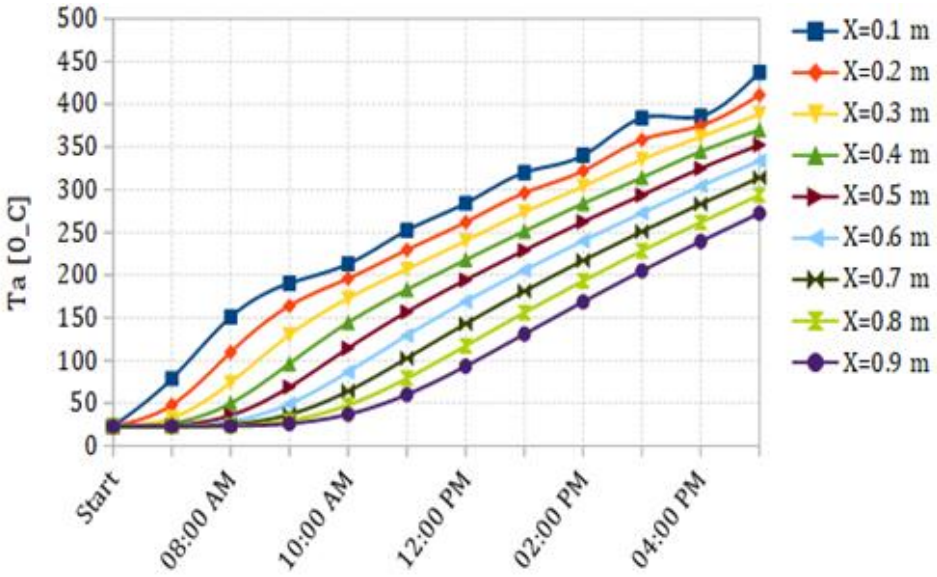

Figure 5-23: T_a versus charging hours from 07:00 AM to 5:00 PM for Semera solar radiation in August for the recommended day.

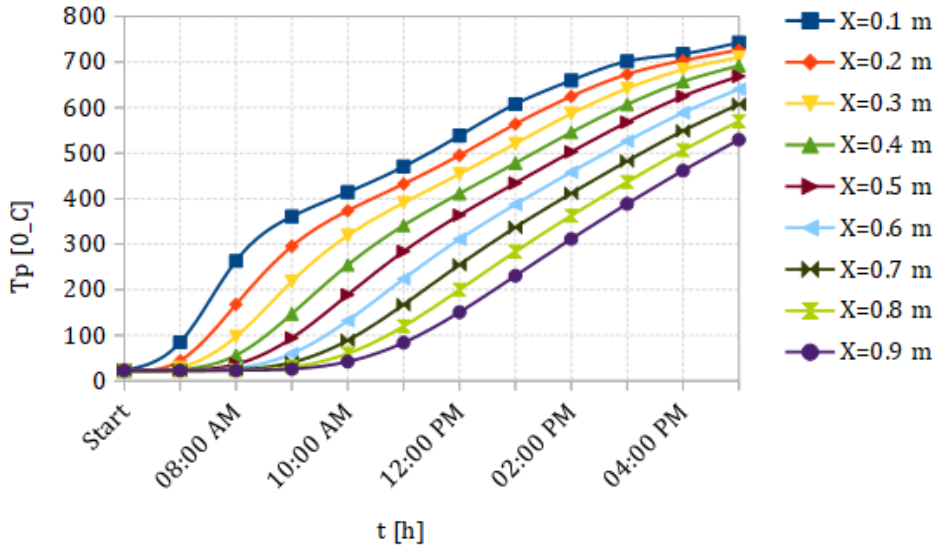

Figure 5-24: T_p versus charging hours from 07:00 AM to 11:00 PM for Semera solar radiation in April for the recommended day.

As it is shown in Figure 5-24, the transient temperature of the packed bed pebbles along the length of the storage has been discussed. The maximum temperatures on the top and bottom faces are about 742.8^{0}C and 529.5^{0}C respectively in April. The average temperature

of the storage after charging for 11 hours is about 654.1^{0}C. The same analysis has been presented for air in the storage as shown in Figure 5-25. The maximum and minimum temperatures range in the storage are about 765.6 ^{0}C and 570.7^{0}C at the top and bottom respectively.

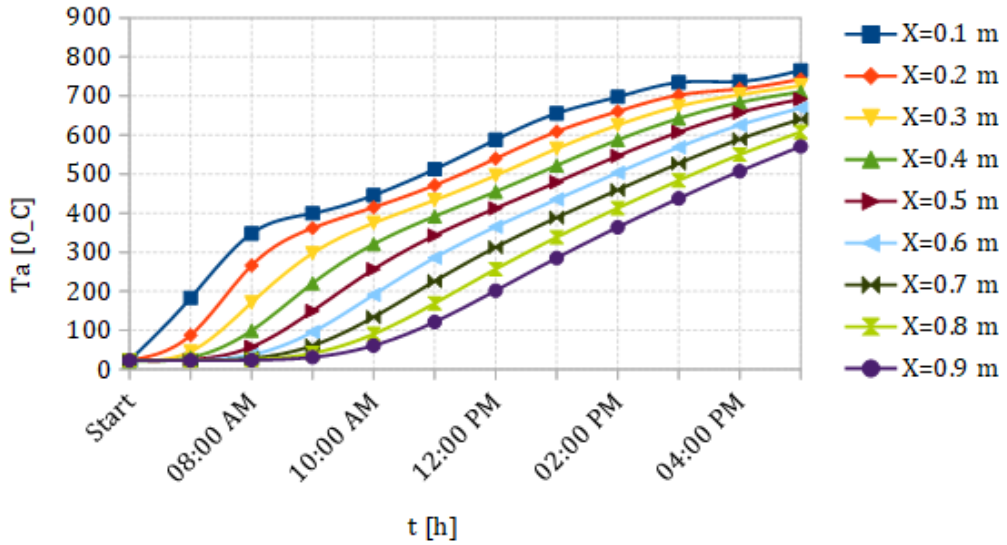

Figure 5-25: T_a versus charging hours from 07:00 AM to 6:00 PM for Semera solar radiation in April for the recommended day.

Therefore, the packed bed thermal storage can store 60.3 MJ and 29.47 MJ of energy after charging for 11 hours Semera solar radiations as it is illustrated in Figure 5-26. The average annual energy storage in the day has been carried out about 46.28 MJ of energy after charging from 7:00 AM to 5:00 PM. This amount of average energy was calculated for all months of the year at each recommended days.

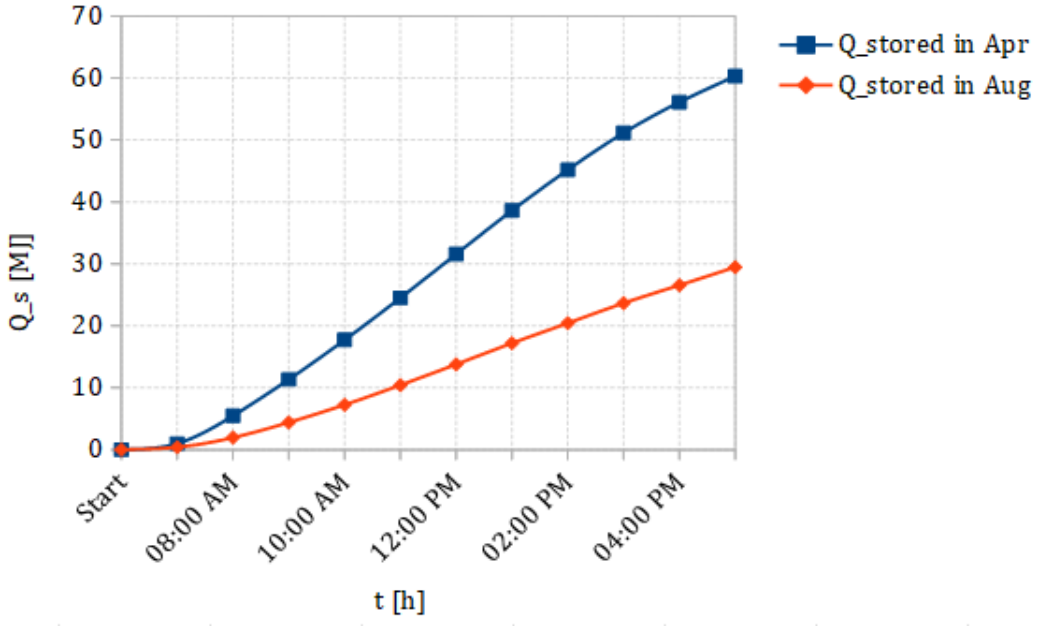

Figure 5-26: Energy stored versus charging hours for both maximum and minimum direct normal irradiance for semera's location.

Discharging Conditions

To simulate the discharging temperature of storage and water boiling, the initial and boundary conditions are the same as Addis Ababa's conditions as it was shown in Table 5-4. For this site, the forced convection and conduction heat transfer modes are concerned for discharging the stored energy from the packed bed of pebbles. This means, the pot is set on the top of storage and the discharging Fan is used to force the air from the ambient to the storage from the bottom throughout the storage. So, the heat is transferred to the pot by the convection and conductions.

Considering this heat transfer mode, the boiling temperatures for 5L of water and degrading temperature of the storage have simulated with respect to discharging hours as shown in Figure 5-27. Hence, the temperature of the water reaches 93 ^{0}C after discharging for 32 minutes. So, the top, middle and bottom temperatures of the storage degraded to 737.63 ^{0}C, 642.1^{0}C, and 252.72^{0}C respectively.

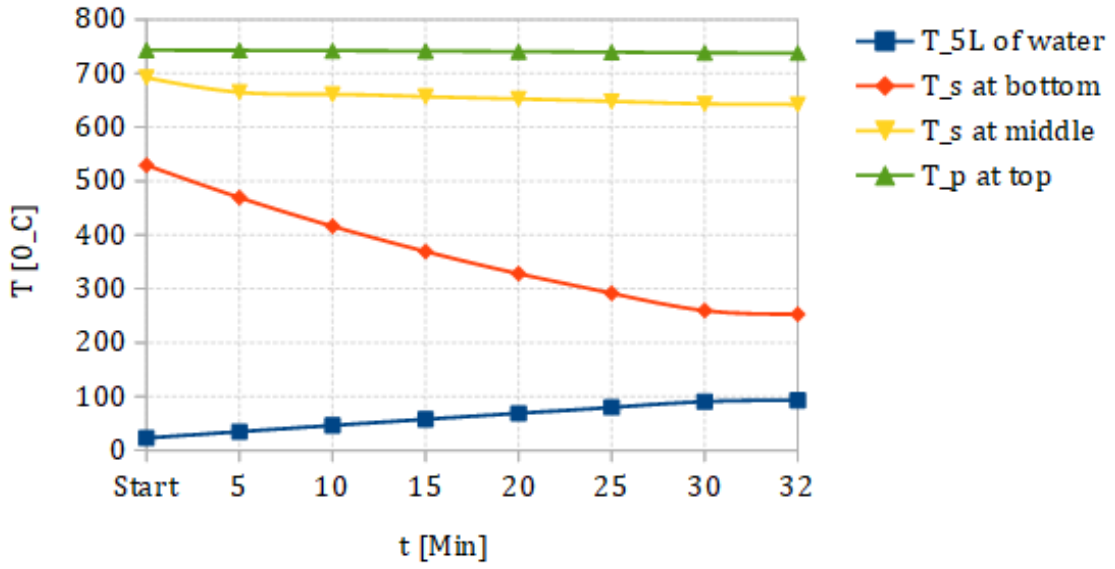

Figure 5-27: Temperature of storage versus temperature of water during the boiling of 5 liters of water with 0.0048kg/s mass flow rate for the maximum direct normal irradiance.

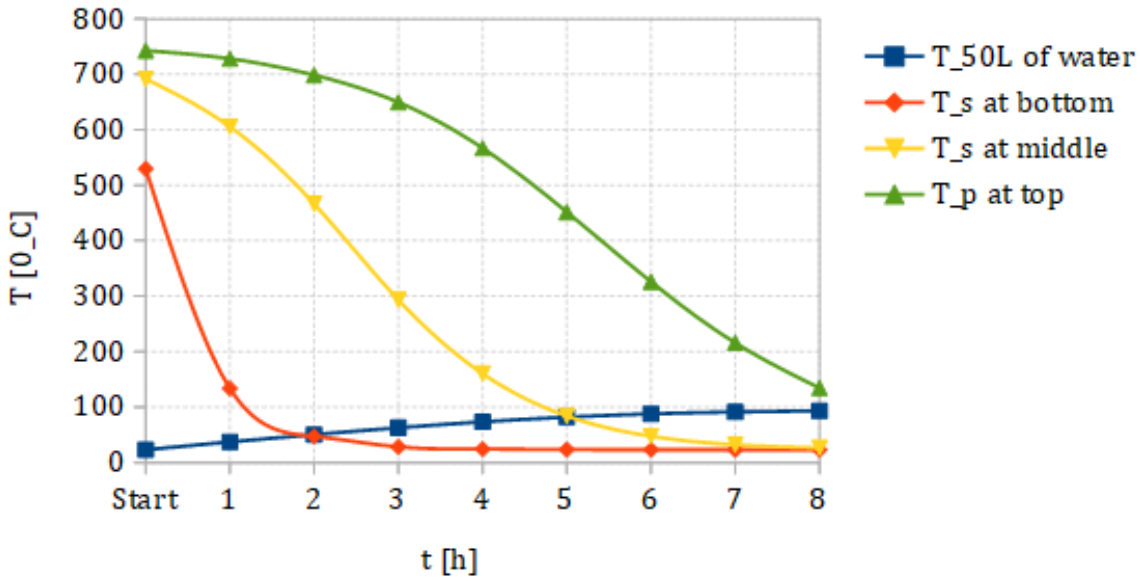

Figure 5-28: Temperature of thermal storage and 50 liters of water during discharging with 0.0048kg/s mass flow rate of air in april for the recommended day.

Figure 5-28 shows the capacity of the storage used to boil 50 liters of water and the temperature degradation during the discharging hours and the time at which the boiling of water reaches 93 ^{0}C have discussed in the figure. After 8 discharging hours the water temperature reaches 93^{0}C and the top, middle, and bottom of the storage reach about 134.4^{0}C, 26.2^{0}C, and 23^{0}C respectively.

In the case of the minimum direct solar irradiance, the following discharging conditions are simulated in Figure 5-29 and Figure 5-30. In Figure 5-29, 5 liters of water have been considered for simulating its boiling temperature and degrading temperature of water based on the water boiling test standard principle. Therefore, the temperature of the water reaches 93 ^{0}C after 63 discharging minutes, and the temperatures of the storage at the top, middle, and bottom of the storage have degraded to 392.15^{0}C, 293.15^{0}C, and 68.92^{0}C respectively.

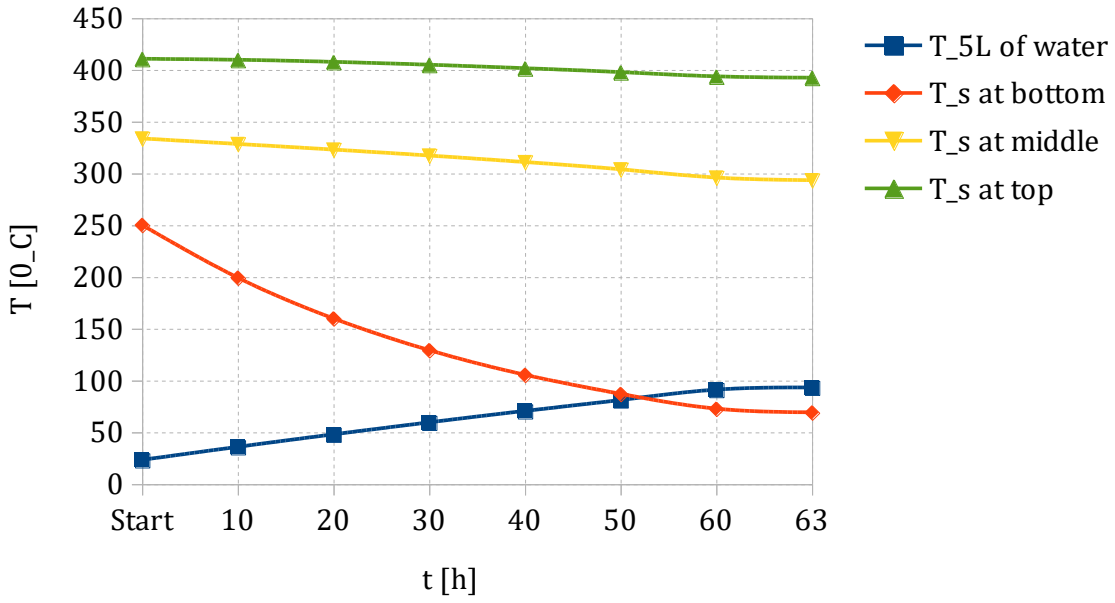

Figure 5-29: temperature of storage versus temperature of water during the boiling of 5 liters of water with 0.0048kg/s the lowest DNI

However, another 21 liters of water are taken for simulating the temperature of storage during discharge time which is presented in Figure 5-30. The modeled storage in August can boil 21 liters of water after discharging for 6.5 hours. The top, middle, and bottom parts of the storage temperature reach 136.36^{0}C, 29.78^{0,} and 23.01^{0}C respectively.

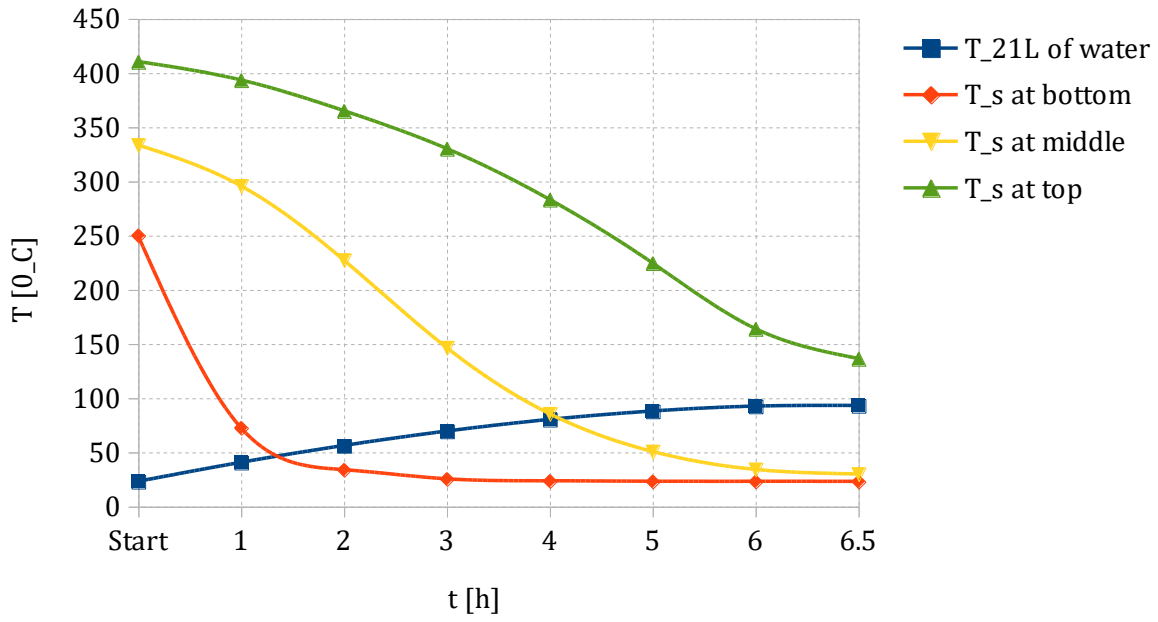

Figure 5-30: Temperature of thermal storage and 21 liters of water during discharging with 0.0048kg/s in the August for the represented day

Table 5-8: Comparisons of efficiencies and energies of solar storage for Semera solar radiations

	DNI Maximum	**DNI Minimum**
Solar Energy [MJ]	91.49	49.92
Stored Energy [MJ]	60.3	29.47
Useful Energy [MJ]	1.45	1.45
The volume of water boiled [Liter]	5	5
Cooking rate [Min]	32	63
Stored Efficiency [%]	65.9	59.1
Cooking (thermal) Efficiency [%]	55.5	52.7
Overall Efficiency [%]	36.6	31.1

5.6. Comparisons of a Pebble Bed Storage Performance for Addis Ababa and Semera Solar Radiations

In this topic, energy storage, thermal efficiency, stored efficiency, and overall efficiency have been discussed based on the solar radiation of the site. Table 5-9 and Figure 5-31 deal with the comparison of these parameters.

Table 5-9: Comparisons of a pebble bed solar storage performance for Addis Ababa and Semera average beam Solar Irradiance

	Addis Ababa			Semera		
	Highest I_b	Lowest I_b	Average I_b	Highest I_b	Lowest I_b	Average I_b
E_{solar} [MJ]	60.1	18.1	41.2	91.49	49.92	73.54
E_{stored} [MJ]	40.1	12.85	28.5	60.3	29.47	46.24
η_{stored} [%]	66.7	70.9	69.1	65.9	59.1	62.6
$\eta_{thermal}$ [%]	45	31.1	38.2	55.5	52.7	52.53
$\eta_{Overall}$ [%]	30	22.08	26.5	36.6	31.1	32.9

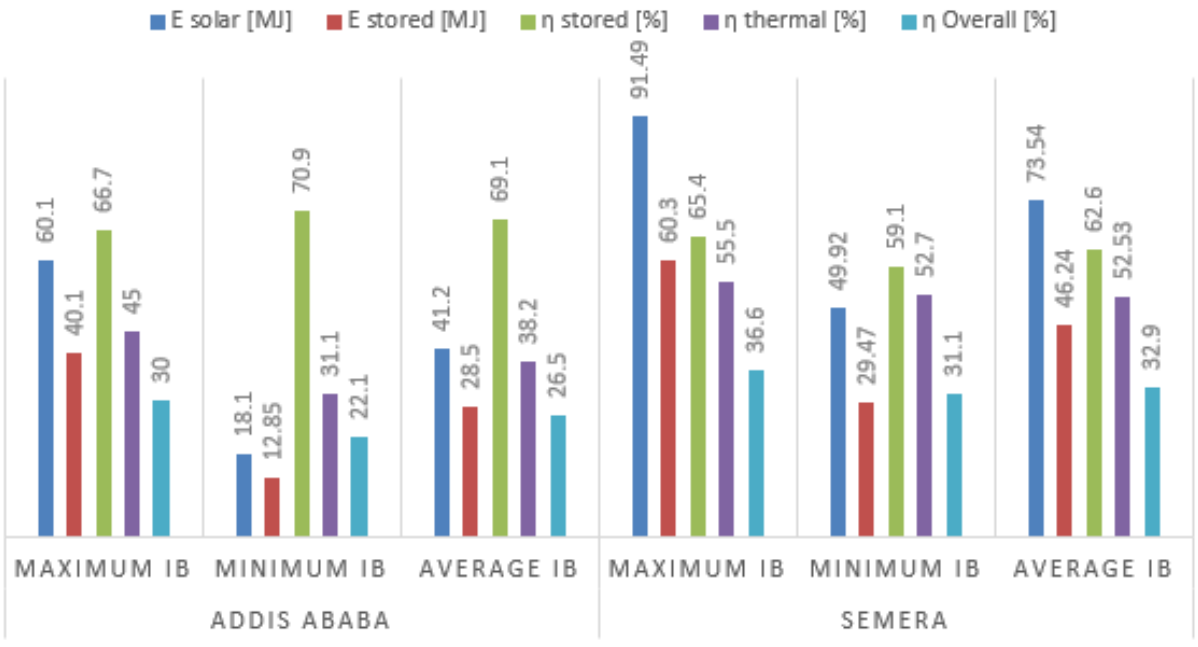

Figure 5-31: Comparison of energy and efficiencies of pebble bed thermal storage for Addis Ababa and Semera solar conditions

CHAPTER SIX:

6. PERFORMANCE ANALYSIS OF A PCM THERMAL STORAGE FOR COOKING

6.1. Physical Concept

Solar radiation is concentrated on the receiver or absorber on the focal point of parabolic dish concentrator as shown in Figure 5-1 and then thermal energy is transported from the absorber of the parabolic dish by hot air to the thermal storage ,which is the phase change materials (PCM) in this case. A charging fan circulates the air from the outlet of the thermal storage through the receiver of the parabolic dish and then through thermal storage. The spherical PCM capsules are packed in the cylindrical storage tank leaving sufficient space for the hot air flow. The cylindrical tank is insulated with fiber glass. Hot air pipes connect the discharge side of the receiver to the inlet of thermal storage and the outlet side of the thermal storage to the suction side of the receiver. The receiver sidewalls and the pipes are also insulated with mineralwool.

The design parameters of the thermal storage based on energy demand of cooking presented in chapter 4 , which are used for the simulations and performance analysis of PCM thermal storage in next sections, are presented in Table 6-1. In addition, thermo-physical properties of PCM required for the same purpose are given in Table 6-2.

Table 6-1: Design parameters of the PCM thermal storage system

Parameters	Nomenclature	Values
Height of tank	H	0.5m
Diameter of tank	D	0.3m
Porosity	ε	0.4
The diameter of PCM capsules	d	25mm
Mass flow rate	$\dot{m}_a$	0.0048kg/s

Table 6-2: 60%$NaNO_3$ – 40% KNO_3 PCM thermo-physical properties [20]

Parameters	Nomenclature	Values	Units
Density at temp≤220 °C	ρ_s	1800	[kg/m^3]
Density at temp≤220 °C	ρ_l	1700	[kg/m^3]
Thermal conductivity	k	0.8	[W/mK]
Latent heat of fusion	h_{fus}	108.67±1.43	[kJ/kg]
Specific heat capacity	$C_{ppcm,s}$	1.25	[kJ/kg K]
Specific heat capacity	$C_{ppcm,l}$	1.6	[kJ/kg K]
Melting temperature of PCM	T_m	220	[^{0}C]

6.2. Mathematical Model

For modeling of PCM thermal storage the following assumptions were made.

- The PCM capsules are uniform, homogenous, and isotropic bodies with thermophysical properties constant with temperature;
- Natural convection in the liquid phase of PCM is negligible
- The hot air temperature does not vary radially or can be approximated as uniform on a layer .

Therefore, one dimensional two-phase energy equations can approximate the heat transfer between air and PCM capsules during charging and discharging from which the time dependent spatial temperature distributions can be determined.

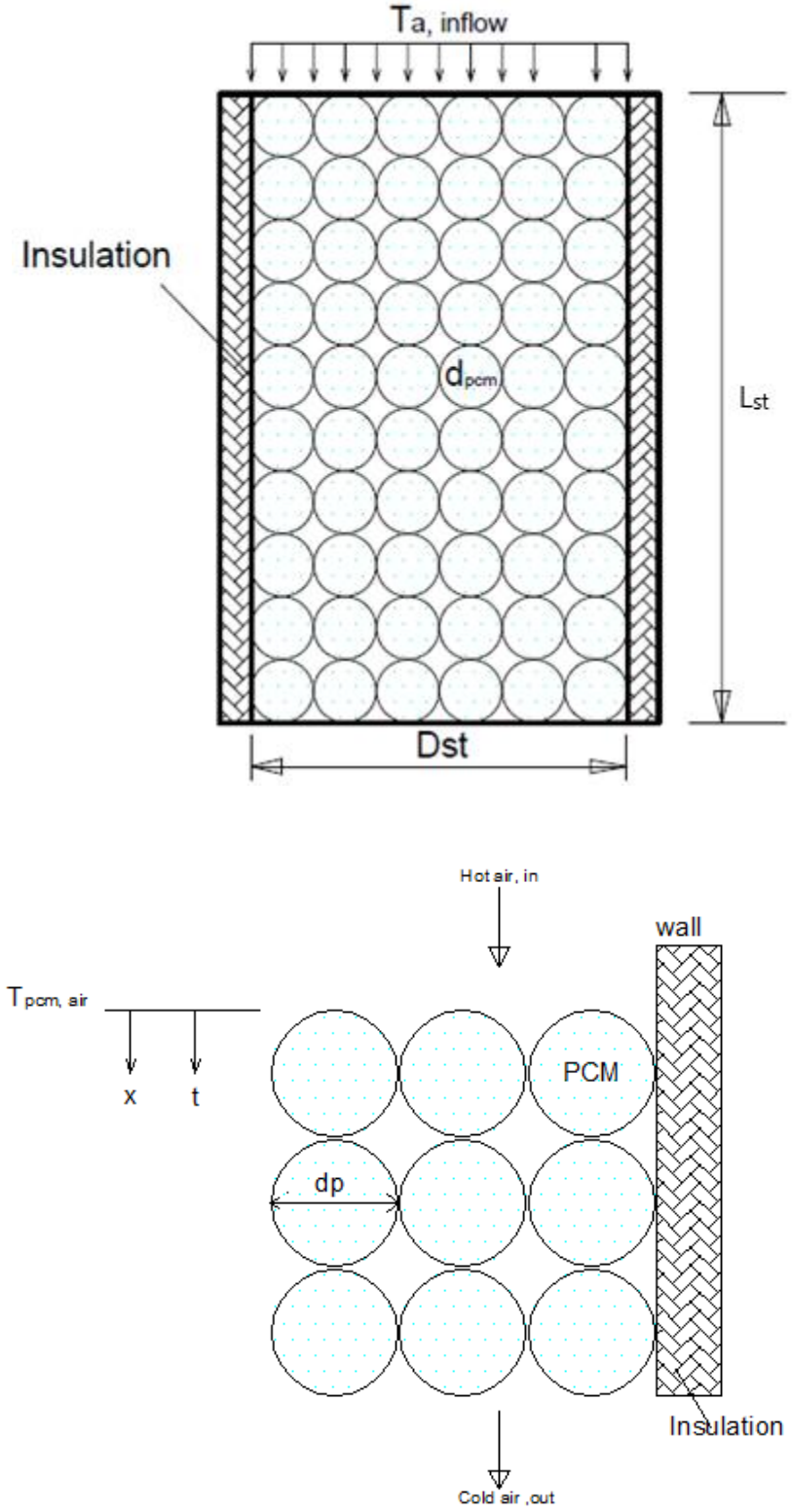

Figure 6-1: Schematic diagram showing the geometry of the packed PCM.

Transient heat transfer equation for air

The partial differential equation for the air is the same as that of the pebble bed case

$$\varepsilon A_{cs}\rho_a c_{pa}\frac{\partial T_a}{\partial t}+h_v A_{cs}(T_a-T_{pcm})+\dot{m}c_{pa}\frac{\partial T_a}{\partial x}+U_{wal}PL(T_a-T_{amb})=0 \quad (6.1)$$

It shall be noted that ε (porosity) is the volume fraction of air ,while 1-ε is the volume fraction of pebbles.

Transient heat equations for solid PCM capsules

As it was discussed on pebble bed thermal energy storage, the modeling of heat transfer within PCM follows a similar procedure for the solid phase. The only difference is when the PCM starts melting and enters the liquid-solid phase region.

The change of temperature of PCM capsules with a change in time is determined as the convective heat gains from the air to the PCM capsules plus the net heat trasnfer in axial direction (from PCM capsules beneath and above).

$$\rho_{pcm}(1-\varepsilon)A_{cs}c_{ppcm,s}\frac{\partial T_{pcm}}{\partial t}-h_v A_{cs}(T_a-T_{pcm})-\frac{\partial}{\partial x}(k_{pcm}A_{cs}\frac{\partial T_{pcm}}{\partial x})=0 \quad (6.2)$$

Governing equation for melting fraction in the latent heat section

The heat transfer from solid-liquid phase transformation region of PCM require can be modeled by using molten fraction with the time difference. The molten fraction is used to predict the quality of a liquid PCM and is given by

$$X=\frac{m_{liq,pcm}}{m_{total}} \quad (6.3)$$

Where, X is the molten fraction of PCM

After the PCM temperature reaches the fusion temperature, the energy supplied to the PCM is stored in the material in the form of latent heat. The rate of change of the enthalpy of PCM is caused by the rate of heat obtained from PCM, $\dot{Q}$.

$$\frac{dH}{dt}=\dot{Q} \quad (6.4)$$

$$\frac{d(\rho_{pcm}V_{pcm}h)}{dt}=\dot{Q} \quad (6.5)$$

$$\rho_{pcm} V_{pcm} \frac{dh}{dt} = \dot{Q} \tag{6.6}$$

$$\rho_{pcm} V_{pcm} \frac{d(C_{ppcm,s} T + X h_L)}{dt} = \dot{Q} \tag{6.7}$$

Where: h_L is the latent heat of PCM (J/kg), ρ_{pcm} is density of PCM (kg/m^3), V_{pcm} is the volume of the PCM (m^3), $C_{PPCM,S}$ is the specific heat of solid PCM $\left(\frac{J}{kgK}\right)$, X is the molten fraction (-).

$$\rho_{pcm} V_{pcm} \left[C_{ppcm,s} \frac{dT}{dt} + \frac{dX h_L}{dt} \right] = \dot{Q} \tag{6.8}$$

There is no temperature change during phase transition and the first derivative of the temperature is zero:

$$\frac{dT}{dt} = 0$$

$$\rho_{pcm} V_{pcm} h_L \frac{dX}{dt} = \dot{Q} \tag{6.9}$$

The liquid fraction is calculated from

$$\frac{dX}{dt} = \frac{\dot{Q}}{\rho_{pcm} V_{pcm} h_L} \tag{6.10}$$

Dividing both side by the total volume(void plus PCM) and simplifying yields

$$(1-\varepsilon)(\rho h)_{eff,fus} \frac{dX}{dt} = h_v (T_a - T_{PCM}) \tag{6.11}$$

$$\frac{dX}{dt} = \frac{h_v}{(1-\varepsilon)(\rho h)_{eff,fus}} (T_a - T_{PCM}) \tag{6.12}$$

$$\text{Where, } (\rho h)_{eff,fus} = \frac{\rho_{pcm} h_L V_{pcm}}{V_{total}}$$

Transient heat transfer equations for liquid PCM capsules

The change of temperature of liquid PCM capsules with a change in time is determined as the convective heat gains from the air to the PCM capsules .

$$\rho_{pcm,l} (1-\varepsilon) A_{cs} c_{ppcm,l} \frac{\partial T_{pcm}}{\partial t} - h_v A_{cs} (T_a - T_{pcm}) = 0 \tag{6.13}$$

Where, $\rho_{pcm,l}$ and $c_{ppcm,l}$ are density and specific heat capacity of PCM for liquid region

6.3. Computational Model

Using finite difference method , the one dimensional two phases heat transfer partial diferential equations is discretized with forward difference in time. Hence, Equation (6.1) of heat transfer fluid or air is apparoximated by the following discrete equation.

$$\frac{T_{a,i}^{n+1}-T_{a,i}^{n}}{\Delta t}=\frac{h_v}{\varepsilon\rho_a c_{pa}}(T_{pcm,i}^{n}-T_{a,i}^{n})-\frac{\dot{m}}{\varepsilon A_{cs}\rho_a}\frac{T_{a,i+1}^{n}-T_{a,i}^{n}}{\Delta x}-\frac{U_{wal}P}{\varepsilon A_{cs}\rho_a c_{pa}}(T_{amb,i}^{n}-T_{a,i}^{n}) \tag{6.14}$$

Using forward differences for temporal discretiation and central difference scheme for spatial discretization, the partial difference equations of heat transfer in PCM capsules during solid phase or equation (6.2), the discrete equation shown in equation (6.15) is obtained.

$$\frac{T_{pcm,i}^{n+1}-T_{pcm,i}^{n}}{\Delta t}=\frac{h_v\left(T_{a,i}^{n}-T_{pcm,i}^{n}\right)}{(1-\varepsilon)\rho_{pcm,s}c_{ppcm,s}}+\frac{k_{pcm,s}}{(1-\varepsilon)\rho_{pcm,s}c_{ppcm,s}}\left(\frac{T_{pcm,i+1}^{n}-2T_{pcm,i}^{n}+T_{pcm,i-1}^{n}}{\Delta x^2}\right) \tag{6.15}$$

For heat transfer during phase change in the PCM, the melt fraction is obtained by discretization of equation (6.12) using forward differene scheme as follows.

$$X_i^{n+1}=X_i^{n}+\frac{\Delta t h_{eff,PCM}}{(1-\varepsilon)(\rho h)_{eff,fus}}\left(T_{a,i}^{n}-T_{pcm,i}^{n}\right) \tag{6.16}$$

Where *n* and *n+1* indicate the current and next time step. Also, *i* and *i+1* indicates the current and next space step.

The temperature of the PCM during the liquid phase is obatined by discretizing Equation (6.13) using forward differene method in time step as shown in equation (6.17).

$$\frac{T_{pcm,i}^{n+1}-T_{pcm,i}^{n}}{\Delta t}=\frac{h_v}{\rho_{pcm,l}(1-\varepsilon)c_{ppcm,l}}\left(T_{pcm,i}^{n}-T_{pcm,i}^{n}\right) \tag{6.17}$$

During recirculation, the temperature of the air is updated as follows considering the conentrated and absorbed solar radiation, the heat capacity of the absorber and the heat loss from the receiver .

$$T_{a,out}^{n+1} = T_{a,in}^{n} + \frac{\eta_{0p} A_{ap} I_b(t)}{\dot{m} c_{pa}} - \frac{A_{abs} U_{rl} (T_{abs}^{n} - T_a)}{\dot{m} c_{pa}} - \frac{\rho_{abs} V_{abs} C_{p,abs} (T_{abs}^{n} - T_{abs}^{n-1})}{\Delta t \dot{m} c_{pa}} \quad (6.18)$$

In similar way, the temperature of the absorber is updated considering the difference between the absorbed energy and the sum of heat loss from reciever and energy transported by air to the thermal storage is given in equation (6.19)

$$T_{abs}^{n} = T_{abs}^{n-1} + \frac{\left(\eta_{0p} A_{ap} I_b(t) - A_{abs} U_{rl} (T_{abs}^{n-1} - T_{amb}) - \dot{m} c_{pa} (T_a^{n} - T_a^{n-1}) \rho_{abs} V_{abs} c_{pabs}\right) dt}{\rho_{abs} V_{abs} C_{p,abs}} \quad (6.19)$$

Energy Balance During Water Boiling

During discharging heat is transferred from storage to the material to be cooked. Simplifying the cooking process as water boiling, the temperature variation is given as follows from the heat transferred to the pan minus the radiation and convection losses of the pan:

$$\dot{Q}_w = \dot{Q}_{pan} - \dot{Q}_{rad} - \dot{Q}_{conv} \quad (6.20)$$

Where,

$\dot{Q}_w$ is the rate of heat transfer to water

$\dot{Q}_{pan}$ is the rate of heat transfere to the pan $= \frac{T_{st} - T_w}{R_{th}}$

$\dot{Q}_r$ is the rate of radiation heat loss $= \sigma S_{\text{pan}} (T_w^4 - T_{amb}^4)$

$\dot{Q}_{cv}$ is the rate of convective heat loss $= hA_{csp}(T_w - T_{amb})$

Where, m_w is mass of water, C_{pw} is specific heat of water, R_{th} is thermal resistance of pan, T_w is temperature of water, T_{st} is temperature of storage, T_{amb} is ambient air, σ is Stefan boltzman constant S_{pan} is surface area of pan, h is convective heat transfer coefficient and A_{csp} is cross-sectional area of pan.

From energy balance , the temperature of the water is obtained as follows, discretizing equation (6.20) with forward difference scheme as follows .

$$T_w^{n+1} = T_w^n + \frac{\dot{Q}_{pan}(t) - (\dot{Q}_r(t) + \dot{Q}_{cv}(t))}{m_w c_{pw}} \Delta t \tag{6.21}$$

Efficiency

The stored thermal energy is obtained from the change in the enthalpy of the packed PCM capsules during charging.

$$E_{stored} = A_{cs}(1-\varepsilon)\int_0^L \left(\rho_{pcm,s} c_{pcm,s}(T_{pcm(x)} - T_o) + \rho_{pcm} X_{(x)} h_{L,pcm} + \rho_{pcm,l} c_{pcm,l}(T_{pcm(x)} - T_m)\right)dx \tag{6.22}$$

The thermal storage efficiency is determined as the ratio of the stored thermal energy to the solar energy incident on the receiver as follows.

$$\eta_{TS} = \frac{A_{cs}(1-\varepsilon)\int_0^L \left(\rho_{pcm,s} c_{pcm,s}(T_{pcm(x)} - T_o) + \rho_{pcm} X_{(x)} h_{L,pcm} + \rho_{pcm,l} c_{pcm,l}(T_{pcm(x)} - T_m)\right)dx}{\int_0^{t_c} I_b A_{ap} dt} \tag{6.23}$$

The cooking thermal efficiency is evaluated as the ratio of the useful heat transferred to the cooking media during discharging to the stored thermal energy for cooking.

$$\eta_{th} = \frac{m_w c_w (T_{w,f} - T_{w,i})}{A_{cs}(1-\varepsilon)\int_0^L \left(\rho_{pcm,s} c_{pcm,s}(T_{pcm(x)} - T_o) + \rho_{pcm} X_{(x)} h_{L,pcm} + \rho_{pcm,l} c_{pcm,l}(T_{pcm(x)} - T_m)\right)dx} \tag{6.24}$$

The overall efficiency of the cooking is evaluated as the ratio of the useful heat in the cooking media to the solar energy incident on the receiver surface during charging.

$$\eta_o = \frac{m_w c_w (T_{w,f} - T_{w,i})}{\int_0^{t_c} I_b A_{ap} dt} \tag{6.25}$$

6.4. Verification of Computational Model

Figure 6-2 shows comparison of average PCM temperature variation using computational model of this work and experimental test results using hytherm 600 as heat transfer fluid and A164 as PCM [23]. The thermal storage has 170mm diameter and 360mm height and contains 209 PCM capsules with 31 mm diameter. The porosity or void fratction is 0.6. The modeling was done under the same codition of the experiment. As it is shown in Figure 6-2, there is good coorelation between the computational model and experimental results

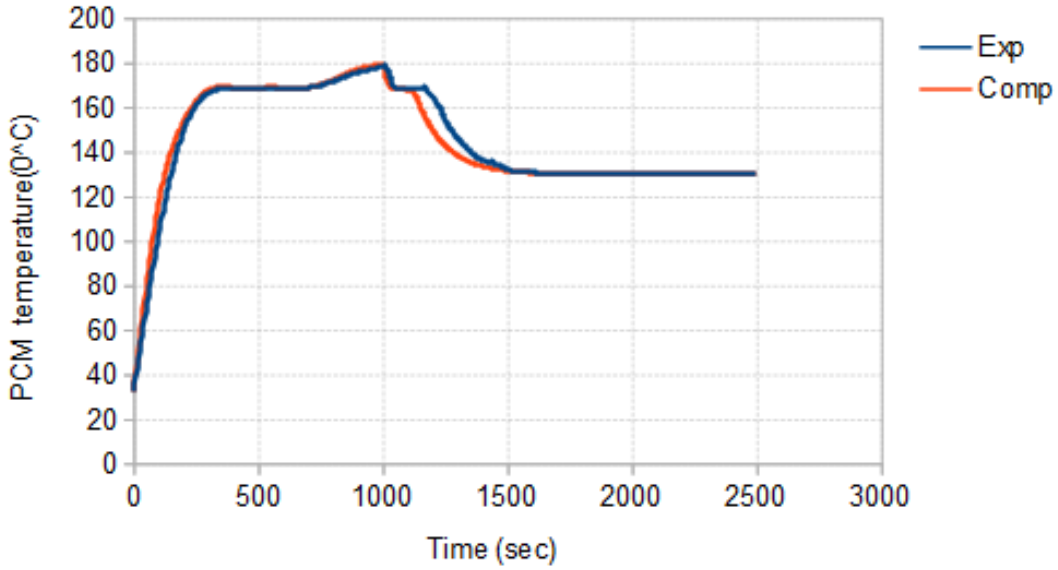

Figure 6-2: Validation of average temperature of PCM computational model by experimental results charging and discharging temperature of heat transfer fluid 180 ^{0}C and 130 ^{0}C, and fusion temperature of 168.7^{0}C.

Figure 6-3 shows comparison of average melt fraction result of computational model and experimental results as function for the same condition.

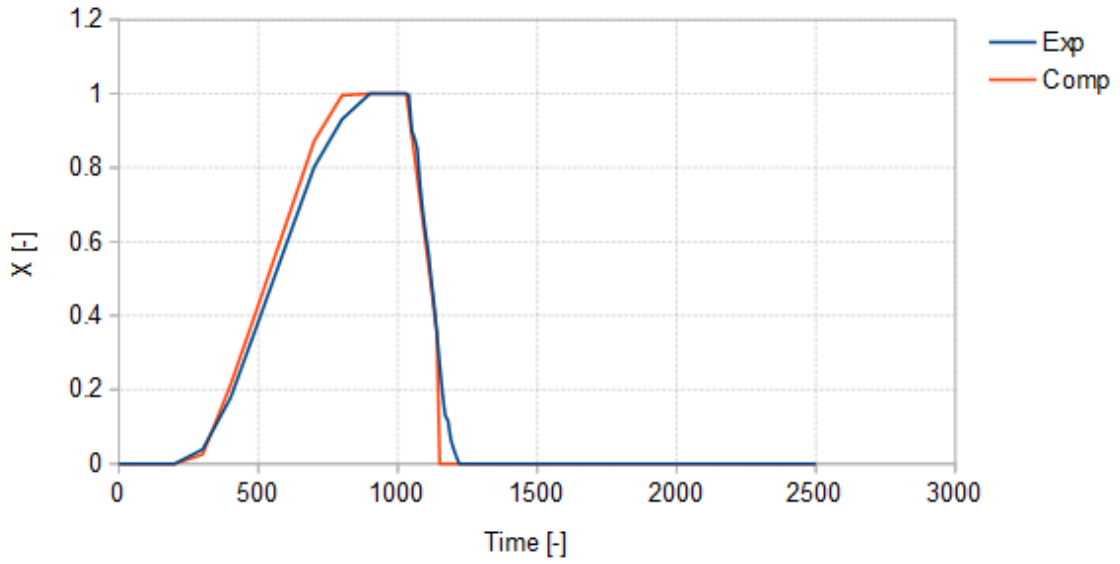

Figure 6-3*:* Validation of average melt fraction as function of time of computational model with experimental results for inlet charging temperature of 180 ^{0}C.

Figure 6-4 shows the comparison of the simulation model with experimental results of heat transfer fluid temperature at inlet and outlet of the thermal storage when the inlet charging temperature is 185^{0}C and good agreement is obtained.

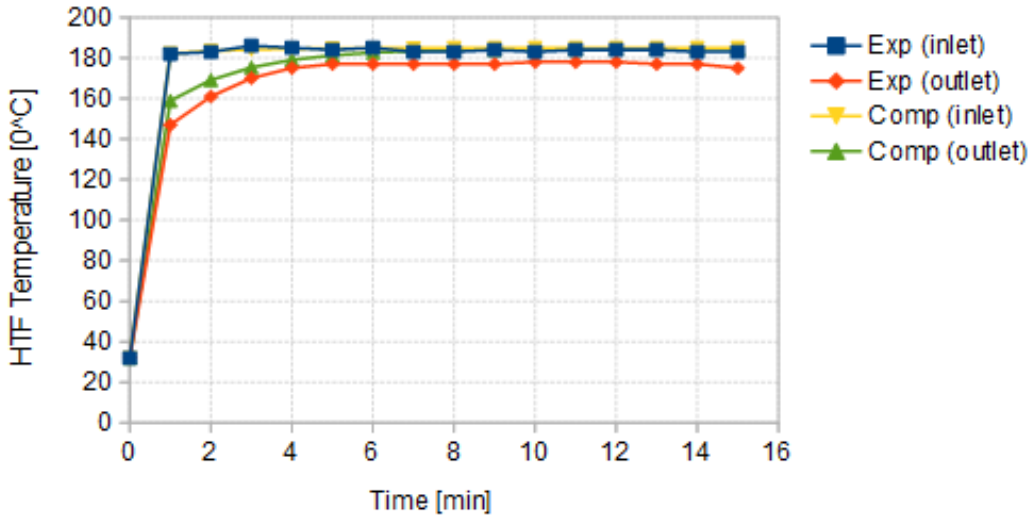

Figure 6-4*:* Validation of numerical model results with experimental test results [23] of heat transfer fluid temperature at inlet and outlet of thermal storage.

Based on comparison of of experimental test and computational model results, it can be concluded that the computational model of the PCM thermal storage can reasonably predict the performance of PCM thermal storage .

6.5. Results and Discussions

Simulation was conducted to predict the performance of PCM thermal storage at Addis Ababa and Semera using solar irradiance data of Addis Ababa and Semera and the thermal storage tank with dimensions of 300mm diameter and 500 mm height with 25mm diameter of PCM capsules as input using air as heat transfer fluid. For discretization, the thermal storage was divided into layers of 0.05m thickness. In addition, a time step of 1sec was used. The boundaries and the initial conditions imposed on this model are given in Table 6-3**.**

Table 6-3: Initial conditions, t = 0s and boundary conditions, t>0s adopted in numerical simulation

PCM	$T_{pcm}(i,n) = T_{init}$
	$x(i,n) = 0$
HTF	$\dot{m}_a(i,n) = const.$
	$T_a(0,n) = T_{in}(t)$

6.5.1. Simulation of PCM Thermal Storage under Addis Ababa Climatic Condition

Charging Conditions

Using the beam solar irradiance presented in chapter 4, the transient temperature distributions within the PCM thermal storage has been investigated. Also, the molten fraction of PCM and performance analysis are also discussed under this topic as per the solar irradiance of Addis Ababa. Here, the results of temperature distributions and molten fractions within the storage are shown in the consecutive results.

Figure 6-5 indicates the temperature variation in PCM thermal storage with charging time. The PCM thermal storage was charged using parabolic solar concentrator for 5 hours. The temperatures reached 543.99 ^{0}c, 410.74 ^{0}c and 275.38 ^{0}c at x=0.1m, 0.3m and 0.5m, respectively. The temperature of the PCM increased until the solid PCM start melting. Then,

the temperature becomes constant and the PCM starts melting. After the PCM is completely melted, the temperature of the liquified region until inreases. All PCM capsules in the storage are fully liquified after charging for 4.5 hours for the day of the highest solar radiation in the year for Addis Ababa case. In 5 hours, 23.13MJ of energy was stored in the PCM thermal storag..

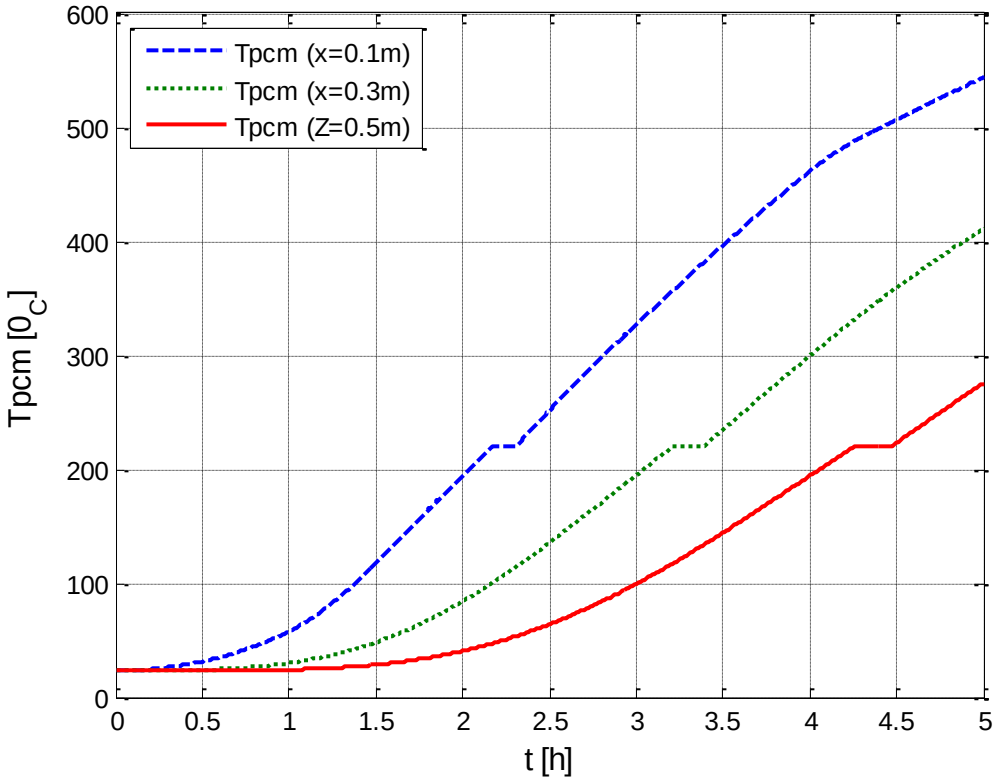

Figure 6-5: Temperature variation of PCM during charging for 5 hours for the day of maximum solar radiation at Addis Ababa.

Figure 6-6 shows comparison of temperature variation of air and PCM at the top and bottom of the thermal storage during charging for 5 hours. The PCM melted when the temperature reached 220 ^{0}C.

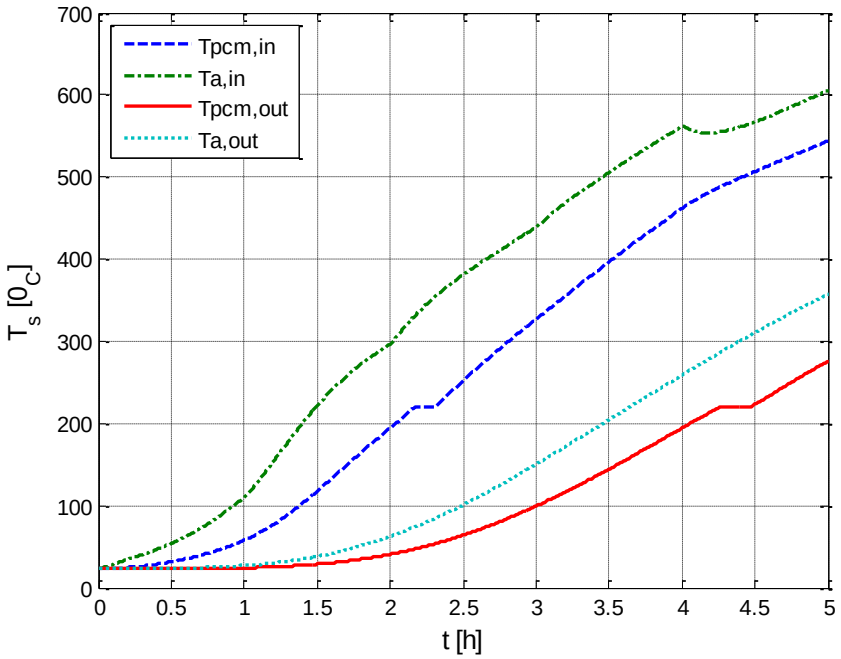

Figure 6-6: Comparison of the temperature of air and PCM during charging on maximum solar radaiation day at Addis Ababa.

Figure 6-7 shows the phase transformation and the melt fraction variation at 3 nodes during charging. The PCM was completely melted after 4.5 hours of charging.

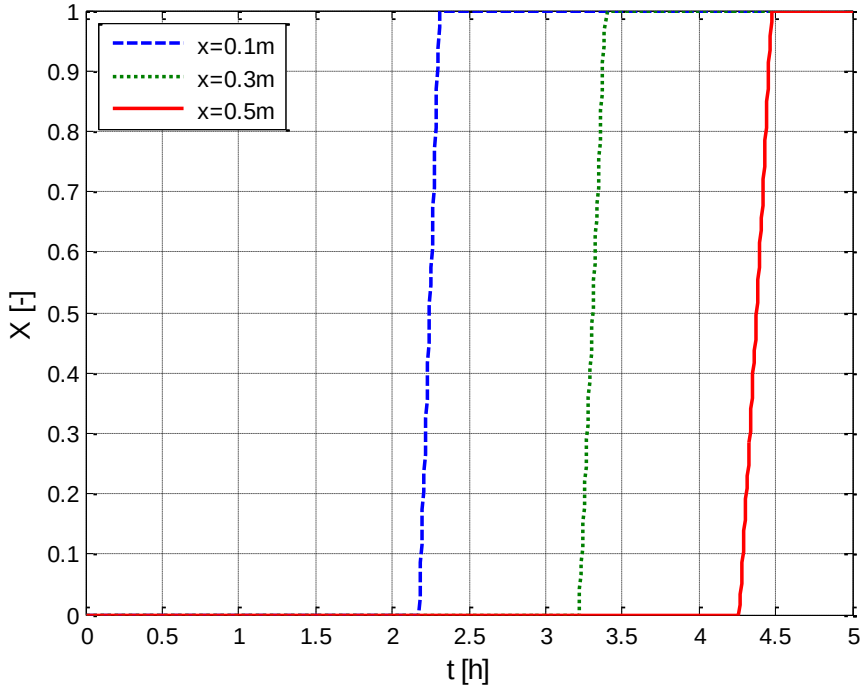

Figure 6-7: Melt fraction of PCM versus time during charging for the day of the highest solar radiation at Addis Ababa

Again, the temperature variation of PCM with time at different height of the thermal storage during charging are given in Figure 6-8 for the day of the lowest solar radiation at Addis Ababa which was in June. The PCM required more than 11 hours of charging to melt completely. At th end 18.56 MJ of energy was stored in the PCM thermal storage.

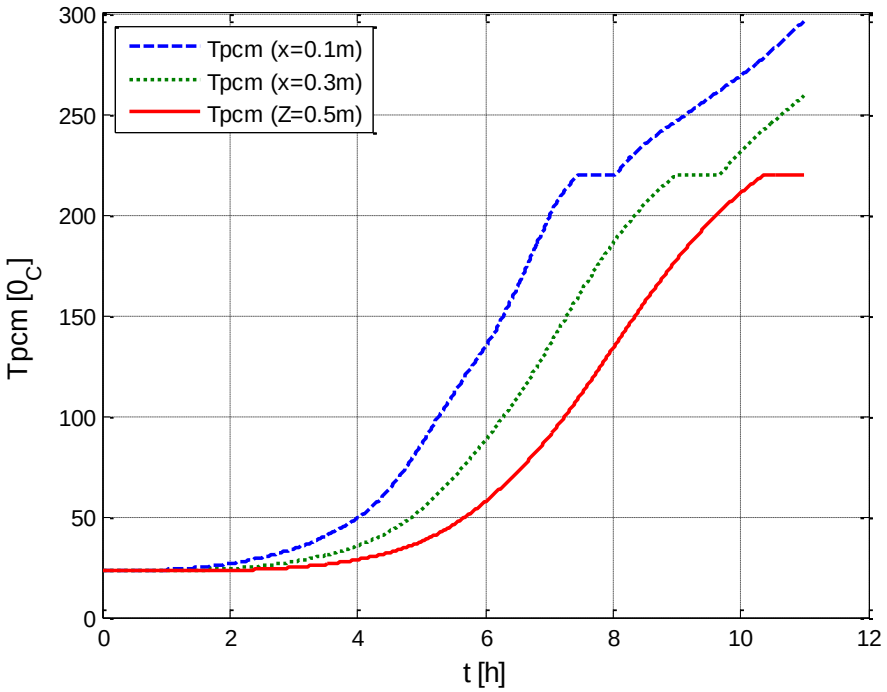

Figure 6-8: Temperature variation of PCM during harging for 11 hours for the day of minimum radaiation at Addis Ababa

The comparisons of inlet and outlet air temperature variation with temperature variation of the PCM at the same location during charging for 11 hours is illustrated in Figure 6-9. Figure 6-10 shows the phase transformation of PCM during charging. The PCM required 6.37 hours to liquify completely.

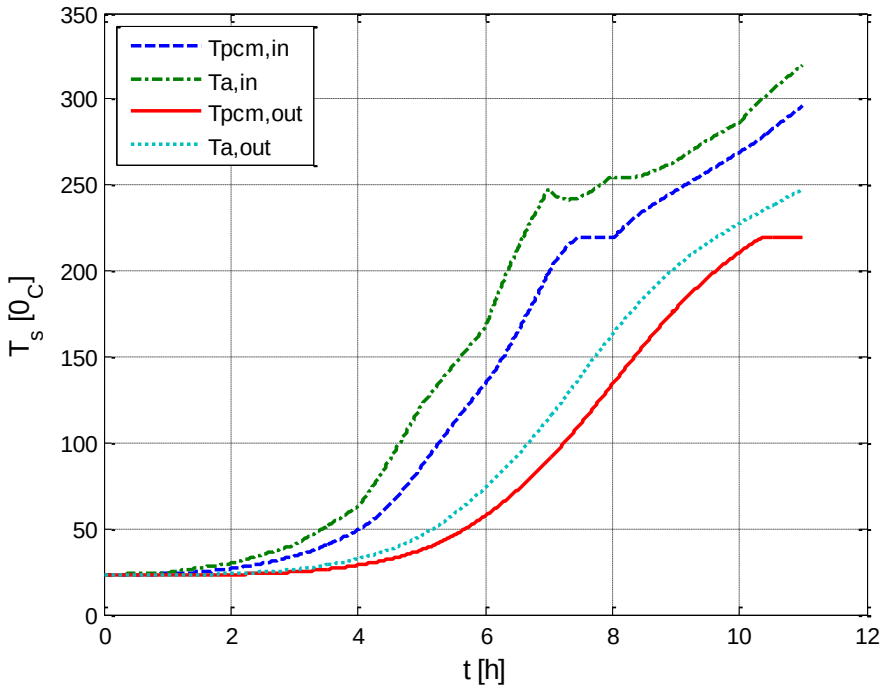

Figure 6-9: Comparison of the temperature variation of air and PCM during charging for the day of minimum radaiation at Addis Ababa

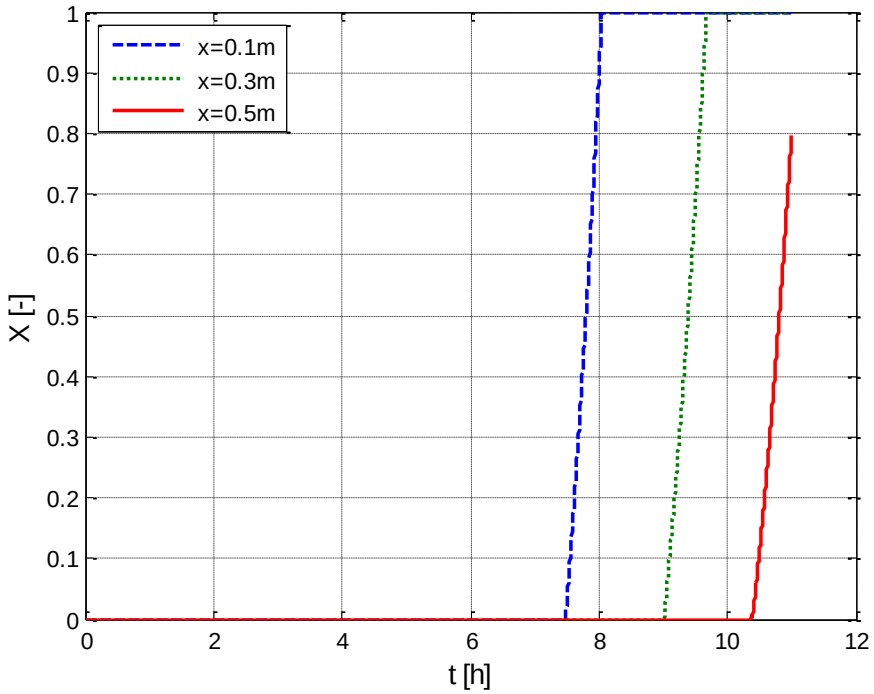

Figure 6-10: Melt fraction of PCM versus time during charging for the day of minimum solar radiation at Addis Ababa

6.5.2. Charging for the case of Semera solar radiations

The same simulations were also conducted for Semera in north east part of Ethiopia for the day of maximum solar radiation and the temperature variation of the PCM, the temperature variation of air at inlet and outlet of thermal storage and the melt fraction during a phase change were obtained after 3.5 hours of charging as shown from Figure 6-11 to Figure 6-13. As Semera has high solar radiation only 3.36 hours was required for complete melting of the PCM and the temperature at the top of thermal storage reached above 600 ^{o}C.

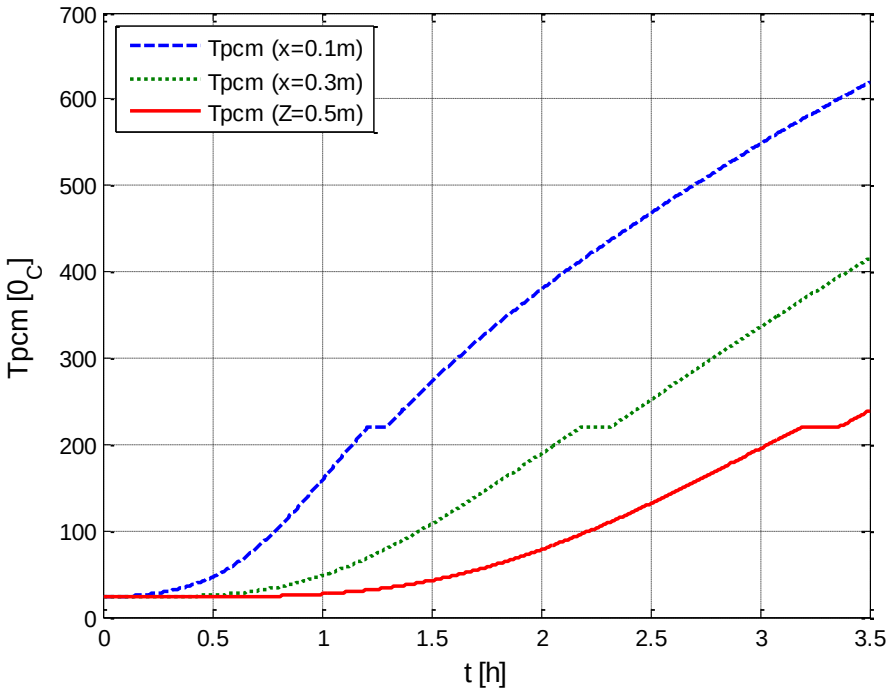

Figure 6-11: Temperature distributions of PCM versus charging hours for the day of the highest solar radiation in Semera.

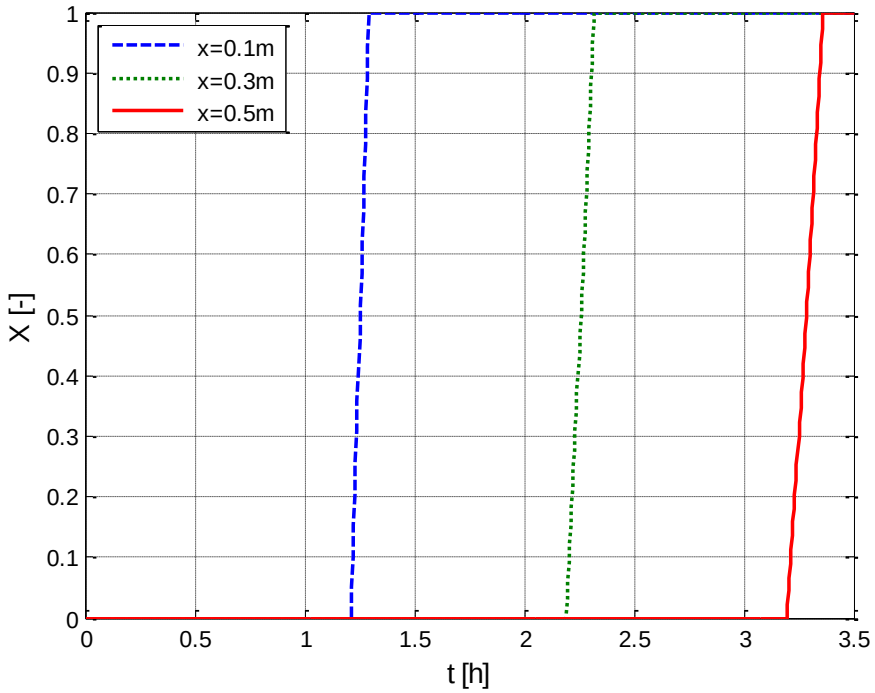

Figure 6-12: Melting fraction of PCM versus charging hours for the day of the highest solar radiation for Semera case

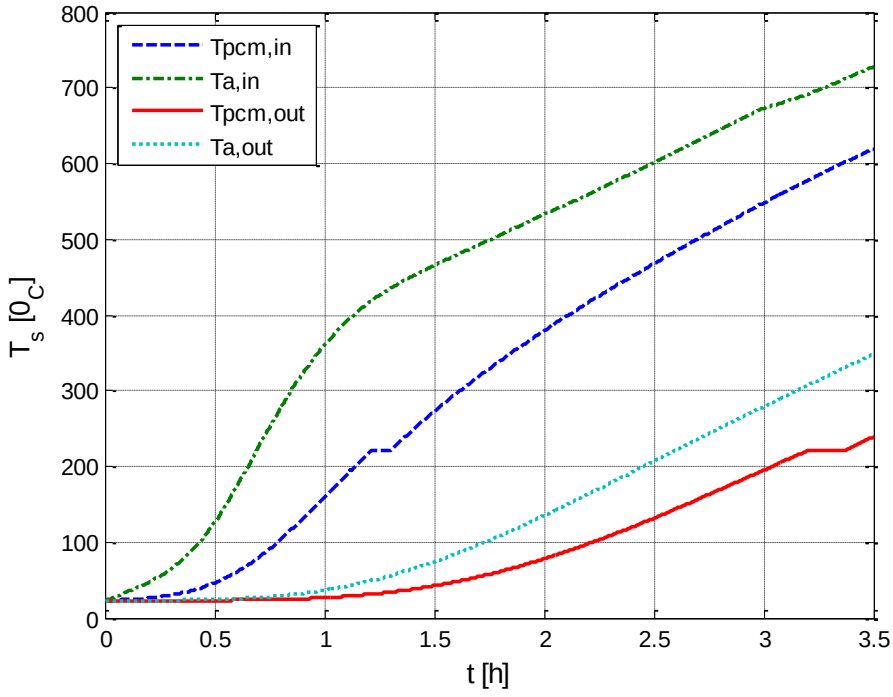

Figure 6-13: Comparison of temperatures variation of air and PCM at the inlet and outlet of the storage charging for 3.5 hours for the day of the highest solar radiation in Semera.

For the case of the day of the lowest solar radiation in Semera, which is in August, the simulation resulted in the temperature variation of the PCM, the temperature variation of air at inet and outlet of thermal storage and the melt fraction during phase change were obtained during 5.5 hours of charging as shown from Figure 6-11 to Figure 6-16. The case of the lowest radiation almost 2 more hours was required for complete melting of the PCM and the temperature at the top of thermal storage reached only 425 ^{o}C.

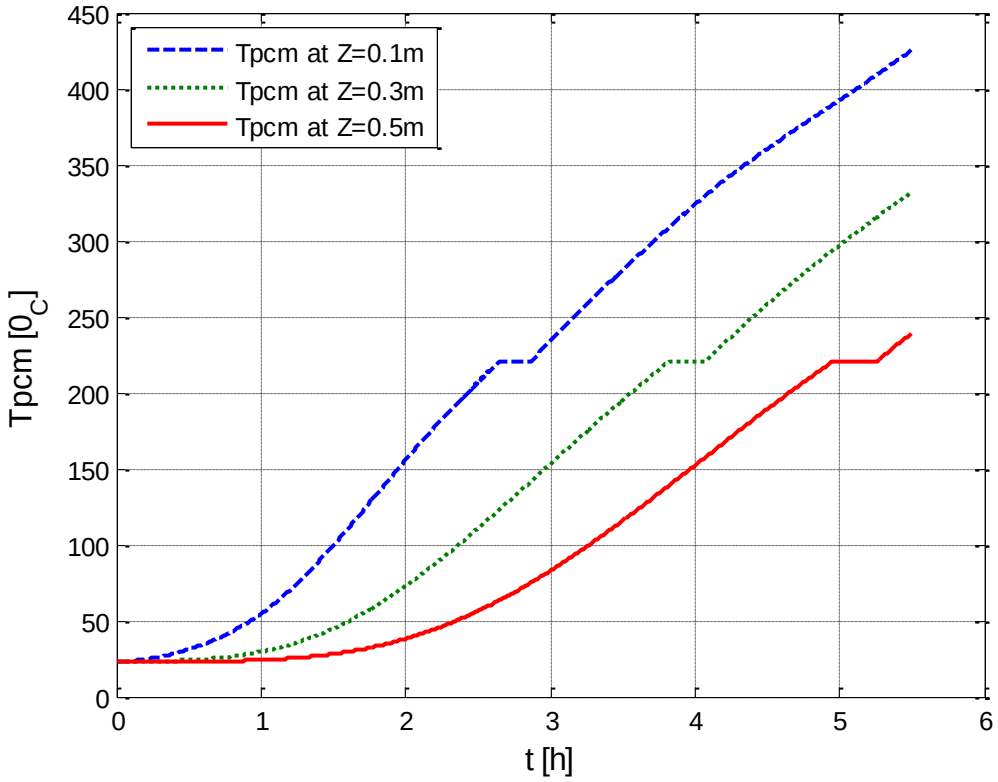

Figure 6-14: Temperature of PCM storage versus charging hours for the day of the lowest solar radiation in the case of Semera.

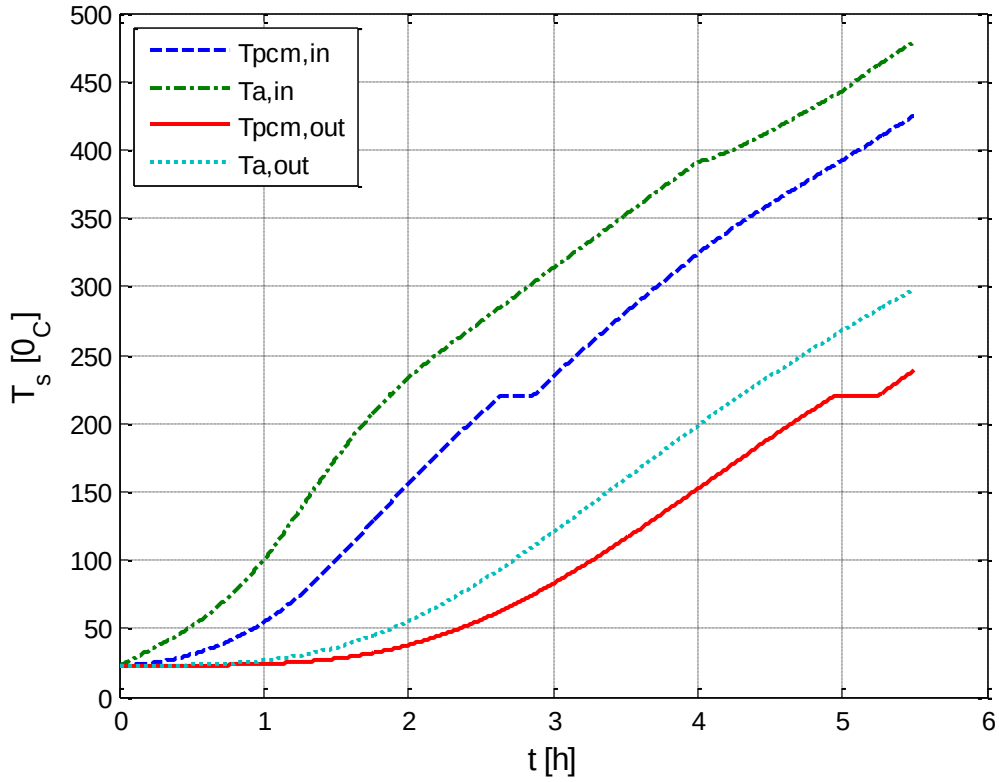

Figure 6-15: Comparison of the temperature of air and PCM at the inlet and outlet storage for the day of lowest solar radiation in Semera

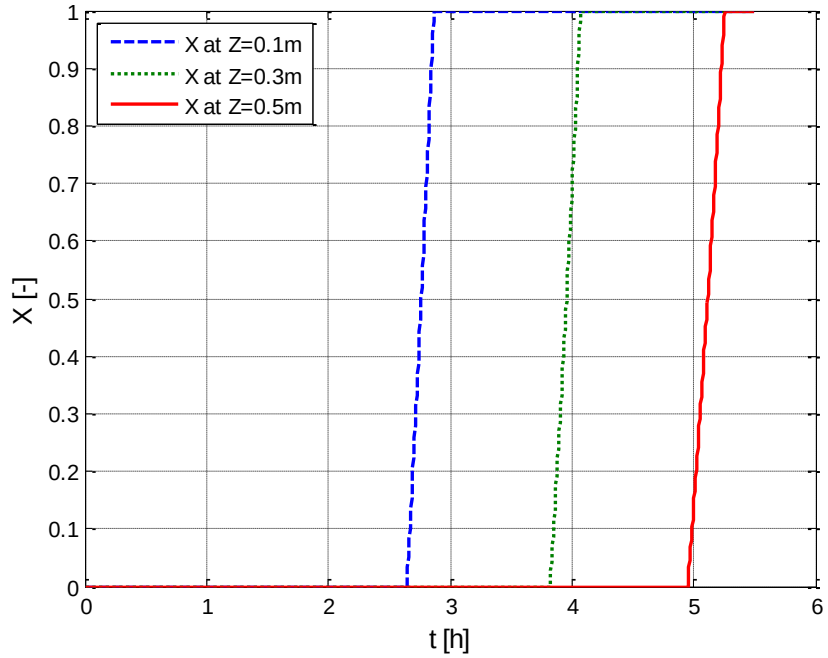

Figure 6-16: Melting fraction versus charging time for the day of the lowest solar radiation in Semera

Discharging Conditions of PCM Thermal Storage

The heat stored in the PCM thermal storage can be discharged by forced convection placing the pot on the top of storage during using a fan. That blows ambient air across PCM capscules through the tank. Table 6-4 describes the initial and boundary conditions of PCM thermal storage used during heat extraction when the cooking process is carried out.

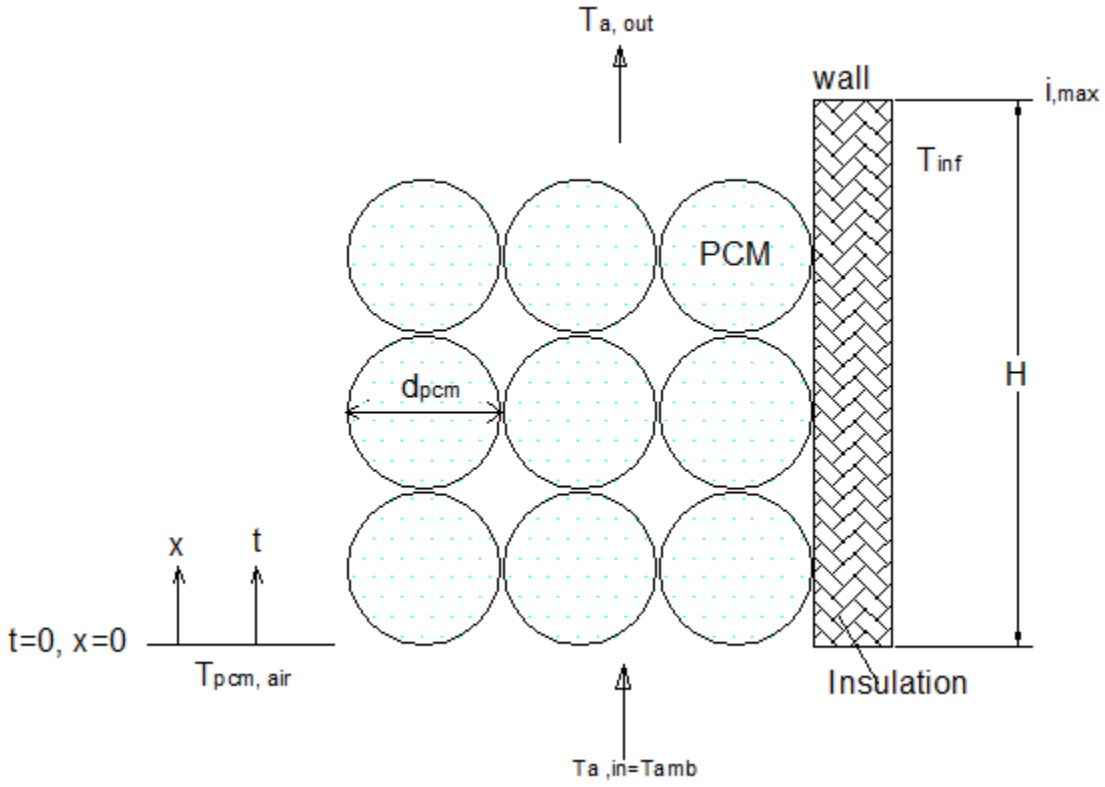

Figure 6-17: Schematic drawing shows discretization of PCM storage during discharging conditions

Table 6-4: Initial and boundary conditions for discharging conditions

$T_{a(t,\ x=0)} = 23\ ^0C$	Space step = 0.1m	Time step $(\Delta t) = 1s$
$T_{p\ (t=0,\ x=L)} = T_{p,\ charge}$	Number of space nodes = 6	t_{max} = 4h

The temperatures of the PCM has degraded after discharging for 4 hours using 0.0048kg/s mass flow rate of ambient air. The temperature of water boiling in Addis Ababa is around 93^0C. Figure 6-20 shows temperature variation of the thermal storage and water with respect to time during discharge or water boiling (cooking). The maximum capacity of water boiled in the case of Addis Ababa for the day of the highest solar radiation is 17 liters in 4

hours. The top, middle and bottom temperature of PCM thermal storage and the temperature of the water in the pan are shown Figure 6-18. The soldfiation of PCM thermal storage is also described by melt fraction in Figure 6-19 .

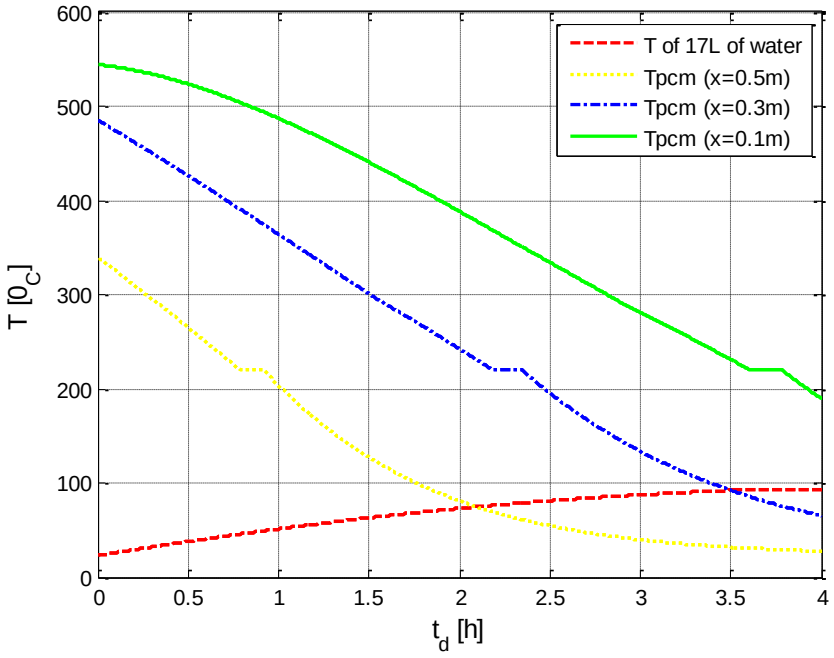

Figure 6-20: Temperature of water and PCM during water boiling in the case of Addis Ababa for the day of the highest solar radiation

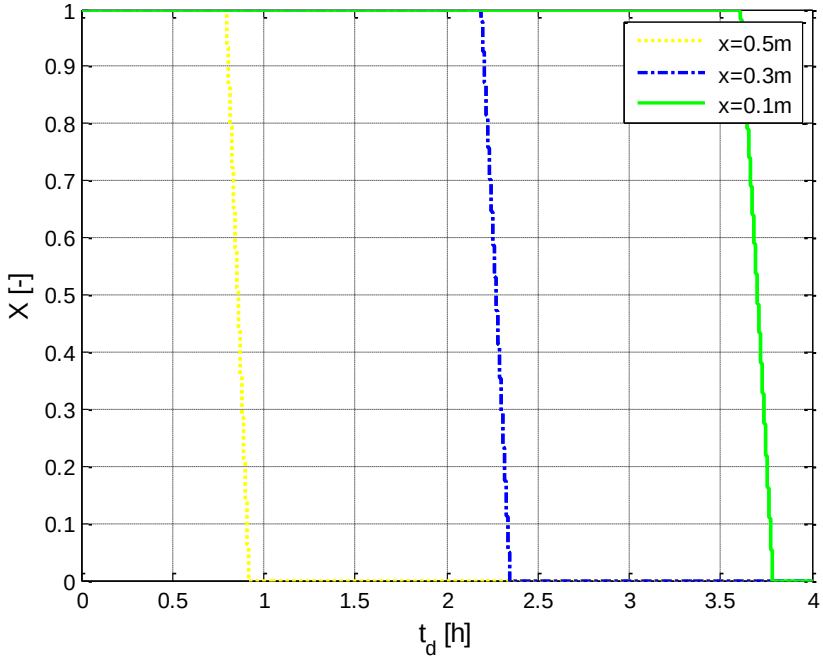

Figure 6-21: Solidification of PCM versus time during water boiling for the day of highest in Addis Ababa. (X is melt fraction)

Figure 6-22 and Figure 6-23 show the temperature degradation and solidification of the PCM thermal storage after discharging for 4 hours in the case Addis Ababa for the day of the lowest solar radiation. The maximum capacity of water boiled was 8.5 liters.

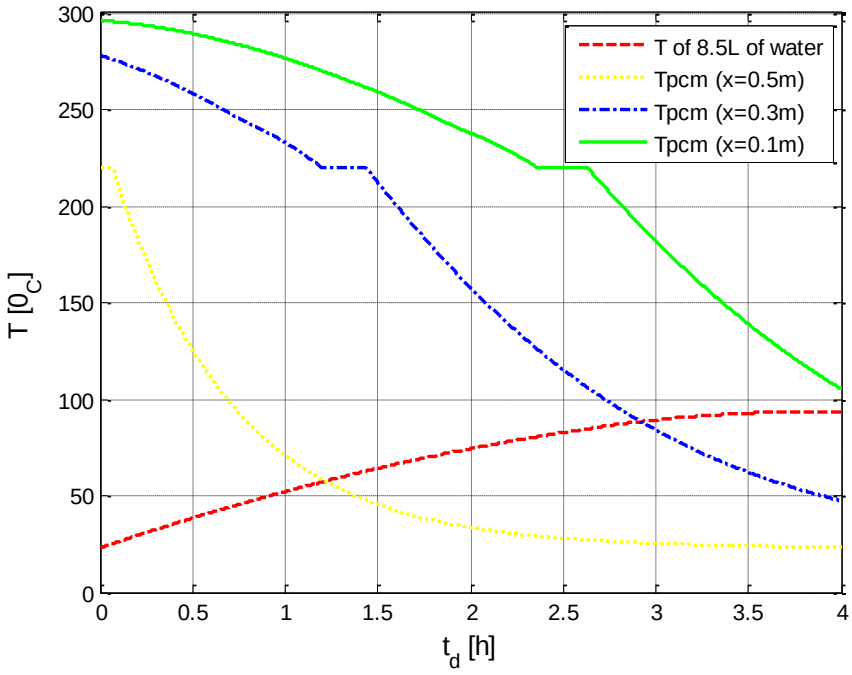

Figure 6-22: Temperature of water and PCM during water boiling in the case of Addis Ababa for the day of the lowest solar radiation.

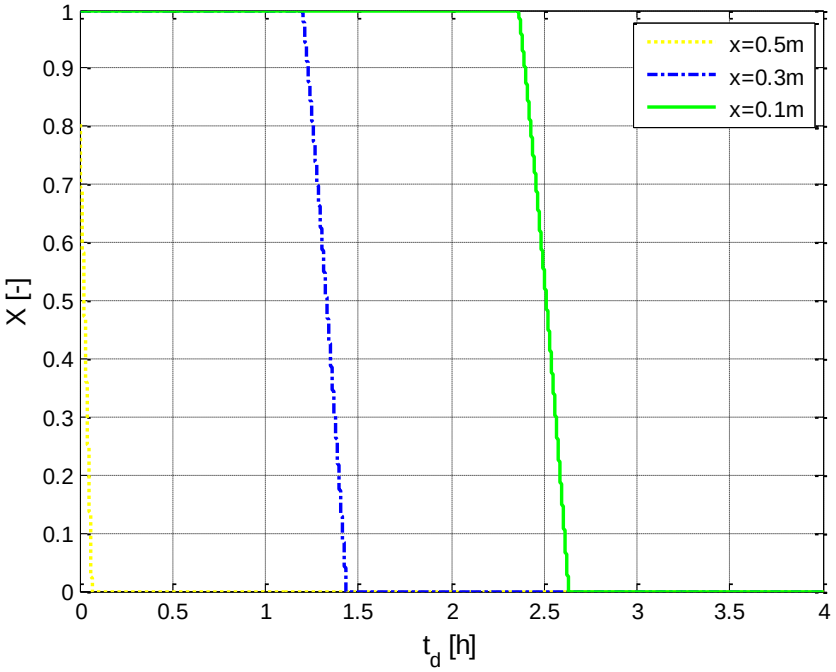

Figure 6-23: Solidification of PCM versus time during water boiling in the case of Addis Ababa for the day of the lowest solar radiation.

The temperatures degradation and the solidifications at different height of PCM thermal storage are shown in Figure 6-24 and Figure 6-25 during the cooking conducted under the day of the highest solar radiation of Semera. The top and bottom of the storage are degraded to 185.81^{0}C and 26.93^{0}C respectively while the temperature of water reaches to 93^{0}C. The liquid PCM in the storage is fully solidified in about 3.74 hours.

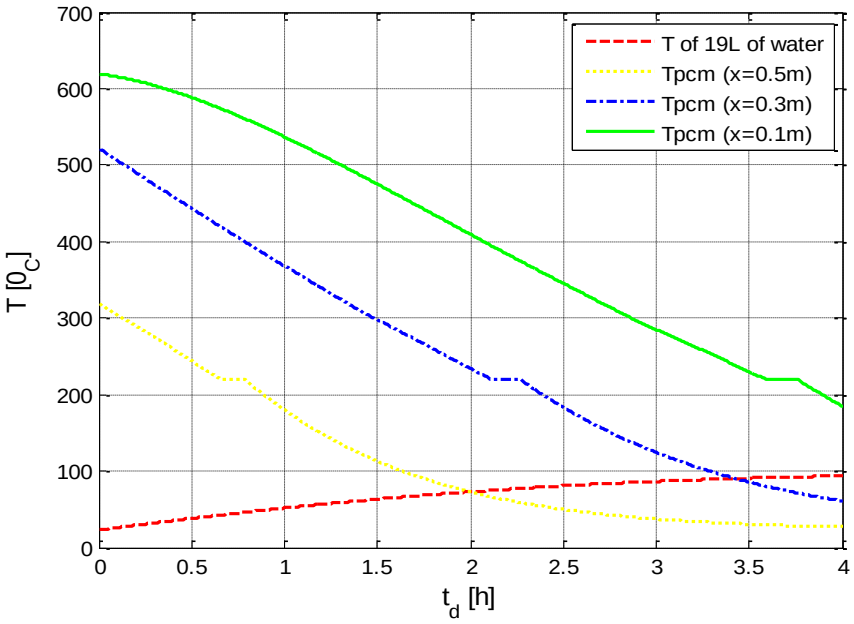

Figure 6-24: Temperature variation of water and PCM during water boiling in the case of Semera for the day of the highest solar radiation.

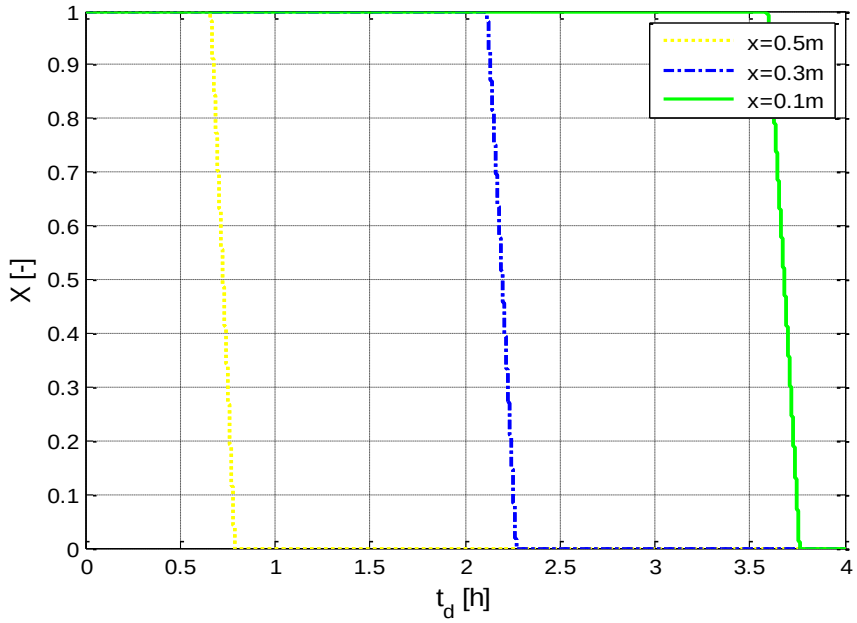

Figure 6-25: Solidification of PCM versus discharging time during water boiling in the case of Semera for the day of the highest solar radiation

Figure 6-26 and Figure 6-27 show the temperature degradations and solidifications of PCM along the height of the PCM thermal storage during water boiling at Semera for the day of the lowest solar radiation during 13 liters of water boiling in 4 hours.

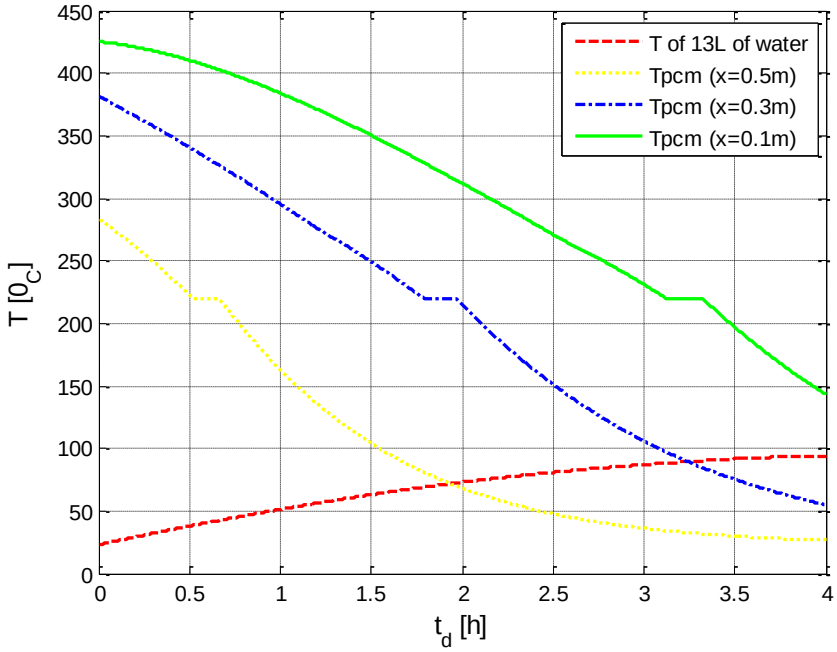

Figure 6-26: Temperature of water and PCM during water boiling in the case of Semera for the day of the lowest solar radiation

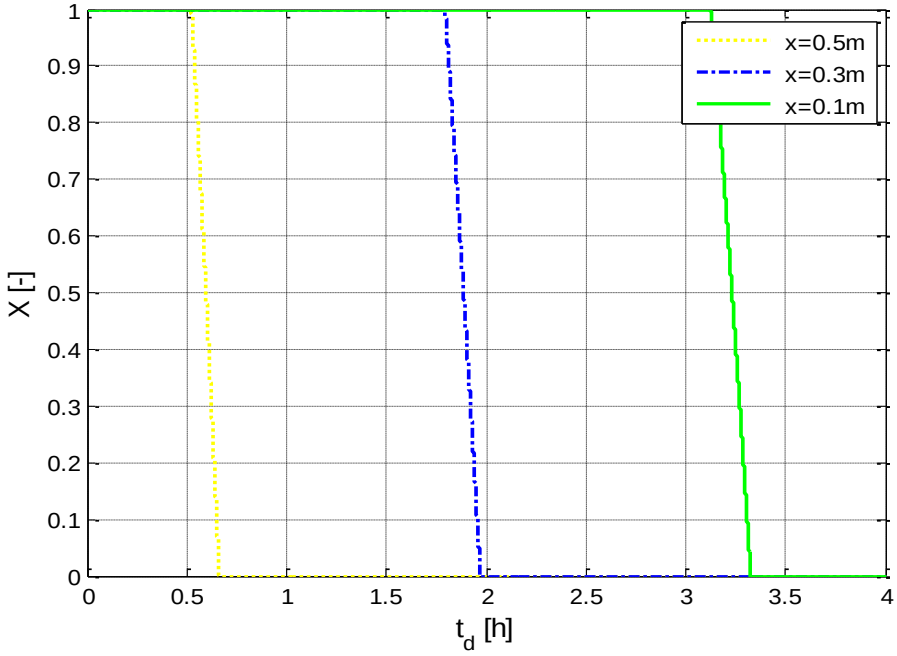

Figure 6-27: Solidification of PCM versus time during water boiling in the case of Semera for the day of the highest solar radiation

For the long term storage in the day of the highest and lowest solar radiation the efficiencies of the storage were estimated as illustrated in table below.

Table 6-5: Energy and efficiency results for both sites

	Addis Ababa			Semera		
	Highest I_b	Lowest I_b	Average I_b	Highest I_b	Lowest I_b	Average I_b
E_{solar} [MJ]	60.1	18.1	41.2	91.49	49.92	73.54
E_{stored} [MJ]	47.42	14.59	30.96	65.36	38.98	52.17
Useful Energy [MJ]	1.45	1.45	1.45	1.45	1.45	1.45
The volume of water boiled [Liter]	5	5	5	5	5	5
η_{stored} [%]	78.91	80.61	79.76	71.44	78.08	73.78
$\eta_{thermal}$ [%]	67.95	54.71	61.33	72.03	68.09	70.06
$\eta_{Overall}$ [%]	53.62	44.10	48.91	51.45	53.16	52.31

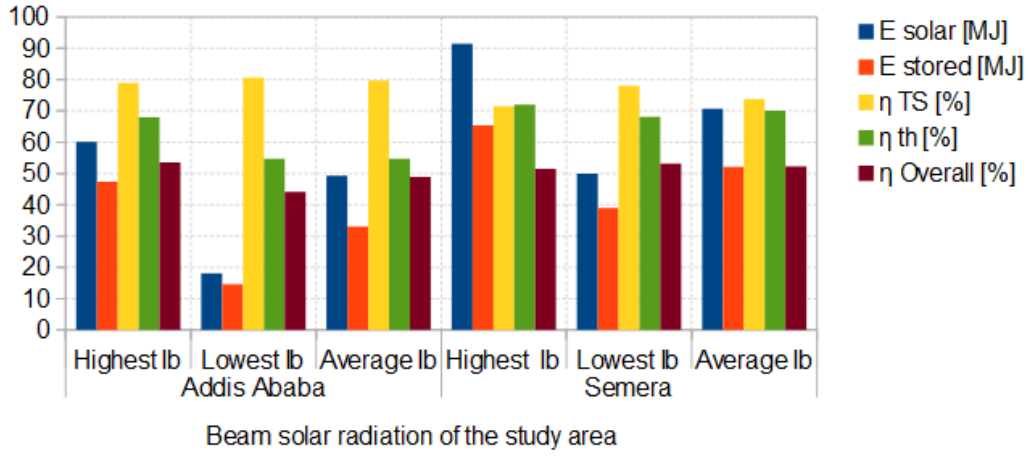

Figure 6-28: Comparison of energies and efficiencies in the study of PCM thermal storage at different loation with maximum and minimum solar radiation.

Performance comparisons of a PCM thermal storage for Addis Ababa and Semera solar radiations for the day of the highest and the lowest solar radiations are shown in Table 6-5 and Figure 6-28.

Table 6-6: Performance comparisons when cooking is carried out by forced convection and conduction during the highest and lowest solar radiations of Addis Ababa

	Addis Ababa			
	Forced convection		Conduction	
	Highest I_b	Lowest I_b	Highest I_b	Lowest I_b
E_{solar} [MJ]	60.1	18.1	60.1	18.1
E_{stored} [MJ]	47.42	14.59	47.42	14.59
η_{stored} [%]	78.91	80.61	78.91	80.61
$\eta_{thermal}$ [%]	67.95	54.71	45.58	30.12
$\eta_{Overall}$ [%]	53.62	44.10	35.96	24.28

Table 6-6 shows comparison of thermal and overall cooking efficiencies when the cooking was conducted under Addis Ababa climate conditions for the days of the highest and lowest solar radiations.

CHAPTER SEVEN

7. ECONOMIC ANALYSIS AND COMPARISONS OF SOLAR THERMAL STORAGE

7.1. Economic Analysis

The Levelized Cost of energy which is to be compared with Ethiopian electricity utility in the current conditions and an expected payback period of the project is analyzed. The Ethiopian electricity tariff is given as 0.06$/kWh for households currently and has a plan to upgrade to 0.09$/kWh in 2021 [62]. Therefore, the electricity is saved using alternative sources of energy and the levelized ost of energy and payback periods of thermal storage are evaluated.

7.1.1. Levelized cost of energy (LCOE)

The levelized cost of energy is can be defined as the present value of the price of the energy which is given in cents per kilowatt-hour (cents/kWh), considering the life of the project and the cost consumed during aquistion,he installation, operation, and maintenance. The general equation of the levelized ost of energy is given as [63]

$$LCOE = \frac{Lifecycle\ Cost\ (\$)}{Life\ time\ energy\ production\ (kWh)}$$

7.1.2. Payback period

The payback period is the time in which the initial cost of the investment is to be recovered through the cash inflow generated by the project/investment. The formula to calculate the payback period is given as [64]

$$Pay\ back\ period = \frac{Initial\ Investement}{Net\ Cash\ Flow\ per\ Period}$$

The results of the levelizedCost of energy and payback periods are summarized in the following tables.

7.1.3. Packed Pebbles Bed Thermal Storage Economic Analysis

Table 7-1: Estimated total cost packed bed pebbles

No	Parts	Total Cost	Units
1	Receiver	350	[birr]
2	Dish with a tracking system	7000	[birr]
3	Storage Tank	500	[birr]
4	Blower	700	[birr]
5	Pipe/ hose	250	[birr]
6	Other accessories	2200	[birr]
	Total	11000	[birr]

Note: The energy storage given in J should be converted to in kWh. The total energy stored for 5 years is given as

Table 7-2: Levelized cost of energy for pebble bed thermal storage

Sites	Addis Ababa			Semera		
The energy in a day [MJ]	Max	Min	Average	Max	Min	Average
	40.1	12.85	26.5	60.3	29.47	44.885
Energy [kWh]/ day	11.13	3.569	7.36	16.75	8.18	12.47
Energy in kWh/year	4,062.45	1,302.685	2,686.4	6,113.75	2,985.7	4,551.55
Energy in kWh for 5years	20,312.25	6,513.425	13,432	30,568.75	14,928.5	22,757.75
Electricity Price in $ for $ 0.06/kWh (current price) of Ethiopia	1,218.735	390.8055	805.92	1,834.125	895.71	1,365.465
Electricity Price in $ for $ 0.09/kWh (future price) of Ethiopia	1,828.1025	586.2025	1,208.88	2,751.1875	1,343.565	2,048.1975
Initial investment cost [Birr]	11000	11000	11000	11000	11000	11000
Installation cost [Birr]	2750	2750	2750	2750	2750	2750

Maintenance Cost [Birr]		2750	2750	2750	2750	2750	2750
Total cost [Birr]		16500	16500	16500	16500	16500	16500
Total Cost in $		515.625	515.625	515.625	515.625	515.625	515.625
LCOE in $/kWh		0.025	0.079	0.038	0.017	0.034	0.022

Table 7-3: Payback period of pebble bed thermal storage for Addis Ababa

Years	Energy in kWh	Cash inflow [$] Current price	Cash inflow [$] Future price	Cumulative Cost [$] with current price	Cumulative Cost [$] with future price
0	2,686.4	0	0	515.625	515.625
1	2,686.4	161.184	241.776	354.44	273.849
2	5,372.8	322.368	483.552	193.257	32.073
3	8,059.2	483.552	725.104	32.073	-209.479
4	10,745.6	644.736	967.104	-129.111	-441.479
5	13,432.0	805.92	1208.88	-290.295	-693.255

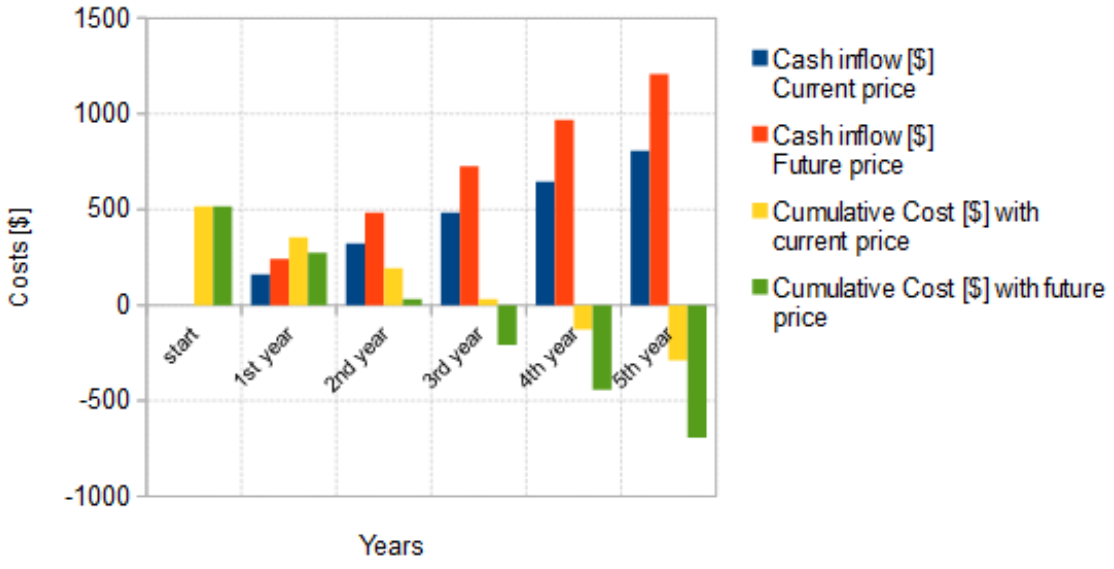

Figure 7-1: Payback period for a pebble bed thermal storage in case of Addis Ababa

Table 7-4: Payback period of pebble bed thermal storage for Semera

Years	Energy in kWh	Cash inflow [$] current price	Cash inflow ($) Future price	Cumulative Cost [$] current price	Cumulative Cost [$] Future price
0	4,551.55	0		515.625	515.625
1	4,551.55	273.093	409.6395	242.532	105.9855
2	9103.1	546.186	819.279	-30.561	-303.654
3	13654.65	819.279	1228.9185	-303.654	-713.2935
4	18206.2	1092.372	1638.558	-576.747	-1122.933
5	22757.75	1365.465	2048.1975	-849.84	-1532.5725

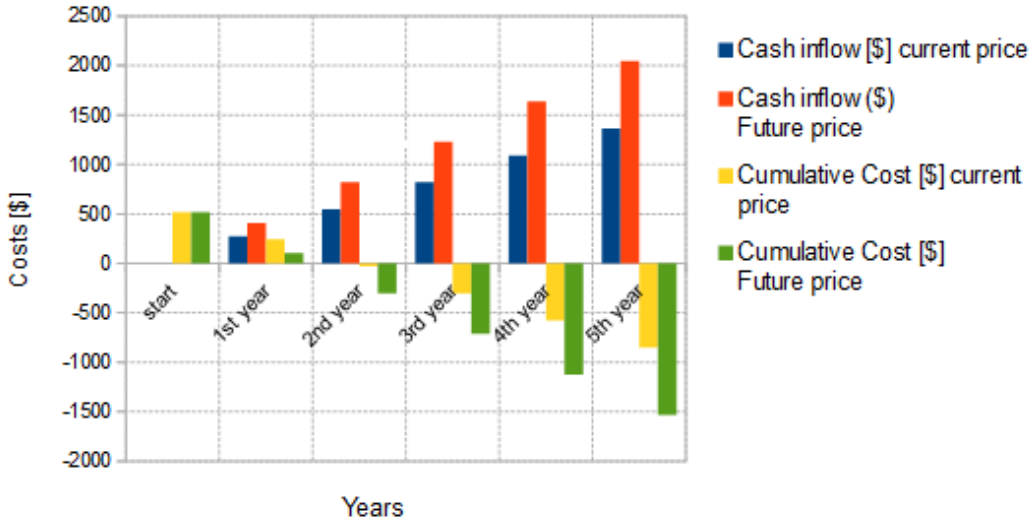

Figure 7-2: Payback period of pebble bed storage in case of Semera

The levelized ost of energy of pebble bed thermal storage is 0.025$/kWh, 0.079$/kWh and 0.038$/kWh for the maximum, minimum, and average Addis Ababa solar irradiances respectively. While it is 0.017$/kWh, 0.034$/kWh, and 0.022$/kWh for the maximum, minimum, and average solar irradiances of Semera ,respectively as shown in Table 7-2. Comparing with the Ethiopian electricity tariff now and in the future, the payback periods of pebble bed thermal storage are evaluated in Table 7-3 and Figure 7-1

7.1.4. PCM Thermal Storage Economic Analysis

Table 7-5: Estimated total cost of PCM thermal storage

No	Parts	Total Cost	Units
1	Receiver	350	[birr]
2	Dish with a tracking system	7000	[birr]
3	Storage Tank	400	[birr]
4	Blower	700	[birr]
5	PCM capsules	500	[birr]
5	Pipe/ hose	250	[birr]
6	Other accessories	2200	[birr]
	Total	11400	[birr]

Note: The energy storage given in joul should be converted to in kWh. The total energy stored for 5 years is given as

Table 7-6: Levelized cost of energy for PCM thermal storage

Sites	Addis Ababa			Semera		
The energy in a day [MJ]	Max	Min	Average	Max	Min	Average
	23.13	17.67	20.40	23.92	19.28	21.60
Energy [kWh]in day	6.42	4.91	5.67	6.64	5.35	6
Energy in kWh/year	2343.3	1792.15	2069.55	2423.6	1952.75	2190
Energy in kWh for 5years	11716.5	8960.75	10347.7	12118	9763.75	10950
Electricity Price in $ for $ 0.06/kWh (current price) of Ethiopia	702.9	537.64	620.86	727.08	585.83	657
Electricity Price in $ for $ 0.09/kWh (future price) of Ethiopia	1054.48	806.46	931.29	1090.62	878.73	985.5
Initial investment cost [Birr]	11400	11400	11400	11400	11400	11400
Installation cost [Birr]	2800	2800	2800	2800	2800	2800

Maintenance Cost [Birr]		2800	2800	2800	2800	2800	2800
Total cost [Birr]		17000	17000	17000	17000	17000	17000
Total Cost in $		531.25	531.25	531.25	531.25	531.25	531.25
LCOE in $/kWh		0.045	0.059	0.051	0.044	0.054	0.048

Table 7-7: Payback period of PCM thermal storage for Addis Ababa

Years	Energy in kWh	Cash inflow [$] Current price	Cash inflow [$] Future price	Cumulative Cost [$] with current price	Cumulative Cost [$] with future price
0	2069.55	0	0	531.25	531.25
1	2069.55	124.17	186.26	407.08	344.99
2	4139.1	248.34	372.52	282.91	158.73
3	6208.65	372.51	558.78	158.74	-27.53
4	8278.2	496.68	745.04	34.57	-213.79
5	10347.75	620.85	931.3	-89.6	-400.05

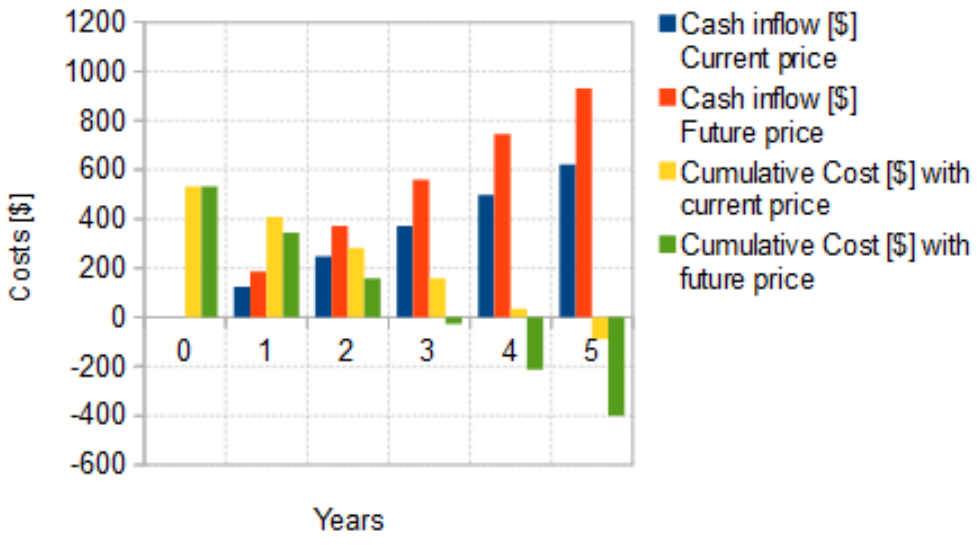

Figure 7-3: Payback period for average PCM stored energy in case of Addis Ababa

Table 7-8: Payback period of PCM thermal storage for Semera

Years	Energy in kWh	Cash inflow [$] Current price	Cash inflow [$] Future price	Cumulative Cost [$] with current price	Cumulative Cost [$] with future price
0	2190	0	0	531.25	531.25
1	2190	131.4	197.1	399.85	334.15
2	4380	262.8	394.2	268.45	137.05
3	6,570	394.2	591.3	137.05	-60.05
4	8,760	525.6	788.4	5.65	-257.15
5	10,950	657	985.5	-125.75	-454.25

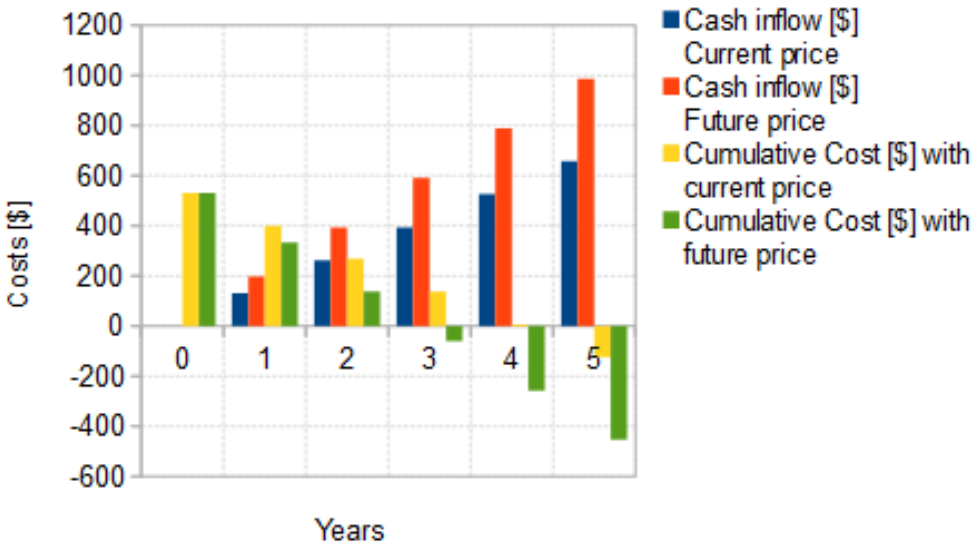

Figure 7-4: Payback period for average PCM stored energy in case of Semera

The Levelized cost of energy of PCM thermal storage is 0.045$/kWh, 0.059$/kWh and 0.051$/kWh for the maximum, minimum, and average in the case of Addis Ababa solar radiation, respectively. While, 0.044$/kWh, 0.054$/kWh, and 0.048$/kWh for the maximum, minimum, and average solar irradiances of Semera respectively as it is shown in Table 7-6 The payback periods of PCM thermal storage are evaluated in Table 7-7 and Figure 7-3 for Addis Ababa and Table 7-8 and Figure 7-4 for Semera cases comparing to eleteriity tariff..

7.2. Comparison of a Packed Pebble and PCM Thermal Storage

A packed pebble bed and PCM thermal storage are compared based on charging and discharging conditions under Addis Ababa and Semera climate conditions at the clear day for similar conditions. The comparison of the packed pebble bed and PCM thermal storage which have simulated for the day of the highest solar radiation of Addis Ababa in the month of 16-March. The pebble bed storage was modeled with a size of $\emptyset 0.3m \times 0.9m$ and PCM was modeled with a size of $\emptyset 0.3m \times 0.5\ m$. After charging for 11hours using beam solar radiation of the selected site and discharging for 4hours, the Table 7-9 compare the performance analysis between pebble bed and PCM thermal storage.

Table 7-9: Performance comparisons between pebble bed and PCM thermal storage

	Addis Ababa						**Semera**					
	Highest I_b		Lowest I_b		Average I_b		Highest I_b		Lowest I_b		Average I_b	
	Pebble	PCM	Pebble	PCM	Pebble	PCM	Pebble	PCM	Pebble	PCM	Pebble	PCM
E_{solar} [MJ]	60.1		18.1		41.2		91.49		49.92		73.54	
E_{stored} [MJ]	40.1	47.42	12.85	14.59	28.5	30.96	60.3	65.36	29.47	38.98	46.24	52.17
η_{stored} [%]	66.7	78.91	70.91	80.61	69.1	79.76	65.9	71.03	59.1	78.08	62.6	70.94
$\eta_{thermal}$ [%]	45	67.95	31.10	54.71	38.2	61.33	55.5	72.03	52.7	68.09	52.53	70.96
$\eta_{Overall}$ [%]	30	53.62	22.08	44.10	26.5	48.91	36.6	51.45	31.1	53.16	32.9	52.31

Based on the comparisons between the two thermal storages PCM thermal storage is more pereferable than pebble bed thermal storage.

CHAPTER EIGHT

8. CONCLUSIONS AND RECOMMENDATIONS

8.1. CONCLUSIONS

Solar thermal energy storage is a great solution for limited energy supply and demand. In developing countries like Ethiopia for more than 80% of the population that depend on biomass fuel for cooking.

The pebble bed thermal storage model describes the successful modeling of sensible heat thermal storage integrated with parabolic solar collector and cookstove at the top of thermal storage. Constant heat inflow and variable heat inflow for heating air with receiver of a parabolic solar collector at constant mass flow approaches were used to evaluate the performance of the pebble bed thermal storage. The computational model of pebble bed thermal storage was validated and the result wass found to be consistent with an experimental work that was reported by Okello [20].

The actual condition, charging of thermal storage by air heating in the receiver of the parabolic solar collector was modeled by the computational model. Boiling of water at the top of thermal storage was simulated under forced convection and conduction heat extraction from the pebbles was performed to simulate discharging of thermal storage during cooking. From the simulation, the storage efficiency was 66.7% for the day with the highest DNI and the thermal efficiency for cooking was for heat transfer with fan and without fan were 45% and 28.72%, respectively. The overall efficiencies of cooking were 30% and 19.14% for the above two cases, respectively. For the day with the lowest DNI, the storage efficiency, thermal efficiency of cooking, and overall efficiency of cooking 70.9%, 31.12%, and 22.08%, respectively. As the overall efficiencies of the cooking stove assuming forced circulation of air through pebbles and conduction across pebble bed represent the limits of best case and worst case efficiency. It can be concluded that the overall efficiency of a solar concentrating cooker with pebble bed thermal storage and air as heat transfer media is between 22% to 30 % for tropical regions in a clear sky day when the sun is overhead at

noon under Addis Ababa climate condition. Also, it can be concluded that the overall cooking efficiency is between 13% to 19% when the cooking was conducted only by conduction.

For PCM thermal storage, the simulation was carried out for both sites and the performance analysis was performed. The PCM has a capacity of storing 47.42MJ of energy, and the thermal storage, thermal cooking and overall cooking efficiencies were 78.91%, 67.95% and 53.62% for the day of the highest and 80.61%, 54.71% and 44.10 % the lowest solar radaition conducted under Addis Ababa solar condition. The energy storage capacity inreased of 7.32 MJ and the thermal storage, thermal and overall cooking efficiencies were 9.71%, % , 23.26% and 22.02% for the day of the highest solar radiation respectively. It can be concluded that the overall cooking efficiency of a solar concentrating cooker with PCM thermal storage and air as heat transfer media is between 44% to 53 % for tropical regions in a clear sky day when the sun is overhead at noon under Addis Ababa climate condition. Also, it can be concluded that the overall cooking efficiency is between 24% to 35% when the cooking was conducted only by conduction.

Under Semera climate condition, the capacity of energy storage was 65.36 MJ of energy, and the thermal storage, thermal and overall cooking efficiencies were 71.03% ,72.03 % and 51.43% for the day of the lowest solar radiation respectively. The energy storage capacity inreased of 5.06 MJ and the thermal storage, thermal and overall cooking efficiencies were 5.13%, % , 16.532% and 14.85% for the day of the highest solar radiation respectively.

The levelized cost of energy and payback period for both storages were evaluated. Although the thermal storage system for solar cookers is attractive due to no limitation on cooking time and place of cooking, heat losses from the system and unavailability of the energy below 100 ^{O}C make the overall efficiency low.

8.2. Recommendation

Solar thermal energy storage is a solution for the limitation of energy supply and energy demand issues happen during the night and cloudy time. Also, it is used for indoor cooking applications. This work develops the computational model and performance analysis of thermal storage that is integrated with a parabolic concentrating solar collector for cooking applications. Two thermal energy storages, pebble bed thermal storage and PCM thermal storage, integrated with parabolic solar concentrators have been modeled. Then, the efficiencies have evaluated based on the actual solar conditions for both Addis Ababa and Semara solar irradiances. It is recommended that the model should be assisted with experimental work and the efficiencies should be validated with experimental work at the actual solar conditions for both sites. Inaddition . the computational model shouldl be investigated using variable mass flow rate for low solar radiations with a experimental validation.

Nomenclature

A	Area	Pr	Prandtl number
Bi	Biot number	R	Resistance
c	Specific heat capacity	Re	Reynold's number
D	Diameter of storage	S	Thickness
d	Diameter	T	Temperature
h	Convective heat transfer coefficient	U	Over all heat transfer coefficient
I	Solar irradiance	V	Volume
k	Thermal conductivity	$\dot{Q}$	The rate of heat transfer
L	Height of the storage	$\dot{m}$	Mass of airflow
m	Mass	X	Molten fraction
P	Perimeter		

Greek letters

ε	Void fraction	ρ	Density
η	Efficiency	σ	Stefan Boltzmann constant
ϵ	Emissivity of pan	v	Kinematic viscosity
μ	Dynamic viscosity		

Subscript

a	air	*pa*	air at constant pressure
abs	absorber	*pan*	pan
amb	ambient air	*pb*	pebble at constant pressure
ap	aperture	*r*	radiation loss
b	beam	*st*	storage
cp	pan circumferential	*th*	thermal
cs	cross – sectional	*v*	volumetric
cv	convective loss	*w*	water
eff	effective	*wal*	wall
i	internal	*pcm,s*	solid PCM
in	inflow	*pcm,l*	liquid PCM
ins	insulation	*pcm*	phase change material

o	outer
op	optical
out	outflow
P	pebble
th	cooking thermal
TS	thermal storage
Overall	over all

REFERENCE

[1] U. R. Prasanna, "Modeling, optimization and design of a solar thermal energy transport system for hybrid cooking application," no. July, p. 245, 2010.

[2] A. H. Tesfay, O. J. Nydal, and M. B. Kahsay, "Energy storage integrated solar stove: A case of solar Injera baking in Ethiopia," IEEE, pp. 659–666, 2014.

[3] A. Asfaw, "Sustainable household energy for Addis Ababa ," J. Sustain. Dev., vol. 8, pp. 1–11, 2012.

[4] R. M. Muthusivagami, R. Velraj, and R. Sethumadhavan, "Solar cookers with and without thermal storage"A review," Renew. Sustain. Energy Rev., pp. 1–11, 2009.

[5] S. B. Joshi and A. R. Jani, "Design, development and testing of a small scale hybrid solar cooker," Sol. Energy, vol. 122, pp. 148–155, 2015.

[6] H. Singh, R. P. Saini, and J. S. Saini, "A review on packed bed solar energy storage systems," Renew. Sustain. Energy Rev., vol. 14, no. 3, pp. 1059–1069, 2010.

[7] L. Nkhonjera, T. Bello-Ochende, G. John, and C. K. King'ondu, "A review of thermal energy storage designs, heat storage materials and cooking performance of solar cookers with heat storage," Renew. Sustain. Energy Rev., vol. 75, no. February, pp. 157–167, 2017.

[8] N. L. Panwar, S. C. Kaushik, and S. Kothari, "State of the art of solar cooking : An overview," Renew. Sustain. Energy Rev., vol. 16, no. 6, pp. 3776–3785, 2012.

[9] M. Mussard, A solar concentrator with heat storage and self-circulating liquid, no. September. 2013.

[10] T. S. Veslum, "Absorber for concentrating solar heat collectors," no. July, 2011.

[11] P. Sharma and R. Sarma, "Design and evaluation of open volumetric air receiver for process heat applications," Energy Procedia, vol. 57, pp. 2994–3003, 2014.

[12] B. A. Veremachi, A. Zia, B. C. Cuamba, J. Lovseth, and O. J. Nydal, "Parabolic dish concentrating collector for indirect solar cooking," Glob. J. Sci. Front. Res., vol. 17, no. 1, 2017.

[13] I. L. Mohammed, "Design and development of parabolic dish solar water heater," Int. J. Eng. Res. Appl., vol. 2, no. 1, pp. 822–830, 2012.

[14] S. Kuravi, J. Trahan, D. Y. Goswami, M. M. Rahman, and E. K. Stefanakos, "Thermal

energy storage technologies and systems for concentrating solar power plants," Prog. Energy Combust. Sci., vol. 39, no. 4, pp. 285–319, 2013.

[15] A. Sharma, V. V. Tyagi, C. R. Chen, and D. Buddhi, "Review on thermal energy storage with phase change materials and applications," Renew. Sustain. Energy Rev., vol. 13, no. 2, pp. 318–345, 2009.

[16] G. Zanganeh, "High-temperature thermal energy storage for concentrated solar power with air as heat transfer fluid," no. 21802, 2014.

[17] M. Hänchen, S. Brückner, and A. Steinfeld, "High-temperature thermal storage using a packed bed of rocks - Heat transfer analysis and experimental validation," Appl. Therm. Eng., vol. 31, no. 10, pp. 1798–1806, 2011.

[18] S. A. Zavattoni, M. C. Barbato, A. Pedretti, G. Zanganeh, and A. Steinfeld, "High temperature rock-bed TES system suitable for industrial-scale CSP plant - CFD analysis under charge/discharge cyclic conditions," Energy Procedia, vol. 46, pp. 124–133, 2014.

[19] N. G. Barton, "Simulations of air-blown thermal storage in a rock bed," Appl. Therm. Eng., vol. 55, no. 1–2, pp. 43–50, 2013.

[20] D. Okello, C. W. Foong, O. J. Nydal, and E. J. K. Banda, "An experimental investigation on the combined use of phase change material and rock particles for high temperature ($ 350 ° C) heat storage," Energy Convers. Manag., vol. 79, pp. 1–8, 2014.

[21] K. G. Allen, T. W. Von Backström, and D. G. Kröger, "Packed rock bed thermal storage in power plants: Design considerations," Energy Procedia, vol. 49, pp. 666–675, 2013.

[22] K. G. Allen, "Rock bed thermal storage for concentrating solar power plants," no. April, pp. 1–205, 2014.

[23] A. Raul, M. Jain, S. Gaikwad, and S. K. Saha, "Modelling and experimental study of latent heat thermal energy storage with encapsulated PCMs for solar thermal applications," Appl. Therm. Eng., vol. 143, no. July, pp. 415–428, 2018.

[24] B. Muñoz-sánchez, I. Iparraguirre-torres, V. Madina-arrese, and U. Izagirre-etxeberria, "Encapsulated high temperature PCM as active filler material in a thermocline-based thermal storage system," Energy Procedia, vol. 69, pp. 937–946, 2015.

[25] B. Fortunato, S. M. Camporeale, and T. Marco, "Simple mathematical model of a thermal storage with PCM," no. June 2014, 2012.

[26] D. Tarwidi, “Modeling and numerical simulation of solar cooker with PCM as thermal energy storage,” Inf. Commun. Technol., no. May 2015, 2016.

[27] A. Kylili, M. Theodoridou, I. Ioannou, and P. A. Fokaides, “Numerical heat transfer analysis of Phase Change Material (PCM) - enhanced plasters,” pp. 1–7, 2016.

[28] A. Oliveira, “PCM energy storage model : A case study for a solar-ejector cooling cycle,” 2016.

[29] H. Peng, H. Dong, and X. Ling, “Thermal investigation of PCM-based high temperature thermal energy storage in packed bed,” Energy Convers. Manag., vol. 81, pp. 420–427, 2014.

[30] A. Marcello, L. E. Mansueti, and R. Gianoli, “Transient simulation of phase change material (PCM) storage integrated in a domestic hot water (DHW) heat pump system,” 2017.

[31] M. R. H. and A. A. Salam, “Simulation and optimization of solar thermal system integrated with PCM thermal energy storage for seawater desalination,” 2011.

[32] J. F. Belmonte and A. E. Molina, “Air-based solar systems for building heating with PCM fluidized bed energy storage,” vol. 130, pp. 150–165, 2016.

[33] D. Heim and J. A. Clarke, “Numerical modelling and thermal simulation of PCM – gypsum composites with ESP-r,” vol. 36, pp. 795–805, 2004.

[34] A. Illah, N. Korti, and F. Z. Tlemsani, “Experimental investigation of latent heat storage in a coil in PCM storage unit,” J. Energy Storage, vol. 5, pp. 177–186, 2016.

[35] N. Beemkumar and A. Karthikeyan, “Experimental Investigation on Enhancement of Heat Transfer in Thermal Energy Storage System using Paraffin Wax as PCM,” vol. 767, pp. 457–462, 2015.

[36] O. S. Alajo, V. C. Ibekwe, and E. C. Nsofor, “Experimental Study on the Performance of a PCM-Based Solar Energy Storage System,” no. 11, pp. 195–203, 2013.

[37] M. J. Kabbara and N. Ben Abdallah, “Experimental investigation on phase change material based thermal energy storage unit,” Procedia - Procedia Comput. Sci., vol. 19, no. Seit, pp. 694–701, 2013.

[38] H. M. A. Hassan, “Development and evaluation of a CFD model to simulate thermal performance of phase change material (PCM) based energy storage systems,” 2014.

[39] A. J. Parry, P. C. Eames, and F. B. Agyenim, “Modeling of thermal energy storage shell-

and-tube heat exchanger modeling of thermal energy storage," Heat Transf. Eng., no. August 2013, pp. 37–41.

[40] K. G. Allen, "Performance characteristics of packed bed thermal energy storage for solar thermal power plants," no. March, 2010.

[41] R. Gamez, "Computational modeling of solar energy storage in rock beds," no. November, 2011.

[42] M. D. Muhammad, "Review of PCMs and heat transfer enhancement methods applied in parabolic trough solar plants thermal storage systems," Niger. J. Technol., vol. 37, no. 1, pp. 96–107, 2018.

[43] A. Mawire, Solar thermal energy storage for solar cookers. Elsevier Ltd., 2015.

[44] M. Mussard, A. Gueno, and O. J. Nydal, "Experimental study of solar cooking using heat storage in comparison with direct heating," Sol. Energy, vol. 98, no. PC, pp. 375–383, 2013.

[45] A. Mawire and M. McPherson, "Experimental and simulated temperature distribution of an oil-pebble bed thermal energy storage system with a variable heat source," Appl. Therm. Eng., vol. 29, no. 5–6, pp. 1086–1095, 2009.

[46] A. Haileselassie, M. Bayray, and O. Jørgen, "Design and development of solar thermal Injera baking : steam based direct baking," Energy Procedia, vol. 57, pp. 2946–2955, 2014.

[47] A. A. Hassen and D. A. Amibe, "Finite element modeling of solar powered Injera," pp. 1–8.

[48] D. Okello, O. J. Nydal, K. Nyeinga, and E. J. K. Banda, "Experimental investigation on heat extraction from a rock bed heat storage system for high temperature applications," vol. 27, no. 2, pp. 30–37, 2016.

[49] D. Okello, O. J. Nydal, and E. J. K. Banda, "Experimental investigation of thermal de-stratification in rock bed TES systems for high temperature applications," Energy Convers. Manag., vol. 86, pp. 125–131, 2014.

[50] H. K. and K. S. Sharma, S D, Takeshi Iwata, "Thermal performance of a solar cooker based on an evacuated tube solar collector with a PCM storage unit," vol. 78, pp. 416–426, 2005.

[51] S. J. Ruebush, "A computational study of thermal storage techniques for solar cooking

devices for use in," 2013.

[52] A. Haileselassie, M. Bayray, and O. Jørgen, "Solar powered heat storage for Injera baking in Ethiopia," Energy Procedia, vol. 57, pp. 1603–1612, 2014.

[53] K. Schwarzer and M. Euge, "Characterisation and design methods of solar cookers," vol. 82, pp. 157–163, 2008.

[54] A. S. K, "Sizing of a packed bed storage for solar air heating systems," Arch. SID, vol. 16, no. 2, pp. 155–162, 2003.

[55] Fouad and A. K. A. H. and A. M. S. S. Al Azawi, "Design parameter effects on the thermal performance of special packed bed for heat storage," 2007.

[56] J. A. Duffie and W. A. Beckman, Solar engineering of thermal processes, Fourth edi. 2013.

[57] R. Khanna, G. Zanganeh, and A. Steinfeld, "Storing Sunlight," 2013.

[58] Y. Kadri, "Design of a solar dish concentrator according to the needed energy for a given application a given application," no. December 2013, pp. 18–25, 2016.

[59] J. A. Alarcón, J. E. Hortúa, and A. L. G, "Design and construction of a solar collector parabolic dish for rural zones in Colombia," Tecciencia, vol. 7, no. 14, pp. 14–22, 2013.

[60] F. P. INCROPERA, Fundamentals of heat and mass transfer, Seventh ed. 2011.

[61] Ashrae, "Thermal properties of food stuff" 2006

[62] The World Bank, "Ethiopia renewable energy guarantees program",2019

[63] C. S. Lai and M. D. Mcculloch , "Levelized cost of energy for PV and grid scale energy storage systems," pp. 1–11.

[64] G.Reniers and N.Paltrinieri, "Cost-benefit analysis of safety measures", 2016

APPENDIX

Table A: Thermo physical properties of air (Incropera et al., 2007 page 941) [60]

T [k] Air	ρ [kg/m³]	C_p [kJ/kg.k]	v. 10^6 [m²/s]	pr	μ. 10^7 [N.S/m²]	α. 10^6 m²/s	k. 10^3 W/mk
100	3.5562	1.032	9.34	0.786	71.1	2.54	9.34
150	2.3364	1.012	13.8	0.758	103.4	5.84	13.8
200	1.7458	1.007	18.1	0.737	132.5	10.3	18.1
250	1.3947	1.006	22.3	0.720	159.6	15.9	22.3
300	1.1614	1.007	26.3	0.707	184.6	22.5	26.3
350	0.9950	1.009	30.0	0.700	208.2	29.9	30.0
400	0.8711	1.014	33.8	0.690	230.1	38.3	33.8
450	0.7740	1.021	37.3	0.686	250.7	47.2	37.3
500	0.6964	1.030	40.7	0.684	270.1	56.7	40.7
550	0.6329	1.040	43.9	0.683	288.4	66.7	43.9
600	0.5804	1.051	46.9	0.685	305.8	76.9	46.9
650	0.5356	1.063	49.7	0.690	322.5	87.3	49.7
700	0.4643	1.075	50.7	0.695	338.8	98.0	52.4

Table B: 5 Years Average Hourly Total, Beam and Diffuse Solar Irradiance of Addis Ababa (2012 To 2016) for recommended day in months

	17-Jan			**16-Feb**			**16-Mar**		
Hours	**I**	**Id**	**Ib**	**I**	**Id**	**Ib**	**I**	**Id**	**Ib**
12:00AM	0.4188	0.0586	0.3601	0.515	0.075	0.44	0.515	0.1009	0.4141
1:00AM	0.4188	0.0586	0.3601	0.5	0.0728	0.4272	0.505	0.099	0.406
2:00AM	0.425	0.0595	0.3655	0.5	0.0728	0.4272	0.51	0.0999	0.4101
3:00AM	0.4188	0.0586	0.3601	0.495	0.0721	0.4229	0.515	0.1009	0.4141
4:00AM	0.4188	0.0586	0.3601	0.495	0.0721	0.4229	0.435	0.0852	0.3498
5:00AM	0.425	0.0595	0.3655	0.51	0.0742	0.4358	0.51	0.0999	0.4101
6:00AM	0.9625	0.1347	0.8278	1.025	0.1492	0.8758	3.165	0.6202	2.5448
7:00AM	47.944	6.7103	41.233	56.045	8.1588	47.886	86.245	16.899	69.346
8:00AM	171.86	24.053	147.8	226.74	33.008	193.73	266.88	52.294	214.59
9:00AM	346.18	48.452	297.73	393.84	57.333	336.5	439.06	86.031	353.02

10:00AM	539.09	75.452	463.64	580.92	84.567	496.35	548.88	107.55	441.33
11:00AM	614.99	86.075	528.92	653.24	95.095	558.14	708.66	138.86	569.8
12:00PM	637.74	89.26	548.48	641.9	93.444	548.45	816.23	159.94	656.29
1:00PM	612.52	85.729	526.79	651.77	94.881	556.88	855.34	167.6	687.74
2:00PM	553.53	77.472	476.05	642.37	93.514	548.86	698.16	136.8	561.36
3:00PM	422.69	59.161	363.53	598.36	87.106	511.25	423.7	83.021	340.67
4:00PM	275.55	38.566	236.98	397.49	57.865	339.63	368.29	72.165	296.13
5:00PM	107.92	15.104	92.814	170.05	24.754	145.29	175.96	34.479	141.48
6:00PM	10.844	1.5177	9.326	22.955	3.3417	19.613	20.595	4.0355	16.559
7:00PM	0.4438	0.0621	0.3816	0.54	0.0786	0.4614	0.535	0.1048	0.4302
8:00PM	0.4313	0.0604	0.3709	0.52	0.0757	0.4443	0.51	0.0999	0.4101
9:00PM	0.4313	0.0604	0.3709	0.51	0.0742	0.4358	0.525	0.1029	0.4221
10:00PM	0.4125	0.0577	0.3548	0.5	0.0728	0.4272	0.51	0.0999	0.4101
11:00PM	0.425	0.0595	0.3655	0.51	0.0742	0.4358	0.505	0.099	0.406
	15-Apr			**15-May**			**11-Jun**		
Hours	**I**	**Id**	**Ib**	**I**	**Id**	**Ib**	**I**	**Id**	**Ib**
12:00AM	0.5	0.0687	0.4313	0.51	0.0977	0.4123	0.515	0.1459	0.3691
1:00AM	0.515	0.0708	0.4442	0.51	0.0977	0.4123	0.505	0.143	0.362
2:00AM	0.515	0.0708	0.4442	0.51	0.0977	0.4123	0.505	0.143	0.362
3:00AM	0.515	0.0708	0.4442	0.525	0.1005	0.4245	0.515	0.1459	0.3691
4:00AM	0.505	0.0694	0.4356	0.51	0.0977	0.4123	0.515	0.1459	0.3691
5:00AM	0.49	0.0674	0.4226	0.515	0.0986	0.4164	0.53	0.1501	0.3799
6:00AM	7.245	0.9961	6.2489	16.68	3.1944	13.486	15.31	4.3366	10.973
7:00AM	109.79	15.094	94.696	146.19	27.997	118.19	116.52	33.005	83.515
8:00AM	270.64	37.208	233.43	342.91	65.671	277.23	266.76	75.561	191.2
9:00AM	469.21	64.509	404.7	497.1	95.201	401.9	432.02	122.37	309.65
10:00AM	601.39	82.68	518.7	547.78	104.91	442.87	559.24	158.41	400.83
11:00AM	643.34	88.448	554.89	661.5	126.69	534.81	496.49	140.63	355.86
12:00PM	590.6	81.198	509.4	682.24	130.66	551.58	425.55	120.54	305.01
1:00PM	668.62	91.923	576.69	633.89	121.4	512.49	359.25	101.76	257.49
2:00PM	635.38	87.354	548.03	495.55	94.904	400.65	284.62	80.62	204
3:00PM	365.67	50.273	315.39	374.04	71.633	302.4	246.65	69.863	176.78
4:00PM	260.08	35.757	224.32	320.28	61.338	258.94	154.57	43.783	110.79
5:00PM	123.4	16.965	106.43	161.7	30.968	130.73	71.74	20.321	51.419
6:00PM	16.835	2.3145	14.52	24.735	4.7371	19.998	17.665	5.0037	12.661
7:00PM	0.53	0.0729	0.4571	0.575	0.1101	0.4649	0.64	0.1813	0.4587
8:00PM	0.51	0.0701	0.4399	0.54	0.1034	0.4366	0.515	0.1459	0.3691

9:00PM	0.515	0.0708	0.4442	0.52	0.0996	0.4204	0.51	0.1445	0.3655
10:00PM	0.51	0.0701	0.4399	0.5062	0.0969	0.4093	0.52	0.1473	0.3727
11:00PM	0.515	0.0708	0.4442	0.5062	0.0969	0.4093	0.515	0.1459	0.3691
	17-Jul			**16-Aug**			**15-Sep**		
Hours	**I**	**Id**	**Ib**	**I**	**Id**	**Ib**	**I**	**Id**	**Ib**
12:00AM	0.51	0.1543	0.3557	0.515	0.2161	0.2989	0.4188	0.1035	0.3153
1:00AM	0.505	0.1528	0.3522	0.515	0.2161	0.2989	0.4188	0.1035	0.3153
2:00AM	0.505	0.1528	0.3522	0.5	0.2098	0.2902	0.4125	0.1019	0.3106
3:00AM	0.515	0.1558	0.3592	0.515	0.2161	0.2989	0.4188	0.1035	0.3153
4:00AM	0.515	0.1558	0.3592	0.505	0.2119	0.2931	0.4313	0.1066	0.3247
5:00AM	0.52	0.1573	0.3627	0.51	0.214	0.296	0.4125	0.1019	0.3106
6:00AM	7.745	2.3429	5.4021	5.495	2.3058	3.1892	9.3375	2.3075	7.03
7:00AM	69.86	21.133	48.727	72.675	30.496	42.179	125.53	31.022	94.509
8:00AM	201.34	60.907	140.43	200.05	83.944	116.11	308.29	76.187	232.11
9:00AM	315.19	95.346	219.84	385.77	161.88	223.89	460.88	113.89	346.98
10:00AM	415.08	125.56	289.51	409.94	172.02	237.92	642.53	158.78	483.74
11:00AM	614.45	185.88	428.57	528.83	221.9	306.92	713.38	176.29	537.08
12:00PM	553.27	167.37	385.9	690.69	289.82	400.86	604.14	149.3	454.84
1:00PM	550.89	166.65	384.24	622.51	261.22	361.29	614.26	151.8	462.46
2:00PM	469.1	141.91	327.19	426.01	178.76	247.25	408.26	100.89	307.37
3:00PM	250.31	75.72	174.59	300.06	125.91	174.15	274.3	67.787	206.51
4:00PM	225.06	68.083	156.98	237.58	99.693	137.89	157.81	39	118.81
5:00PM	101.81	30.798	71.012	127.55	53.522	74.028	89.75	22.18	67.57
6:00PM	18.62	5.6327	12.987	13.46	5.648	7.812	9.9188	2.4512	7.4676
7:00PM	0.67	0.2027	0.4673	0.54	0.2266	0.3134	0.425	0.105	0.32
8:00PM	0.51	0.1543	0.3557	0.505	0.2119	0.2931	0.4063	0.1004	0.3059
9:00PM	0.505	0.1528	0.3522	0.51	0.214	0.296	0.4313	0.1066	0.3247
10:00PM	0.515	0.1558	0.3592	0.505	0.2119	0.2931	0.4188	0.1035	0.3153
11:00PM	0.5	0.1513	0.3487	0.505	0.2119	0.2931	0.4	0.0989	0.3011
	15-Oct			**14-Nov**			**10-Dec**		
Hours	**I**	**Id**	**Ib**	**I**	**Id**	**Ib**	**I**	**Id**	**Ib**
12:00AM	0.4063	0.1068	0.2994	0.4188	0.134	0.2847	0.435	0.1516	0.2834
1:00AM	0.4125	0.1085	0.304	0.425	0.136	0.289	0.44	0.1534	0.2866
2:00AM	0.4125	0.1085	0.304	0.4188	0.134	0.2847	0.43	0.1499	0.2801
3:00AM	0.425	0.1117	0.3133	0.4313	0.138	0.2932	0.43	0.1499	0.2801
4:00AM	0.4125	0.1085	0.304	0.4125	0.132	0.2805	0.435	0.1516	0.2834

5:00AM	0.4063	0.1068	0.2994	0.4188	0.134	0.2847	0.425	0.1481	0.2769
6:00AM	14.706	3.8667	10.84	7.6938	2.4624	5.2314	3.21	1.1188	2.0912
7:00AM	143.47	37.722	105.75	101.42	32.459	68.96	74.71	26.04	48.67
8:00AM	356.38	93.704	262.68	261.94	83.833	178.1	246.35	85.862	160.48
9:00AM	530.93	139.6	391.33	467.46	149.61	317.85	416.85	145.29	271.56
10:00AM	676.56	177.89	498.67	541.68	173.36	368.32	554.21	193.16	361.04
11:00AM	763.73	200.81	562.92	614.68	196.73	417.95	659.54	229.88	429.66
12:00PM	721.74	189.77	531.97	658.32	210.69	447.62	701.56	244.52	457.03
1:00PM	684.93	180.09	504.84	554.94	177.61	377.33	691.92	241.16	450.75
2:00PM	500.2	131.52	368.68	630.63	201.83	428.79	591.97	206.33	385.64
3:00PM	442.11	116.24	325.86	482.57	154.45	328.12	452.18	157.6	294.57
4:00PM	294.45	77.42	217.03	279.73	89.528	190.2	266.12	92.754	173.37
5:00PM	95.85	25.202	70.648	59.35	18.995	40.355	58.22	20.292	37.928
6:00PM	3.8813	1.0205	2.8607	1.85	0.5921	1.2579	3.465	1.2077	2.2573
7:00PM	0.4188	0.1101	0.3086	0.4063	0.13	0.2762	0.44	0.1534	0.2866
8:00PM	0.4125	0.1085	0.304	0.425	0.136	0.289	0.44	0.1534	0.2866
9:00PM	0.425	0.1117	0.3133	0.4	0.128	0.272	0.435	0.1516	0.2834
10:00PM	0.4063	0.1068	0.2994	0.4125	0.132	0.2805	0.435	0.1516	0.2834
11:00PM	0.4063	0.1068	0.2994	0.4125	0.132	0.2805	0.435	0.1516	0.2834

Table C: Hourly Total, Beam and Diffuse Solar Irradiance of Semera for recommended days in months

Hours	17-Jan			16-Feb			16-Mar		
	I	**I_d**	**I_b**	**I**	**I_d**	**I_b**	**I**	**I_d**	**I_b**
12:00AM	0	0	0	0	0	0	0	0	0
1:00AM	0	0	0	0	0	0	0	0	0
2:00AM	0	0	0	0	0	0	0	0	0
3:00AM	0	0	0	0	0	0	0	0	0
4:00AM	0	0	0	0	0	0	0	0	0
5:00AM	0	0	0	0	0	0	0	0	0
6:00AM	321.3	19.88	301.4	400.8	24.61	376.2	421.1	36.13	385
7:00AM	558.9	115.8	443.1	647.7	103.3	544.5	631.9	120.6	511.3

8:00AM	705.9	182.8	523	837.5	177.2	660.2	770.1	184.4	585.7
9:00AM	790.1	229.5	560.6	960.3	228.3	732.1	845.4	219.9	625.6
10:00AM	839.7	256.7	583	1025	258.3	766.5	902.2	252.3	649.9
11:00AM	858.8	270.2	588.6	1052	276.4	775.4	920.1	267	653.2
12:00PM	856.5	259.1	597.4	1032	269.5	762.2	911.6	258.2	653.4
1:00PM	819.4	236.5	582.9	970.3	243	727.3	879.4	248.6	630.8
2:00PM	748.6	207.3	541.3	863	205.4	657.5	820.1	216.3	603.8
3:00PM	640.2	164.7	475.5	750.8	163.2	587.6	737.4	173.9	563.5
4:00PM	514.6	106.6	408	579	107	471.9	609	112.5	496.5
5:00PM	330.2	29.07	301.1	310	38.12	271.9	414.1	43.04	371.1
6:00PM	0	0	0	0	0	0	0	0	0
7:00PM	0	0	0	0	0	0	0	0	0
8:00PM	0	0	0	0	0	0	0	0	0
9:00PM	0	0	0	0	0	0	0	0	0
10:00PM	0	0	0	0	0	0	0	0	0
11:00PM	0	0	0	0	0	0	0	0	0
Hours	**15-Apr**			**15-May**			**11-Jun**		
	I	**I_d**	**I_b**	**I**	**I_d**	**I_b**	**I**	**I_d**	**I_b**
12:00AM	0	0	0	0	0	0	0	0	0
1:00AM	0	0	0	0	0	0	0	0	0
2:00AM	0	0	0	0	0	0	0	0	0
3:00AM	0	0	0	0	0	0	0	0	0
4:00AM	0	0	0	0	0	0	0	0	0
5:00AM	0	0	0	0	0	0	0	0	0
6:00AM	425	58.4	366.5	461.3	50.12	411.2	551.6	57.56	494
7:00AM	718.3	98.8	619.5	702.2	122.6	579.6	640.6	113.2	527.4
8:00AM	880.4	121.0	759.3	870.6	179.5	691.1	801	179.6	621.4
9:00AM	985	135.4	849.6	973	209.9	763.1	914.7	215.4	699.2

10:00AM	1028	141.3	886.4	1027	230	797	938.7	240.8	697.9
11:00AM	1044	143.5	900.2	1040	239.2	800.5	938.7	243.9	694.8
12:00PM	1031	141.8	889.3	1024	228.6	795.1	857.1	236	621.1
1:00PM	989	136.0	853.1	983	213.2	769.7	801	171.4	629.7
2:00PM	891.9	122.6	769.3	905.9	181.2	724.7	641.1	152	489.1
3:00PM	794.3	109.2	685.1	807.7	139.4	668.3	640.6	93.85	546.8
4:00PM	612.8	84.2	528.5	662.2	88.5	573.7	577.7	78.02	499.6
5:00PM	409.5	56.3	353.2	440.3	19.87	420.4	551.6	17.3	534.3
6:00PM	0	0	0	0	0	0	0	0	0
7:00PM	0	0	0	0	0	0	0	0	0
8:00PM	0	0	0	0	0	0	0	0	0
9:00PM	0	0	0	0	0	0	0	0	0
10:00PM	0	0	0	0	0	0	0	0	0
11:00PM	0	0	0	0	0	0	0	0	0
Hours	**17-Jul**			**16-Aug**			**15-Sep**		
	I	**I_d**	**I_b**	**I**	**I_d**	**I_b**	**I**	**I_d**	**I_b**
12:00AM	0	0	0	0	0	0	0	0	0
1:00AM	0	0	0	0	0	0	0	0	0
2:00AM	0	0	0	0	0	0	0	0	0
3:00AM	0	0	0	0	0	0	0	0	0
4:00AM	0	0	0	0	0	0	0	0	0
5:00AM	0	0	0	0	0	0	0	0	0
6:00AM	492.6	57.8	434.8	420.3	55.22	365.1	452	38.13	413.8
7:00AM	572.1	117.4	454.6	488.1	124.4	363.7	524.9	130.4	394.5
8:00AM	715.3	182.3	533	488.5	131.6	356.8	525.3	131.8	393.4
9:00AM	765.4	209.3	556.1	610.3	213.9	396.4	656.3	194.5	461.8
10:00AM	816.8	236.9	579.9	653.1	238.3	414.8	702.3	225.4	476.8
11:00AM	838.3	257.8	580.5	715.2	263.5	451.7	769.1	229.3	539.8

12:00PM	838.3	245.6	592.7	715.2	269.8	445.4	769.1	317.6	451.5
1:00PM	765.4	235.7	529.7	696.9	255.6	441.3	749.4	234.6	514.8
2:00PM	715.3	204.5	510.8	653.1	255.3	397.8	702.3	228.8	473.4
3:00PM	572.5	152.5	420	610.3	190.3	420	656.3	201.1	455.2
4:00PM	572.1	95.35	476.7	488.1	152.7	335.4	524.9	199.2	325.7
5:00PM	492.6	17.84	474.8	420.3	27.63	392.7	452	39.86	412.1
6:00PM	0	0	0	0	0	0	0	0	0
7:00PM	0	0	0	0	0	0	0	0	0
8:00PM	0	0	0	0	0	0	0	0	0
9:00PM	0	0	0	0	0	0	0	0	0
10:00PM	0	0	0	0	0	0	0	0	0
11:00PM	0	0	0	0	0	0	0	0	0
Hours	**15-Oct**			**14-Nov**			**10-Dec**		
	I	**I_d**	**I_b**	**I**	**I_d**	**I_b**	**I**	**I_d**	**I_b**
12:00AM	0	0	0	0	0	0	0	0	0
1:00AM	0	0	0	0	0	0	0	0	0
2:00AM	0	0	0	0	0	0	0	0	0
3:00AM	0	0	0	0	0	0	0	0	0
4:00AM	0	0	0	0	0	0	0	0	0
5:00AM	0	0	0	0	0	0	0	0	0
6:00AM	580.4	25.13	555.3	650.8	18.32	632.5	638.5	20.13	618.4
7:00AM	607.8	67.31	540.5	721.8	73.09	648.7	668.7	97.72	571
8:00AM	674.1	105.7	568.4	722.3	89.23	633.1	742.1	110.6	631.6
9:00AM	674.5	124.9	549.6	885.6	142.5	743.1	741.6	179.7	561.9
10:00AM	901.8	181.6	720.3	965.7	205.9	759.9	992.2	265.7	726.5
11:00AM	987.7	221.4	766.3	1058	210	847.6	1087	293.1	793.5
12:00PM	987.7	257.4	730.3	1031	227.7	802.9	1087	299.3	787.3
1:00PM	962.4	213.7	748.7	902.5	222.5	680	1059	277.1	781.7

2:00PM	842.8	204.4	638.4	902.5	184	718.6	927.2	244.6	682.7
3:00PM	842.8	174.7	668.1	721.8	154.3	567.5	927.2	210.3	717
4:00PM	674.1	122.1	551.9	621.5	136.1	485.4	741.6	134.8	606.7
5:00PM	580.4	43.16	537.2	621.5	52.93	568.6	638.5	72.23	566.3
6:00PM	0	0	0	0	0	0	0	0	0
7:00PM	0	0	0	0	0	0	0	0	0
8:00PM	0	0	0	0	0	0	0	0	0
9:00PM	0	0	0	0	0	0	0	0	0
10:00PM	0	0	0	0	0	0	0	0	0
11:00PM	0	0	0	0	0	0	0	0	0

Appendex D1: Schematic drawing of solar thermal storage show external feutures

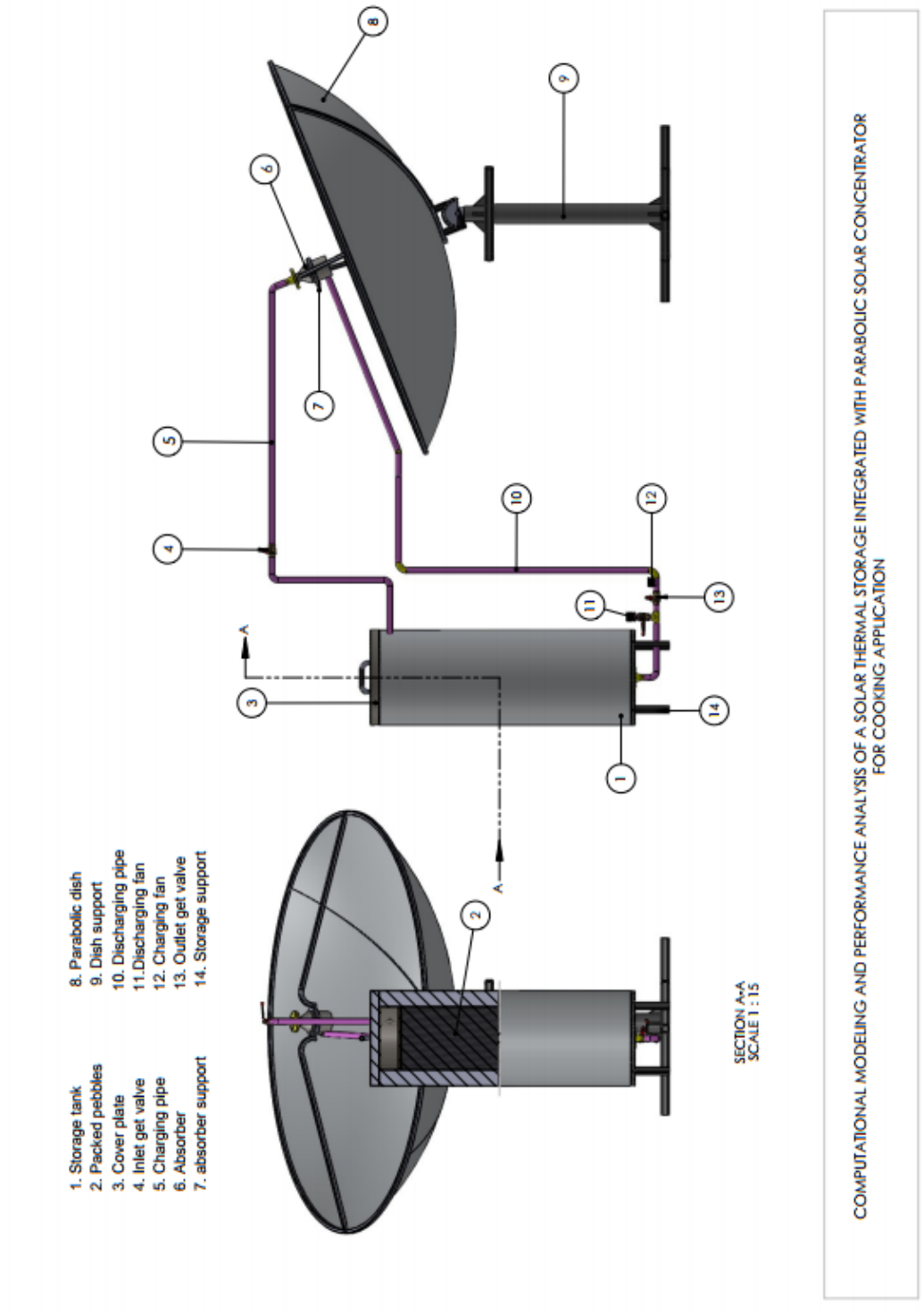

Appendix D2: Schematic drawing of Solar thermal storage shows internal features

1. Storage tank
2. Packed pebbles
3. Cover plate
4. Inlet get valve
5. Charging pipe
6. Absorber
7. Absorber support
8. Parabolic dish
9. Dish support
10. Discharging pipe
11. Discharging fan
12. Charging fan
13. Outlet get valve
14. Storage support

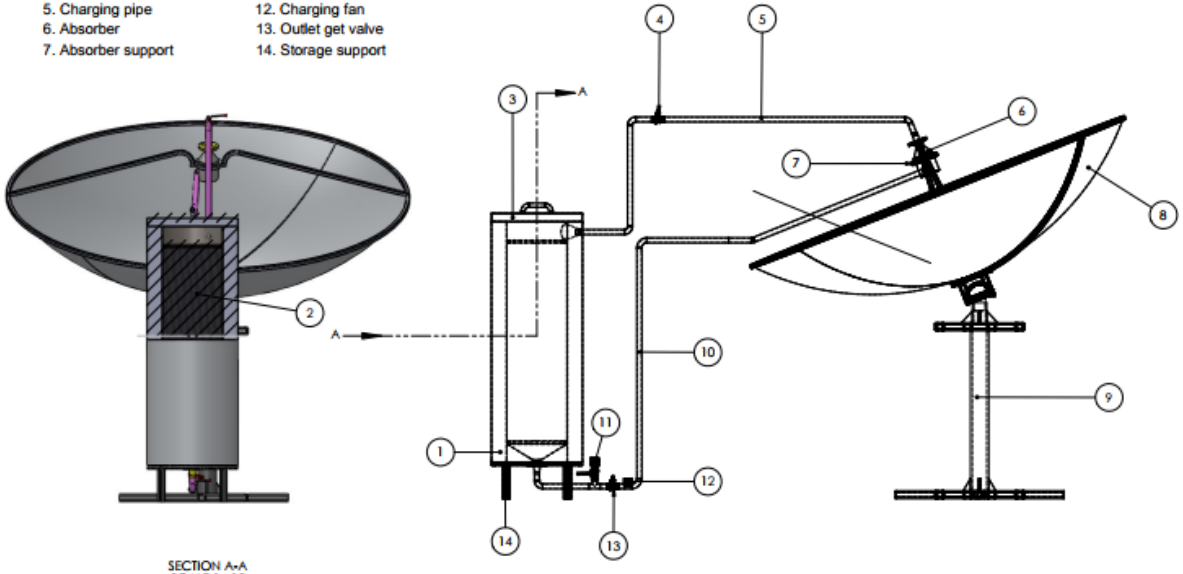

SECTION A-A
SCALE 1 : 15

COMPUTATIONAL MODELING AND PERFORMANCE ANALYSIS OF A SOLAR THERMAL STORAGE INTEGRATED WITH PARABOLIC SOLAR CONCENTRATOR FOR COOKING APPLICATION